2-1-2017

Impedance Optimized Electric Pulses for Enhancing Cutaneous Gene Electrotransfer

Reginald Morley Atkins
University of South Florida, dsherelyn@yahoo.com

Impedance Optimized Electric Pulses for Enhancing Cutaneous Gene Electrotransfer

by

Reginald Morley Atkins Jr.

A dissertation submitted in partial fulfillment
of the requirements for the degree of
Doctor of Philosophy in Biomedical Engineering
Department of Chemical and Biomedical Engineering
College of Engineering
University of South Florida

Major Professor: Mark Jaroszeski, Ph.D.
Wei Chen, Ph.D.
Timothy Fawcett, Ph.D.
Richard Gilbert, Ph.D.
Andrew Hoff, Ph.D.

Date of Approval:
January 30, 2017

Keywords: Electroporation, Bioimpedance Spectroscopy, Gene Delivery, Cell-membrane Permeabilization, Gene Therapy, DNA Transfection

DEDICATION

I dedicate this dissertation to my wife Sherry and son Thorin who have been my primary motivation behind this work. I would also like to thank my parents for their support and finally my Great Aunt Hazel Godwin who believed in me and encouraged me to pursue a selfless life aimed at contributing to the world.

ACKNOWLEDGMENTS

The author expresses his posthumous acknowledgment and sincere appreciation for Professor Anthony Llewellyn's contribution to this research. Without his wisdom and guidance the work would still be in its infancy. His humor, knowledge, and insights are missed. Research reported in this manuscript was supported by National Institute of Arthritis and Musculoskeletal and Skin Diseases of the National Institutes of Health under award number R21AR061136. The content is solely the responsibility of the authors and does not necessarily represent the official views of the National Institutes of Health. The work presented in this document would not be possible without the support and direction of my committee. In particular, major professor Dr. Mark Jaroszeski, and committee member Dr. Timothy Fawcett who have been very generous with their time and patience throughout my academic career. I am also very grateful to Dr. Wei Chen, Dr. Richard Gilbert, and Dr. Andrew Hoff for guidance in their particular areas of expertise. Their contributions allowed the merit of this work to come to fruition.

TABLE OF CONTENTS

LIST OF TABLES

LIST OF FIGURES

ABSTRACT

Electric field mediated gene delivery modalities have preferable safety profiles with the ability to rapidly transfect cells *in vitro* and *in vivo* with high efficiency. However, the current state of the art has relied on trial and error studies that target the average cell within a population present in treated tissue to derive electric pulse parameters. This results in fixed gene electrotransfer (GET) parameters that are not universally optimum. Slow progress towards the validation of a mechanism that explains this phenomena has also hindered its advancement in the clinic. To date, GET methods utilizing feedback control as a means to optimize doses of electric field stimulation have not been investigated. However, with modern electric components the electric characteristics of tissue exposed to electric pulses can be measured in very short time scales allowing for a near instantaneous assessment of the effect these pulses have on cells and tissue. This information is ideal for use in optimizing GET parameters to ensure the conditions necessary for gene delivery can be created regardless of anisotropic tissue architecture and electrode geometry. Bioimpedance theory draws parallels between cell structures and circuit components in an attempt to use circuit theory to describe changes occurring at a cellular and tissue level. In short, a reduction in tissue impedance indicates a reduction to the opposition of current flow in a volume conductor indicating new pathways for current. It has been purported these new pathways exist in the cell membrane and indicate a degree of membrane permeability/destabilization that either indicates or facilitates the uptake of exogenous molecules, such as nucleic acids or plasmid DNA. This study evaluated the use of relative impedance changes from 10 Hz – 10 kHz that occur

in tissue before and after GET to indicate relative increase in tissue and membrane permeability. An optimum reduction in impedance was then identified as an indicator of the degree of membrane permeability required to significantly enhance exogenous DNA uptake into cells. This study showed the use of impedance-based feedback control to optimize GET pulse number in real time to target 80% or 95% reduction in tissue impedance resulted in an 12 and 14 fold increase in transgene expression over controls and a 6 and 7 fold increase in transgene expression over fixed pulse open loop protocols.

CHAPTER 1: BACKGROUND

1.1 Gene Therapy

The discovery of genetic components to chronic diseases and cancers has increased the need to manipulate gene function at the molecular level [1]. With this discovery, novel nucleic acid based therapeutics and methods for treating these pathologies have come to the forefront of medicine. As a result, controlled delivery of nucleic acids to eukaryotic cells has become requisite for advancing research and development of gene-based medicine.

Gene therapy approaches have made substantial progress and show great promise for the treatment of chronic diseases such as arthritis, cardiovascular disease, diabetes, autoimmune disease, and neurodegenerative disease [2] [3] [4] [5] [6] [7]. The central premise of these gene-based therapies relies on either a therapeutic effect induced by properly functioning proteins translated from exogenously delivered genes or the rescue of proper cellular function via the knockdown of a gene and the function of the protein for which it codes. The former case addresses pathologies associated with the absence of a properly functioning protein caused by a deleted gene or a mutant version which results in improperly folded protein with poor bioactivity. Gene therapies resolve this disease state by providing a source for this "missing" protein. The latter case addresses mutated genes that produce proteins with altered catalytic kinetics and/or binding affinities. These often hyperactive proteins perpetuate a disease state while their knockdown can restore proper cell function [8]. Ultimately, the goal of gene therapy is to modulate expression and function of delivered genes to restore or enhance homeostatic activity of cells.

Identifying an absent or improperly folded, non-functioning protein, responsible for a diseased state in turn identifies a gene therapy target. However, the location and function of this protein also determines the target cell type and delivery modality by which therapeutic genes must be delivered to resolve the disease. Some diseases may be associated with a systemically distributed secreted protein that is absent or non-functioning, such as hemophilia or Severe Combined Immunodeficiency Disorder (SCID). In cases such as these, the transfection of specific cell types is often not necessary as long as transfected cells can translate and express functioning proteins. This is because the fate of many secreted proteins in its natural setting is often the same when translated in other cells not normally expressing the delivered gene. This approach lends to less invasive gene delivery methods, such as electroporation or gene electrotransfer with surface electrodes, which indiscriminately target cells within the treatment region without regard to cell type. In contrast, pathologies caused by deleted or mutant proteins with an intracellular or intramembrane function, not secreted by cells, require a gene delivery method that targets the cell type that expresses this gene. In this case, selective transfection is required because only target cells possess the necessary phenotype equipped to modify and regulate the function of this protein. Gene therapy methods targeting specific populations of cells in deep tissue also require more invasive protocols. Viral, chemical, and even physical delivery methods like GET with proper electrodes can target deeper cell populations but assume greater safety risks. Delivery to deep tissue poses a challenge for GET methods, as catheter-based devices would need to be fabricated for the specific disease being targeted. The location of protein function (intracellular/intramembrane or extracellular) and whether or not transfection must be cell type specific are the critical factors necessary for identifying the appropriate gene therapy approach [9]. As a result, some diseases are better suited for certain gene therapy methods than others.

Identifying and targeting pathogenic proteins is not the only consideration when administering gene-based medicine. The complex nature of any gene cannot be underestimated as each gene/protein is intimately connected, usually, with many other gene/proteins either directly through an equilibrium relationship or indirectly through sensitive regulatory feedback systems, which in turn also affect the activity of a plethora of other genes. The forced translation of exogenous genes of interest can interfere with these complex regulatory feedback mechanisms if concentrations or activity is above physiologic levels. This may eventually destabilize cellular function, then tissues, organs, and organ systems away from homeostasis toward a pathogenic state. Considering this, as a safety concern, it is necessary that gene therapies target a desired level and duration of protein expression commensurate for resolving a disease state that also matches physiologic protein levels in order to not disturb homeostatic equilibria. Rate of protein translation can be directly controlled by regulatory elements within exogenous nucleic acid constructs, for example the choice of origin of replication and enhancers in a plasmid vector can provide for high or low rates of protein translation. Expression can also be induced by delivering a secondary agent such as doxycycline or tetracycline when the appropriate tetracycline-dependent promoter is incorporated into plasmids. It is also possible to control duration of expression indirectly by transfecting cells that have a lifespan that matches the desired duration of targeted expression.

Gene therapy applications for treating cancer have taken a fundamentally different approach where genes of interest are delivered to direct the inherent functions of immune cells to target and kill cancer cells. This is also known as immunotherapy. This method attempts to activate or suppress a population of immune cells including: dendritic cells (macrophages), natural killer cells, cytotoxic T lymphocytes, regulatory T cells, helper T cells, or B lymphocytes. All lymphoid derived cells have roles in adaptive immunity that identify and eliminate cells presenting

non-self antigens. Because tumor cells present self-antigens, these immune cells are able to escape identification by dendritic cells and elimination by effector lymphocytes and NK cells. Some gene constructs for immunotherapy encoding for cytokines and growth factors are delivered to activate or suppress immune cells in an attempt to eliminate anergy inducing effects of the tumor microenvironment and tolerance to tumor antigens.

Cancer vaccines work in the same fashion as conventional vaccines, attempting to educate adaptive immune cells to identify cancer cells by exposing them to tumor associated antigens (TAA's). These vaccines contain nucleic acids that code for cancer specific TAA's identified via tumor genome sequencing and require translation of encoded protein by cells to stimulate a therapeutically relevant concentration of antigen to induce an immune response. DNA cancer vaccines can be prophylactic or therapeutic in their mode of action however like traditional vaccines attempt to provide long-term activation of humoral and cell mediated immune components to completely eradicate a tumor and prevent its reoccurrence [10] [11]. Cancer vaccines have been shown to induce anticancer responses against many different cancer types [12] [13] [14] [15].

1.2 Skin as a Platform for Gene Therapy

This research investigated the use of surface electrodes to facilitate electric field mediated gene delivery in skin. Surface electrodes, like the multielectrode array (MEA) used in this study are ideal for delivering genes to superficial cells residing in the epidermis, dermis, and hypodermis as well as superficial tumors. This approach is relatively noninvasive and lends to simple GET application with rapid protocols. The depth of electric field penetration can be determined with electrode spacing; therefore, different layers of skin and populations of cells could theoretically be targeted for transfection by adjusting the distance between electrodes.

Target cells in the epidermis include keratinocytes, lymphocytes, and specialized antigen presenting dendritic cells (macrophages), referred to as Langerhans cells, which comprise up to 8% of epidermal cells [16]. The epidermis is divided into two types, thick or thin skin, which have five and four layers respectively. Thick skin occurring only on the palms of the hands and soles of the feet contains an additional layer called the stratum lucidum. This layer is absent in thin skin which has only four distinct layers and was the target for gene therapy discussed herein. In thin skin, the epidermis ranges in thickness from 75 to 150 μm and is renewed every 15 – 30 days as keratinocytes mature from the highly mitotic basal layer to the dead corneal layer [16]. The life cycle of epidermal cells can be used to control the duration of transgene expression as these cells live for a month at most and cannot migrate to other regions of the body. This provides for temporal and spatial control of transgene expression to cells within a confined treatment region when using physical gene delivery methods that are not selective. However, transfection of Langerhans cells can generate systemic responses due to their migratory nature especially if the delivered gene has an influence on the immune system.

The structure of the epidermis contains two layers with relevant distinctions that significantly affect electrical characteristics and therefore cutaneous GET. The most superficial layer of the epidermis, the stratum corneum, is composed of anuclear, hexagonally shaped corneocytes with an average diameter and height of 40 μm and 0.8 μm respectively [17]. These dead cells are imbedded in a protein and lipid rich matrix and together form a layer approximately 20 μm thick with very little bound water [18]. The three living layers below the stratum corneum, increasing in depth include the stratum granulosum, stratum spinosum, and the stratum basale combine to form the remainder of the epidermis. These layers are composed of living keratinocytes that range in diameter from 35 μm to 55 μm depending on their age and layer with a

height near 10 μm [19]. The volume fraction occupied by water in this layer is roughly 0.7 [20]. As a result, the stratum corneum has a resistivity near 200 - 400 kΩ•m, which is approximately three orders of magnitude greater than the resistivity of the lower electrolyte rich layers of the epidermis where resistivity is near 100 - 200 Ω•m [21].

The integument is an excellent tissue for administering cancer vaccines. A population of dendritic (Langerhans) cells reside in the epidermis as part of the mononuclear phagocyte system. Cancer vaccines require direct exposure of dendritic cells to TAA's to promote antigen binding, processing, and presentation to T cells. Because of their proximity to the skin exterior, surface electrodes have the ability to directly transfect these antigen presenting cells with a TAA encoded plasmid. Transfected dendritic cells then translate, process, and present the TAA to lymphocytes with the potential to generate antigen specific MHC I/II restricted immune responses against tumors. These same dendritic cells may also receive antigenic stimulation from TAA secreted by transfected keratinocytes within the treated region. This could provide the basis for efficacy of cutaneous cancer vaccines.

Similar to cancer vaccines, immunotherapies attempt to modulate humoral and cell mediated immune cell function to reduce autoimmunity or identify and eliminate tumor cells via stimulation of effector T and cells with chemokines, cytokines, antibodies, or other proteins. Healthy cells that having undergone neoplastic transformation to form tumors have been shown to modify their environment and suppress immune function [22] [23]. The microenvironment within tumors contains a host of suppressive cytokines overexpressed by tumors cells and a modified extracellular matrix highly effective at suppressing tumor immunogenicity and identification of tumor cells by antigen presenting cells and effector cells [24]. For example programmable death receptor ligand 1 (PDL1), overexpressed by tumor cells, anergizes lymphocytes and suppresses

the expression of anti-tumor phenotypes necessary for tumor eradication [25]. This allows tumor cells to evade cytotoxic T lymphocytes and unchecked tumor growth to occur. Two approaches for circumventing this immune suppression include the transfection of cytokines to counteract this suppression by directly upregulating T cell activity and the use of checkpoint inhibitors or (antibodies) like anti-PDL1 that neutralize suppressive proteins released by tumors.

1.3 Nucleic Acid Delivery Methods

The copious charge and large size of nucleic acid constructs impede its delivery across the cell membrane. For every nucleic acid within a gene construct there exists a single negative charge resting on a phosphate molecule, the amount of charge on deliverable nucleic acid constructs can accumulate quickly when considering the size of most genes. For example, the plasmid DNA used in this study was composed of 6,732 base pairs, which equated to 13,464 negative charges associated with the phosphodiester backbone only. However, pDNA in this case becomes supercoiled hiding many of those charges. In addition to this charge, the hydrodynamic diameter of supercoiled DNA is typically between 200 nm to 400 nm [26] [27]. Smaller, single stranded genetic constructs are easier to deliver, but still pose a major challenge with respect to traversing the cell membrane. To circumvent these barriers to delivery, a collection of delivery methods classified as either viral, chemical, physical have been developed. Each of these methods have their own advantages and disadvantages. The cell type, location of target cell, desired type of expression (transient or long term), need for selective transfection, cost, safety, and time are important factors to consideration when selecting a gene delivery method.

1.3.1 Viral Delivery Methods

Viral delivery exploits the innate biological machinery viruses utilize to infect host cells. The life cycle of a virus revolves around the delivery of its own DNA or RNA into host cells, for

this reason they have been a popular vehicle for delivering genes. Viral gene delivery can produce higher transduction efficiency and some achieve prolonged gene expression. However, viruses differ in their selectivity for transducing targeted cell types. Some species induce transient expression while others permanently integrate their genes into the host genome. There are also distinct differences in DNA payload capacity [28]. Popular viruses used to deliver genes with their respective payloads include adeno virus (AV) 36kbp of dsDNA, adeno-associated virus (AAV) 4.7 kb of ssDNA, lentivirus (LV) 10 kb ssRNA, retrovirus (RV) 7.5 kb of ssRNA, vaccinia virus (VV) 190 kbp of dsDNA, and herpes simplex virus (HSV) 152 kbp dsDNA [29]. Safety issues with viral methods include immunogenicity and genotoxicity [29]. Stable viral gene insertion into the coding sequence of a host gene can create fusion proteins. This raises the risk for insertional mutagenesis and subsequent carcinogenicity or nonfunctioning proteins [30]. Immunogenicity is also a concern. Patients previously exposed to a virus that induced an immune response could experience anaphylaxis when exposed to the same viral vector used for gene delivery [31]. Limitations in payload capacity can also restrict the size of genes available for delivery. Lastly, procedures associated with viral vector preparation require lengthy protocols, higher costs, and stringent quality control procedures.

1.3.2 Non-Viral Delivery Methods

Safety, time, and economic concerns associated with viral methods have led to the advent of several chemical and physical techniques. Benefits of non-viral methods include shorter protocols, no risk of insertional mutagenesis, non-immunogenic, biocompatibility, little to no toxicity, no genotoxicity, and lower costs.

Chemical delivery methods attempt to neutralize the negative charge on the DNA backbone while also compressing it through encapsulation via electrostatic interactions [32] [33]. Peptides,

polymers, or cationic lipids are the chemical species commonly used to accomplish this [34]. When these polyplexes form, functionalized lipids, polymers, and polypeptides can be conjugated with surface receptors for cell targeting and DNA release/escape [34]. However, issues with polydispersity and heterogeneity present in polymer-based methods reduce control over size of DNA polylpexes resulting in variable transfection efficiencies. As a whole, disadvantages with *in vivo* chemical methods include cytotoxicity and low transfection efficiencies relative to viral and other physical methods [32].

Physical methods employ a physical forcing function to accomplish gene delivery that have preferable safety profiles without the threat of toxicity, immunogenicity, or carcinogenicity. Physical methods typically deliver genes on shorter time scales and require few reagents. There are a collection of different physical methods for delivering pDNA including single cell laser cutting [35], sonoporation [36] [37], biolistic transfection (gene gun) [38], magnetic fields [39], and electric fields [40] [41] [42]. Physical and chemical methods produce transient transfection only. This requires periodic transfection to maintain therapeutic levels of the encoded protein. Gene electrotransfer, the application of electric fields to tissue, represents a physical method that relies upon the permeabilizing effect of pulsed electric fields [43] [44] [45] [46]. When a specific electric field is employed to deliver genes, extracellular nucleic acids pass through the membrane via a mechanism that is not clearly understood has been explained through various mechanisms, including the formation of transient pores within the membrane that allow DNA access to the cell interior [47] [48]. These genetic constructs translocate to the nucleus where the gene expression process begins. Permeabilizing electric fields are established by applicators containing electrodes in direct contact with the target tissue. Typical electrode spacing requires the delivery of electrical pulses on the order of tens of volts for hundreds of milliseconds to generate field strengths within

hundreds of V/cm [49] [50]. Electric fields generated in tissues cause ions in the local extracellular space and within cells to collect on the inner and outer leaflets of cell membranes similar to the charging of a capacitor [51]. As the ions accumulate, the transmembrane potential eventually reaches the breakdown voltage of the insulating phospholipid bilayer resulting in current flow through the membrane and permeabilization [52]. Rearrangements in cell membrane structure following permeabilization provide new pathways for current resulting in measurable changes in electrical conductivity. Changes in conductivity can then be used to indicate when changes in membrane permeability occur [53]. Thus, the changes in tissue conductivity and capacitance allows impedance spectroscopy to be used as a tool for quantifying changes in the electrical characteristics of cells/tissue during gene electrotransfer [53] [54] [55].

Current *in vivo* electrotransfer treatment protocols typically apply a fixed set of pulses to the tissue to optimize the electric field delivery parameters to obtain a desired gene delivery. The pulse characteristics (field strength, pulse duration, number of pulses, etc.) are typically empirically derived based upon mean responses from preclinical studies. When determining these optimal parameters there is currently no method available to account for differences between individuals with respect to chemical environment and tissue architecture. Similarly, empirical approaches do not permit the ability of real-time alterations of pulse parameters in response to any measured parameter (such as impedance or conductivity changes in the tissue) during electrical treatment nor do they provide any indication of successful gene delivery. Although GET has been successful and will likely have many applications in the near future, it is likely that it can be ultimately improved by measuring changes in electrical properties of tissue during electric field pulsing and then adjusting pulse parameters in real-time to achieve membrane permeability optimum for DNA delivery.

The application of gene therapy in medicine holds great promise; however, the ability to ensure its delivery has not been resolved. The current state of the art employs fixed GET pulsing parameters that fail to account for differences in tissue architecture across organisms. The goal of this research was to characterize the relationship between electric field induced changes in tissue impedance with gene expression. Successful characterization of this relationship provided a variable for optimizing GET in real-time that describes changes in membrane permeability induced by pulsed electric field. This information was then used to adjust EF pulse parameters to modulate cell membrane permeability towards an optimum and thus control gene delivery to cells. Initial work identified a correlation between gene expression and impedance taken before, during, and after electric pulses were administered to tissue. After which a deeper analysis of the frequency dependent nature of impedance was performed to develop an appropriate equivalent circuit model. This relationship will be ideal for implementation in electroporation treatment algorithms to accomplish targeted gene delivery across patients. Optimizing in real-time during treatment ensures gene delivery occurred and allows the full potential of physical gene therapy to be realized. This dissertation summarizes work performed and the motivation for characterizing impedance as a feedback tool to be used during electroporation.

1.4 Bioimpedance

The analysis, characterization, and manipulation of biological tissue for the purposes of extracting information or application of medicine requires methods that do not disturb the natural processes occurring within the living system. This demands these methods be rapid, non-invasive, and non-toxic. Optical techniques such as X-rays, MRI, and fluorescence based imaging exist with this capability but are limited in the type of effect they can induce. Chemical methods are generally too slow and toxic. However, electric field based methods possess a unique ability to

characterize living systems without perturbing them as well as the ability to force changes within them. Historically, the gene delivery field has used high magnitude electric fields on the order of hundreds of V/cm to kV/cm to induce the uptake of nucleic acids by cells. Recently this same field has begun to use low magnitude electric fields (5 V/cm) that have been shown not to affect delivery *in vivo* when surface electrodes are used [56]. These label free interrogation pulses have also been shown to have the ability to evaluate the change in electrical characteristics of living tissue after electric field stimulation [56].

The application of this method in biological systems is referred to as bioimpedance spectroscopy and has been practiced for many decades to characterize biological tissues [57] [58] [59]. Simply stated, impedance is the sum of resistance and reactance in alternating current systems. Where sources of opposition to current flow exist in not only in resistive components but also in structures with the ability to store charge (capacitance) and in structures that can generate a back electromotive force (inductance). The utility of impedance spectroscopy comes from the information it can provide concerning these capacitive and inductive components. When biological structures possess capacitive mechanisms, modeling them as these components can reveal what may be occurring physiologically in a biological system. Bioimpedance was used in this study in this way to determine what effect electric fields were having on cell membranes as a way to guide electric field pulsing, the gene delivery forcing function.

Electrical impedance is a complex number, represented by the letter Z with units of resistance or ohms (Ω) that provides information about the magnitude of the complex ratio of voltage to current and difference in phase between the voltage and current as a function of alternating current frequency (ω). Impedance can be defined in Cartesian form (eqn. 1) or in polar form (eqn. 2),

$$Z(\omega) = R + jX \qquad (1)$$

$$Z(\omega) = |Z|e^{j\theta} = |Z|(cos\theta + jsin\theta) \qquad (2)$$

where R is a measure of the real component of resistance (Ω), θ is the phase angle, and the imaginary component X is termed reactance, which is the sum of capacitive and inductive contributions to impedance defined as X_C and X_L respectively with units of ohms Ω. Capacitive reactance and inductive reactance are functions of frequency and capacitance and inductance respectively as defined below.

$$X_C = \frac{1}{j\omega C} = \frac{1}{\omega C} e^{-\frac{\pi}{2}} \qquad (3)$$

$$X_L = j\omega L = \omega L e^{\frac{\pi}{2}} \qquad (4)$$

The magnitude of impedance and phase angle shift can be calculated as the length of the position vector in the complex plane to a frequency dependent impedance locus and the angle this vector makes with the positive x-axis respectively as shown below.

$$|Z| = \sqrt{R^2 + (X_L - X_C)^2} \qquad (5)$$

$$\theta = tan^{-1}\left(\frac{X}{R}\right) \qquad (6)$$

CHAPTER 2: MOTIVATION AND SPECIFIC AIMS

2.1 Motivation

Current GET methods employ fixed, empirically derived parameters that do not compensate for differences in tissue architecture between organisms nor do they attempt to evaluate cellular response to electric pulses to ensure optimum conditions for DNA delivery are attained. These open loop methods have no way of assessing the changes in tissue permeability that result from electric field stimulation. Without being able to measure the degree of permeability induced by electric fields it is difficult to determine whether a lack of gene therapy efficacy was due to the gene construct or suboptimal membrane permeabilization. Furthermore, open loop or fixed pulse methods lack the control needed to target a desired degree of membrane permeability and a corresponding targeted amount of delivery. These limitations of the current state of the art provided the motivation to integrate feedback control into GET. This was done in an effort to create closed loop methods that use the response of tissue during GET to adjust electric field parameters in real-time to achieve the targeted permeability necessary to ensure successful gene delivery occurs.

This research investigated the use of an impedance spectroscope to assess the relative change in membrane permeability present in cells between GET pulses and to guide the number of pulses applied based on these changes. Relative changes in impedance were used to decide whether or not electric field pulsing should cease or continue which provided for tissue specific electric field dosing. Pulsing continued in each sector until tissue impedance was reduced by a

specified percent relative to baseline. Pulsing in this manner provided tissue specific doses of electric field exposure accounting for differences in tissue architecture between treatment sectors and was expected to enhance gene delivery when compared to open loop, fixed pulse protocols. A closed loop protocol was developed to identify the stop impedance and corresponding permeability that correlated with maximum transgene expression. Therefore, this research was designed to test the hypothesis that changes in tissue impedance could be used to identify and target cell/tissue permeability in a closed loop feedback GET protocol to ensure the membrane permeability necessary for maximum DNA delivery were created. Ultimately, this project significantly improved the efficacy of GET technology to accomplish controlled gene delivery.

2.2 Specific Aims

This dissertation describes the characterization, validation, and utilization of impedance spectroscopy for the real-time optimization of *in vivo* gene electrotransfer. In order to develop a closed loop protocol, it was first necessary to establish a correlation between impedance and gene expression as a function of electric field strength. It was hypothesized that a reduction in tissue impedance indicated the presence of new current pathways. These new pathways were expected to exist through cells, a result of membrane permeabilization induced by electric field stimulation. Identifying the direction of the correlation between impedance and gene delivery allowed for impedance changes that correspond to high gene expression to be selected. After establishing this correlation, the utility of impedance as a feedback variable for optimizing gene delivery was evaluated. The reporter gene expression present in treatment groups receiving closed loop GET that optimized pulse number to target two different stop impedances at different field strengths was compared to the expression in open loop, fixed pulsing GET groups of the same field strength

to show the impedance based closed loop methods significantly enhanced gene delivery. Each of these items was addressed as a specific aim in this investigation.

The following specific aims fully characterize this technology and optimize GET.

2.2.1 Specific Aim i

The purpose of specific aim i was to characterize the dependence of biological response on impedance changes that resulted from pulses used for pDNA delivery to skin.

2.2.2 Specific Aim ii

(A) Establish a pulsing algorithm that uses feedback to adjust pulsing based upon impedance changes. (B) Deliver pDNA using impedance feedback based pulsing and compare results to open loop pulsing protocols to establish if the impedance guided pulsing scheme enhanced biological response.

CHAPTER 3: MATERIALS AND METHODS

3.1 GET/Impedance Analyzer System

To characterize changes in tissue impedance without affecting permeability conditions, the interrogation signal was required to be low in magnitude relative to the scale of voltages required to generate GET electric fields. Also, in order to accomplish rapid inter-GET pulse impedance measurements without disturbing tissue architecture during the GET protocol, it was also necessary to apply the GET and impedance waveforms with the same electrodes. This required a set of 32 solid state relays to separate low power impedance circuitry from being damaged by the higher voltage GET pulses and for each to apply waveforms from their respective power supplies.

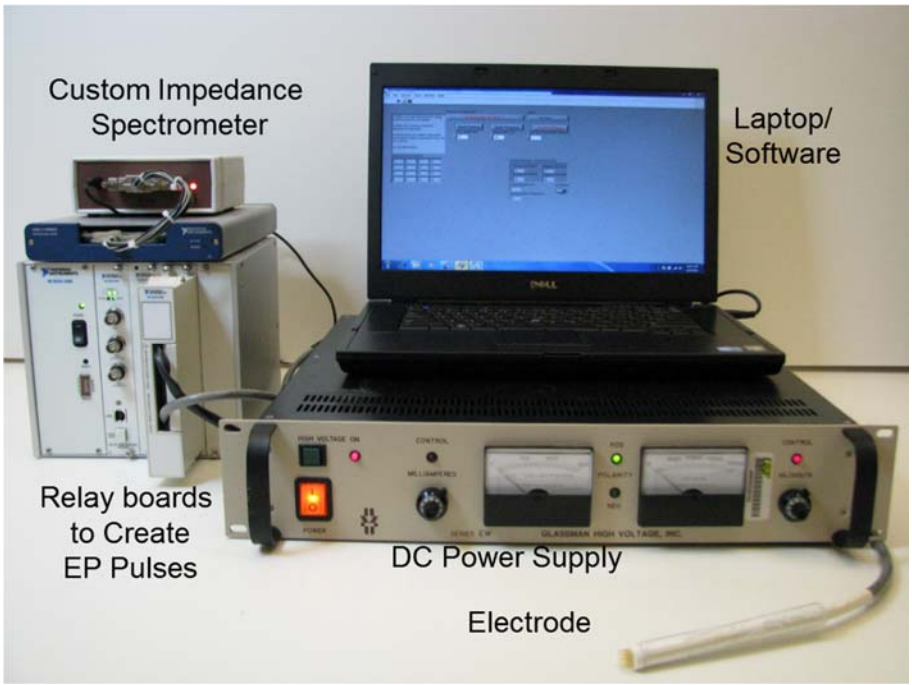

Figure 1: HV power supply, software control/laptop, SCXI chassis, impedance spectrometer and relay boards.

The impedance analyzer/GET system (Figure 1) was controlled by custom LabView software installed on a laptop. GET pulses were generated by a high voltage power supply (Glassman High Voltage Inc., PS/EW02R300-115) and the multi frequency analog sine wave impedance waveforms were generated using a National Instruments (NI) USB-6361 multifunction input/output card. Voltage and current signals through tissue during impedance measurement was measured and buffered by two instrumentation amplifiers (LT1995) before being recorded by the analog input channels of the USB-6361. Sixteen electrodes in the multielectrode array were connected to an (NI) SCXI-1163R module housed in a NI SCXI-1000 chassis containing the 32 solid-state relays. A NI SCXI-1600 USB Data Acquisition and Control Module (200 kS/s) was used to control the isolated solid-state relay module. Sixteen of the relays were connected to the ground terminal and the other sixteen were connected to the positive terminal. The solid-state relays have switching time of approximately 50 ms. The short time scale that allows a near instantaneous image of tissue impedance after pulsing giving this protocol its power and reliability to measure tissue response to electric field stimulation during GET.

The multielectrode array (MEA) used to apply GET pulses and impedance pulses was constructed of 16 gold plated, cylindrical, hemispherical electrodes. Electrodes were configured into a 4x4 square array and spaced 2.5 mm apart, center to center. Spring-loaded electrodes allowed for good electrical contact regardless of tissue topology. Electrodes were numbered 1 through 16 vertically from top to bottom and left to right. The square spaces between 4 electrodes were referred to as treatment sectors 1 through 9, which were labelled with the same directionality as electrodes. Pulsing advanced from sectors one through 9 in numerical order.

The motivation of this study was to show closed loop GET methods could significantly enhance gene delivery. The major difference between these two methods was in the number of

GET pulses that were applied. To ensure a relevant area of membranes became permeabilized pulses were applied in two directions: vertically and horizontally. To ensure a relevant area of tissue was permeabilized in each sector each pulsed direction consisted of a pair of simultaneous parallel pulses from pairs of parallel electrodes. For example in sector one a vertical pulse from each positive potential electrode 1 and 5 to ground potential electrode 2 and 6 was followed by a horizontal pulse from each positive potential electrode 1 and 2 to ground potential electrode 5 and 6. Open loop methods followed a fixed pulsing pattern where each animal received 8 pulses per sector, 2 pairs of simultaneous vertical pulses from parallel sector electrodes (4 pulses) followed by 2 pairs of simultaneous horizontal pulses from parallel sector electrodes (4 pulses) for a total of 8 pulses per sector and 72 pulses per the entire protocol. The pulse number in closed loop methods varied per treatment sector as a function of impedance. Pulsing continued in each treatment sector until the impedance reduction set point had been attained. In closed loop methods, as pulsing advanced to a sector, first a set of four GET pulses were applied then impedance was measured. A single pulse from each parallel pair of electrodes in each sector in each direction for a total of four pulses was applied between each impedance measurement. This pattern of pulsing between impedance measurements in the closed loop pulsing regime was referred to as an exposure, which was equal to 4 pulses. Once target impedance was attained, pulsing advanced to the next sector followed by an impedance measurement.

3.2 Impedance Measurement

The design of the MEA gives the electrodes the dual capability to apply both high voltage electric pulses necessary for inducing membrane permeability as well as the low voltage pulses and current measurement for quantifying tissue impedance. A 1 V continuous sine wave excitation signal was generated by the impedance spectroscope containing a range of linearly spaced

frequencies from 10 Hz to 100 kHz over a duration of 25 ms. This 25 ms impedance measuring signal was injected 50 ms after the fourth double (last) pulse in the fixed pulse DEI groups or after each double pulse in the DEIF groups. After collecting voltage and current waveforms from the 25 ms pulse, a Fast Fourier Transform (FFT) algorithm with a rectangular window implemented in NI Labview 2013 calculated the Fourier transform of both voltage and current waveforms expressed as frequency dependent complex numbers ($F_V(\omega)$ and $F_I(\omega)$ respectively. The ratio of the magnitudes $F_V(\omega)$ relative to $F_I(\omega)$ was used to calculate impedance norms $|Z(\omega)|$. Similarly, the phase of impedance (ϕ_z) was calculated as the ratio of $F_V(\omega)$ (ϕ_V) relative to $F_I(\omega)$ (ϕ_I). Before treatment, to account for impedance associated with the MEA, applicator electrodes were placed on a conductive block of steel etched with a MEA footprint for securing good contact with electrodes. Electrodes were then shorted with the 25 ms impedance signal and impedance instrumentation measurements were acquired for all nine electrode sectors. The instrumentation impedance from each sector was then appropriately subtracted from the corresponding treatment sector spectra obtained from tissue during experiments.

In DEIF groups, after each EF treatment sector double pulse impedance was measured. The mean impedance norm $|Z(\omega)|$ after each double pulse relative to baseline impedance of that sector was calculated. Double pulsing of that sector then continued until the sector impedance was reduced by either 80% or 95% of baseline impedance. Once the targeted reduction in impedance of a sector was met, the next sector received pulsing in each direction at least once followed by an impedance measurement to determine relative change in impedance. Upon advancement of pulsing to next sector, one EF pulse was required before measuring impedance. This required all sectors to receive at least on direct EF pulse.

3.3 Reporter Gene Plasmid

The reporter gene expression vector used in this study was a 6,732 base pair, high expression circular plasmid (gWIZ-Luc, Aldevron) shown in Figure 2 with an inserted luciferase DNA sequence. The regulatory elements in this plasmid allowed for high transgene expression via a proprietary hybrid promoter/enhancer that contained a cytomegalovirus immediate early gene (CMV IE) and the Intron A gene. This expression vector also contained a high-efficiency artificial transcription terminator to ensure timely cleavage and release of the primary mRNA transcript from the transcription complex and 3' end polyadenylation processing to occur. The plasmid also included a Kanamycin resistance gene. Relative differences in gene delivery between different treatment conditions were assessed via an *in vivo* imaging system (IVIS) images that quantified the number of photons emitted per second from the luciferase-catalyzed reduction of injected luciferin substrate. It was expected that as more reporter gene pDNA was delivered to cells, luciferase copy number would increase leading to an increased number of emitted photons and higher radiance values upon substrate injection.

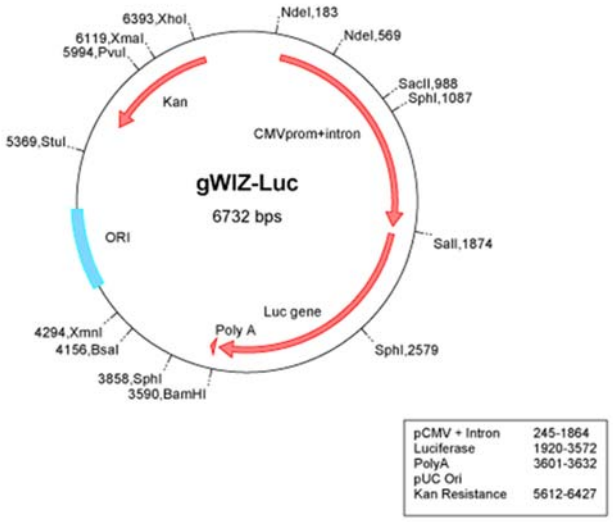

Figure 2: High expression gWIZ™ Luciferase plasmid vector map [60].

CHAPTER 4: SPECIFIC AIM I: IMPEDANCE AND GENE EXPRESSION[1]

4.1 Introduction

The origin of pathologies associated with aberrant genes has been studied extensively [61] [62] [63] [1] [64] [65]. It is now accepted that both inherited and acquired genetic mutations are culpable for many chronic diseases. Technologies with the ability to deliver correctly sequenced genes encoding properly functioning proteins into cells provide an excellent opportunity for the treatment of pathologies caused by DNA mutations that produce absent or non-functioning proteins. However, delivering nucleic acids through cell membranes poses a challenge. Nucleic acid constructs are orders of magnitude larger than most drugs and possess copious negative charge making the translocation of extracellular nucleic acids across the plasma membrane unlikely under normal conditions [66] [67]. To this point, a great demand exists for technology to address this obstacle if medicine is to harness the advantages of gene-based therapies.

An electric field mediated *in vivo* gene delivery method referred to as gene electrotransfer (GET) has emerged as a formidable technique allowing the potential of gene-based therapies to be realized. During GET, it is proposed that electric pulses temporarily permeabilize the cell membrane facilitating exogenous DNA uptake [68]. To improve the efficiency of GET, recent work has shown the status of tissue can be characterized with impedance measurements [69] [70]. Changes in tissue and or cell impedance indicate changes in the membrane permeability present

[1] This chapter was accepted for publication in *Bioelectrochemistry* and is in press. Copyright permission is included in Appendix A.

in GET attributed to electric pulses [68] [71] [72] [73] [74]. This work supports the integration of impedance spectroscopy into GET as a way to enhance the probability that gene delivery occurs by optimizing the number of electric pulses during GET treatment. This was accomplished by measuring tissue impedance between pulses until an impedance level that corresponds to optimum cell membrane permeability and gene delivery has been attained after which pulsing ceased. Real time use of tissue impedance measurements can be used to decide whether more electric pulses are required during a GET to maximize gene delivery. In order to validate the potential of this method it is necessary to juxtapose the efficacy of GET with other methods that have contributed to gene delivery research.

An array of technologies exist for enhancing the intracellular delivery of nucleic acids broadly classified as either viral or non-viral methods. Viral methods employ live viruses to transfect host cells with a gene of interest. This is accomplished with high efficiency but also with safety concerns. Many viral vectors randomly integrate their genome into the host genome increasing the risk for insertional mutagenesis and subsequent malignant transformation [75]. Other viral vectors target specific regions of the host genome for integration but with a limited payload capacity for exogenous nucleic acids [76] [77] [28]. Although effective, viral vectors raise safety concerns associated with their immunogenicity. Natural exposure to viruses over time engenders immunity to their components. These same viruses often induce immune responses when used to deliver genes [30] [31].

Non-viral methods utilize physical or chemical processes to induce gene delivery. Chemical methods that use liposomes and cationic surfactants that encapsulate pDNA exhibit relatively lower transfection efficiencies and cell viability [78] [79] compared to viral methods. Chemical methods often involve a systemic distribution of therapeutics that may lead to unwanted

gene expression in untargeted cells [80]. There are a collection of different methods for delivering pDNA including single cell laser cutting [35], mechanical perturbation via ultrasonic treatment [36] [37], biolistic transfection (gene gun) [38], magnetic fields [81], and electric fields [40] [41] [42]. Unlike chemical methods, physical methods do not require exposure to chemicals. Physical and chemical methods produce transient transfection only with periodic treatments required to maintain high expression levels of the encoded protein.

GET, the application of electric fields to tissue, represents a physical method that relies upon the membrane permeabilizing effect of electric pulses/fields [45] [43] [44] [46]. When a specific electric field is employed to deliver genes, extracellular nucleic acids pass through the membrane via a mechanism that is not clearly understood [47] [48]. These genetic constructs translocate to the nucleus where the gene expression process begins. Permeabilizing electric fields are established by applicators containing electrodes in direct contact with the target tissue. Typical electrode spacing requires the delivery of electrical pulses on the order of tens of volts for hundreds of milliseconds to attain field strengths between 100 V/cm to 200 V/cm [49] [50]. These electric fields generated in the skin cause ions in the local extracellular space and within cells to collect on the inner and outer leaflets of cell membranes similar to the charging of a capacitor [51] [82]. As the ions accumulate, the transmembrane potential eventually reaches a breakdown voltage of the insulating phospholipid bilayer resulting in current flow through the membrane and permeabilization [52]. Rearrangements in cell membrane structure following permeabilization provide new pathways for current resulting in measurable changes in electrical conductivity. Changes in conductivity can then be used to indicate when changes in membrane permeability occur [53] [83] [84] [85]. Such changes in tissue conductivity and capacitance allow impedance

spectroscopy to be used as a tool for quantifying changes in the electrical characteristics of cells/tissue during gene electrotransfer [53] [54] [55] [68] [69] [70] [71] [73] [74] [86].

Current in vivo electro transfer treatment protocols typically apply a fixed set of pulses to the tissue to accomplish gene delivery. The pulse characteristics (field strength, pulse duration, number of pulses, etc.) are typically empirically derived based upon mean responses from preclinical studies. When determining these optimal parameters, there is currently no method available to account for differences between individuals with respect to chemical environment and tissue architecture. Similarly, empirical approaches do not permit the ability of real-time alterations of pulse parameters in response to any measured parameter (such as impedance or conductivity changes in the tissue) during electrical treatment nor do they provide any indication of successful gene delivery. Although gene electrotransfer has been successful and will likely have many applications in the near future, it is likely that it can be ultimately improved by measuring changes in electrical properties during gene electrotransfer. This paper reports on research efforts to identify impedance spectra characteristics of tissue that correlate with successful gene delivery.

4.2 Methods

4.2.1 Hardware

The electric field delivery instrumentation hardware included thirty-two (32) isolated solid-state relays within a single National Instruments (NI) SCXI-1163R module housed in a NI SCXI-1000 chassis. The module is controlled by an NI SCXI-1600 USB Data Acquisition and Control Module (200 kS/s). Sixteen of the relays were connected to the positive terminal while the other sixteen relays were connected to the ground terminal of a high voltage power supply (Glassman High Voltage Inc., PS/EW02R300-115). Impedance spectroscope was created from a National

Instruments (NI) USB-6361 multifunction input/output card that generated a multi-frequency sine analog voltage reference signal buffered by a unity gain high-bandwidth amplifier (Linear Technology LT1358) rated to drive capacitive loads. The differential voltage across and current flowing through the tissue was buffered (LT1359) and measured by a pair of instrumentation amplifiers (LT1995) before being recorded by the analog input channels of the USB-6361. The sampling rate for both the reference signal generation and voltage/current measurements was 1 MHz. The electric field generation and impedance measurement instrumentation were combined into a single composite instrument system that permitted impedance spectra to be obtained before and/or after electric pulses were applied using the same electrode array. This arrangement assured that the electric field and the impedance measurement occurred in the same tissue region. This was achieved with a series of high-voltage reed relays (Cynergy3 DAT71210) that were used to rapidly connect/disconnect the high voltage pulse delivery instrument and the low voltage impedance measurement portion of the instrument. All devices were connected to a laptop computer and controlled via a custom NI Labview 2013 application.

4.2.2 Applicator and Pulsing Sequences

Pulsed electric fields were applied and impedance measurements were made using a direct contact multielectrode array (MEA) applicator, shown in Figure 3A, constructed with sixteen gold-plated 0.54 mm diameter electrodes (S-0-c-3.7-G, Interconnect Devices). Circular electrodes with rounded edges were chosen to reduce edge effects on electric field distribution associated with flat bottom electrodes. The electrodes were spaced 2.5 mm apart center to center creating a square geometry with a side length of 8.0 mm. This array created nine 2.5 mm by 2.5 mm square spaces between electrodes with each spacing referred to a sector of treated tissue. Each electrode in the

MEA applicator was spring loaded, which allowed the applicator tips to conform to match the topology of the animal skin and ensure electrodes remain in good contact with tissue.

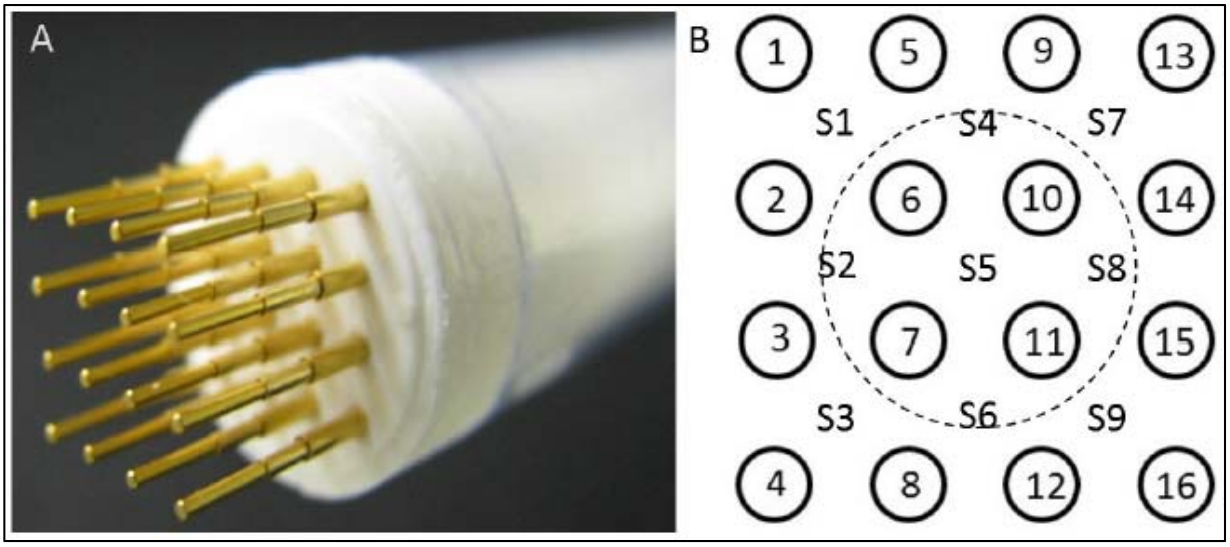

Figure 3: (A) Image of multielectrode array, (B) schematic of electrodes (1-16) with sector labels (S1-S9) numbering sets of 4 electrodes. Dashed line is an indictor of the relative size of an intradermally injected bolus of DNA around electrodes 6, 7, 10, and 11.

Treated animals received DC pulses 150 ms in duration with a 500 ms interval between pulses. Figure 1B shows a schematic of electrode placement on the skin of the animal and numerically identifies each electrode (1-16) and sector (S1-S9). Electric pulsing and post-pulse impedance measurements were conducted in each sector sequentially (S1 through S9). For example, the first pulsing sequence was executed in sector one (S1) with the following pattern: four pulses with electrodes 1 and 5 positive potential and electrodes 2 and 6 ground. Next, four pulses were applied with electrodes 1 and 2 positive and electrodes 5 and 6 ground. Immediately after pulsing S1, impedance measurements were made in this sector using the same horizontal then vertical sequence as was used for pulsing. Then, the system moved to Sector 2 (S2) to start the eight pulses in this sector followed by impedance measurements. Each subsequent sector, S3 - S9, was treated in the same manner. Impedance was measured for all sectors (horizontally and

vertically) immediately before the first voltage pulse in S1 to provide prepulsed values for comparison.

4.2.3 Impedance Measurement

As indicated above, the MEA applicator was used for both the application of electric fields for gene electrotransfer and for impedance measurements. The impedance spectroscope generated a 1 V amplitude continuous sine wave excitation signal containing linearly spaced frequencies from 10 Hz to 100 kHz with a total duration of 25 ms. This 25 ms duration signal began 50 ms after the eighth (last) pulse in each sector. Once the voltage and current waveforms were collected, the Fourier transform of both waveforms was calculated using the Fast Fourier Transform (FFT) algorithm with a rectangle window implemented in NI Labview 2013 expressed as frequency dependent complex numbers (FV (ω) and FI (ω) respectively). The magnitude of the impedance |Z (ω)| was calculated as the ratio of magnitudes of FV (ω) relative to FI (ω) while the phase of the impedance (φ_Z) was calculated as the phase of FV (ω) (φ_V) relative to FI (ω) (φ_I). Prior to any animal impedance spectroscopy measurements, the impedance spectrum of the MEA applicator electrodes were shorted and impedance measurements acquired for all sectors. The contribution to the instrumentation spectra for each sector was then subtracted from all subsequent spectra obtained from tissue.

4.2.4 Treatment

Mixed sex BALB/c mice (Charles Rivers) 8-10 weeks of age were used for this study. The right flank of each animal was shaved 48 hours prior to DNA delivery using standard animal clippers. Immediately before treatment, animals were anesthetized in an induction chamber that was continuously supplied with a 2.5% isoflurane/97.5% oxygen mixture (VetEquip). Once anesthetized, individual animals were removed from the induction chamber and kept anesthetized

under the same 2.5% isoflurane in oxygen mixture attached to a standard scavenged rodent nose cone. Animals were placed on a warming pad to maintain body temperature during delivery procedures.

Nine different animal groups were used to evaluate both the utility of impedance data for predicting the enhanced delivery of luciferase plasmid to murine skin and the impact the low voltage impedance measurement process had on delivery. One treatment group was an untreated control group, which received neither an applied electric field treatment nor a pDNA injection. A second group received pDNA only (DO). Five treatment received pDNA followed by electric pulses and had impedance measurements taken before, during and after electrical treatment (DEI). These 5 groups varied only in the applied electric fields, which were 50 V/cm, 100 V/cm, 150 V/cm, 200 V/cm and 250 V/cm. The remaining two groups received pDNA and electric pulses (DE) and did not have impedance measurements taken. These received electric fields of 150 V/cm and 200 V/cm. DNA was administered intradermally as a bolus injection by a 1ml syringe and 30-gauge needle (BD). Each 50 µl injection contained 100 µg of gWiz Luciferase pDNA (Aldevron) in phosphate buffered saline.

4.2.5 Biological Response, Quantification, and Statistical Analysis

Transfection was quantified from luminescence produced by the oxidation of luciferin by the expressed reporter gene luciferase. Each animal was anaesthetized, as described above, and given a 200 µL intraperitoneal injection of D-luciferin at 15 mg/mL (Gold Biotechnology Inc.). Animals remained anaesthetized for 15 minutes to allow luciferin to diffuse to the treatment site and provide enough time for luciferin luminescence to reach a maximum. Animals were then placed into a Xenogen IVIS 200 series imaging system (Caliper Life Sciences) and radiance (photons/s) was measured over a 10-second exposure time. This procedure was used to collect

luminescence data 2, 4, 7, 10, 14 and 30 days post treatment. Once all data was collected, the mean radiance and standard error of the means for each group at all time points were calculated. Comparison of radiance between groups to determine statistical significance was performed using a single-tailed Students t-test at a 95% significance level.

4.3 Results

4.3.1 Gene Expression

Figure 4 shows luciferase luminescence data for a representative animal for all DO (pDNA only) and DEI (pDNA, electric pulses, and impedance measurements) groups 14 days post treatment. Radiance of the control group that did not receive plasmid injections or exposure to electric fields was taken to determine background luminescence. As expected, pDNA expression increased with increasing field strength for fields below 250 V/cm in which the amount of expression was less than that of 100 V/cm but still greater than the DNA only animals. Measurable expression of luciferase in the DO group was expected, as there is typically some uptake of plasmid by cells at the injection site.

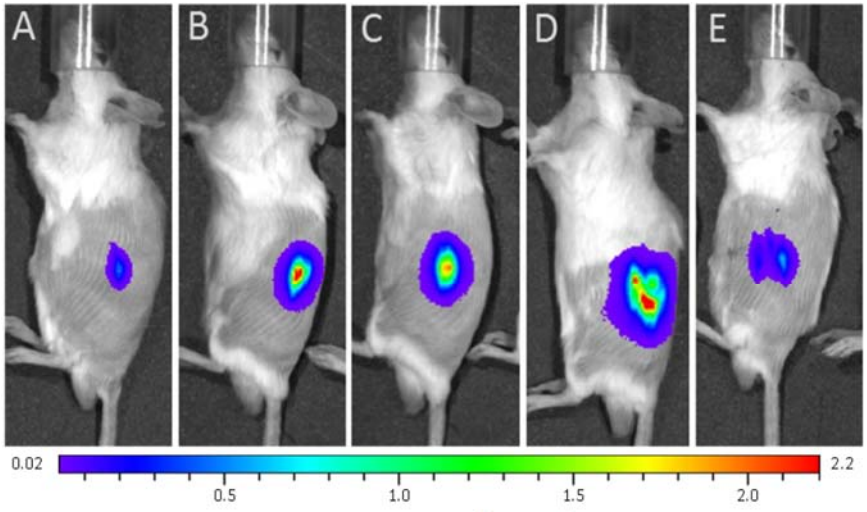

Figure 4: Xenogen images showing luciferase luminescence at day 14 for one representative animal from each group. (A) DO group, (B) DEI-100V/cm group, (C) DEI – 150 V/cm group, (D) DEI-200 V/cm group, and (E) DEI-250 V/cm group.

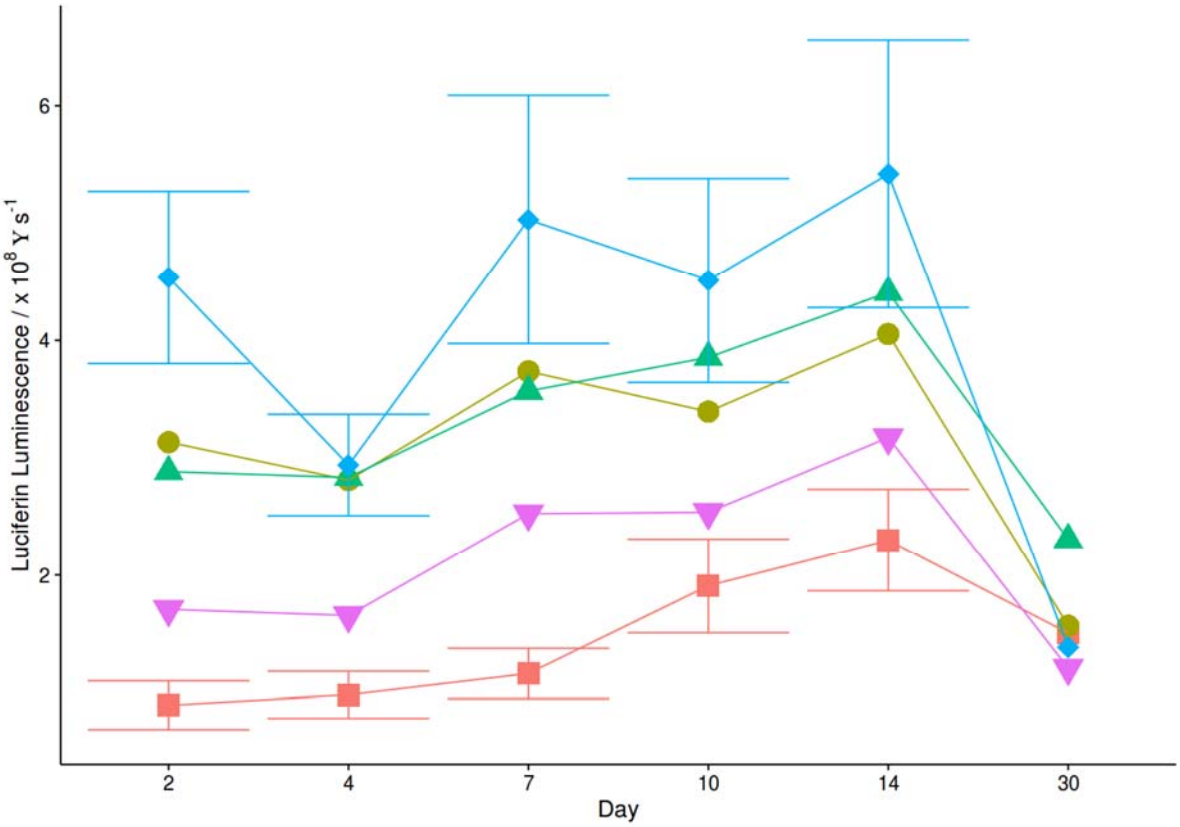

Figure 5: Mean luciferin luminescence for all groups at 2, 4, 7, 10, 14, and 30 days post treatment. Error bars show the standard error of the mean for DO group (■) and DEI groups exposed to 100 V/cm (●), 150 V/cm (▲), 200 V/cm (♦), and 250 V/cm (▼).

Figure 6 shows mean luciferase luminescence data for all DO and DEI groups 2, 4, 7, 10, 14, and 30 days post treatment. As expected, these levels remained constant throughout the duration of the experiment. Luciferase expression levels of the DO, DE (not shown), and DEI groups reached a maximum on day 14 and decayed to background levels by day 30. However, expression levels were near maximum at day 2 for all groups. Biological response (luciferase levels) generally increased as field strength increased, suggesting a greater degree of membrane permeabilization and/or DNA uptake as field strength was increased. A field of 200 V/cm produced the highest expression levels. However, skin treated with a 250 V/cm field (highest field) produced the lowest luciferase expression levels. These were above the levels of the DO group which may have indicated that a portion of cells were irreversibly permeabilized resulting

in cell death. Further evidence of this was based upon macroscopically observable damage to skin. The radiance levels of the DEI groups where highest at day two relative to the DO group. Animals exposed to 200 V/cm had the greatest increase in expression levels as indicated by the means and associated single-tail t-test p-value presented in Table 1. The greatest relative expression levels were produced with a field strength of 200 V/cm, which exhibited a 5-fold increase in mean radiance relative to DO group at day two and dropped to 2.36 fold by day fourteen. The relative

Table 1: Mean luciferin luminescence for all groups at 2, 4, 7, 10, 14, and 30 days post treatment.

	Mean Luciferin Luminenscence / $\times 10^8\ \Upsilon s^{-1}$					
Group	Day 2	Day 4	Day 7	Day 10	Day 14	Day 30
Injection only	0.89	0.98	1.16	1.91	2.3	1.5
DEI-100 V/cm	3.13^{***}	2.81^{**}	3.73^{**}	3.39^{*}	4.05	1.57
DEI-150 V/cm	2.88^{***}	2.83^{***}	3.57^{**}	3.85^{**}	4.41^{**}	2.31
DEI-200 V/cm	4.54^{***}	2.94^{***}	5.03^{**}	4.51^{**}	5.42^{*}	1.39
DEI-250 V/cm	1.71^{*}	1.65^{*}	2.53^{*}	2.54	3.17	1.21
DE-100 V/cm	2.17^{**}	2.44^{**}	2.69^{**}	3.26^{*}	3.58^{*}	1.78
DE-200 V/cm	3.29^{***}	3.37^{***}	3.03^{***}	3.3^{*}	3.91^{*}	1.37

n = 12 animals for all groups

* sig. at $p < 0.05$; ** sig. at $p < 0.01$; *** sig. at $p < 0.001$.

expression levels for 100 V/cm and 150 V/cm field strengths produced relative radiance levels on day two that were 3.13 and 2.9 fold higher than DO group respectively. The 200 V/cm group had statistically higher expression levels over the DO group for fourteen days post treatment (P = 0.0113). The 200 V/cm group demonstrates the highest level of DNA transfection as seen in both the magnitude and duration of radiance values relative to the DO group. Impedance pulses where shown to have no statistically significant effect (P values greater than 0.1 at all time points in a two-tailed t-test) on radiance levels. This was expected as the electric fields (0.25 V/cm) generated

from low voltage impedance measurements were not likely to contribute to DNA uptake. The non-intrusive, label-free nature of low voltage impedance pulses are ideal for real-time electrical characterization without interfering with the biological process(es) being studied.

4.3.2 Impedance Spectroscopy

A Nyquist plot for representative impedance measurements for several representative sectors (S1, S4, S5, and S9 of the 16 pin array, see Figure 6) both before and after electric fields (EF) for a single animal in the 200 V/cm group is shown in Figure 5. The before EF Nyquist curves shown in Figure 5A exhibit the same characteristic semicircular shape indicative of a parallel RC circuit model for cell membranes [72] and only differ by minor changes in tissue electrical properties and measurement noise. The after EF Nyquist curves shown in Figure 5B show a dramatic decrease in the magnitude and shape of impedance relative to skin that had not yet been treated with electric pulses. In addition, the after EF Nyquist curves shown in the Figure 5C are dramatically different between each sector with sector S1 showing the smallest change in impedance and sectors S5 and S9 showing the largest changes in impedance behavior. The Nyquist curves for sectors S1 (top-left sector, first to be receive EF) and S4 (top-middle sector) shown in Figure 4C also exhibit the semicircular shape predicted from the parallel RC circuit model (as seen in the before EF curves for all sectors) but with decreased resistance and capacitance. However, the Nyquist curves for sectors S5 (central sector) and S9 (bottom-right sector, last to receive EP) show a marked deviation from the semicircular shape of a parallel RC circuit.

Figure 6 shows the magnitude of impedance as a function of frequency for representative impedance measurements for all sectors both before and after EF for a representative animal in the 200 V/cm group. Similar to the Nyquist plots in Figure 4, the before EF curves all follow the same shape. However, the variations in tissue impedance are more apparent such that the magnitude of

impedance for sector S1 is higher than that of all other sectors for all frequencies while the impedance of all other sectors are relatively close to each other for the before EF curves. Figure 6 shows the after EF magnitude of impedance for all sectors with sectors S1, S4, and S7 having similar shape while all other sectors follow a different shape. A probable explanation for this is that effect previous electric fields generated in earlier sectors have on initiating the membrane permeabilization mechanism in cells in adjacent sectors. This may explain why sector S5 has the lowest impedance magnitude for all frequencies as sector S5 experiences the highest number of previous electric field exposures.

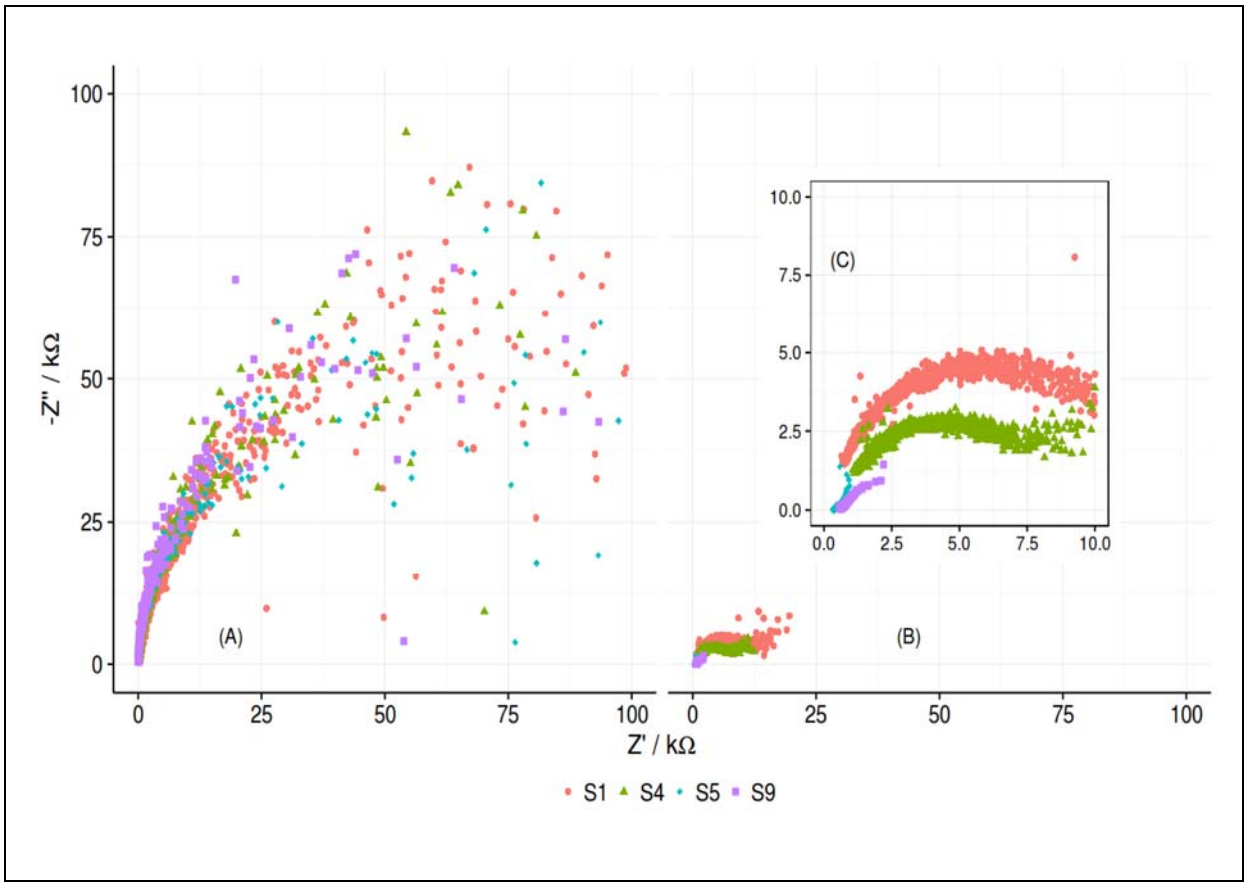

Figure 6: Nyquist plot for a single representative animal in the 200 V/cm group (A) before and (B and C) after electric field for sectors S1, S4, S5, and S9.

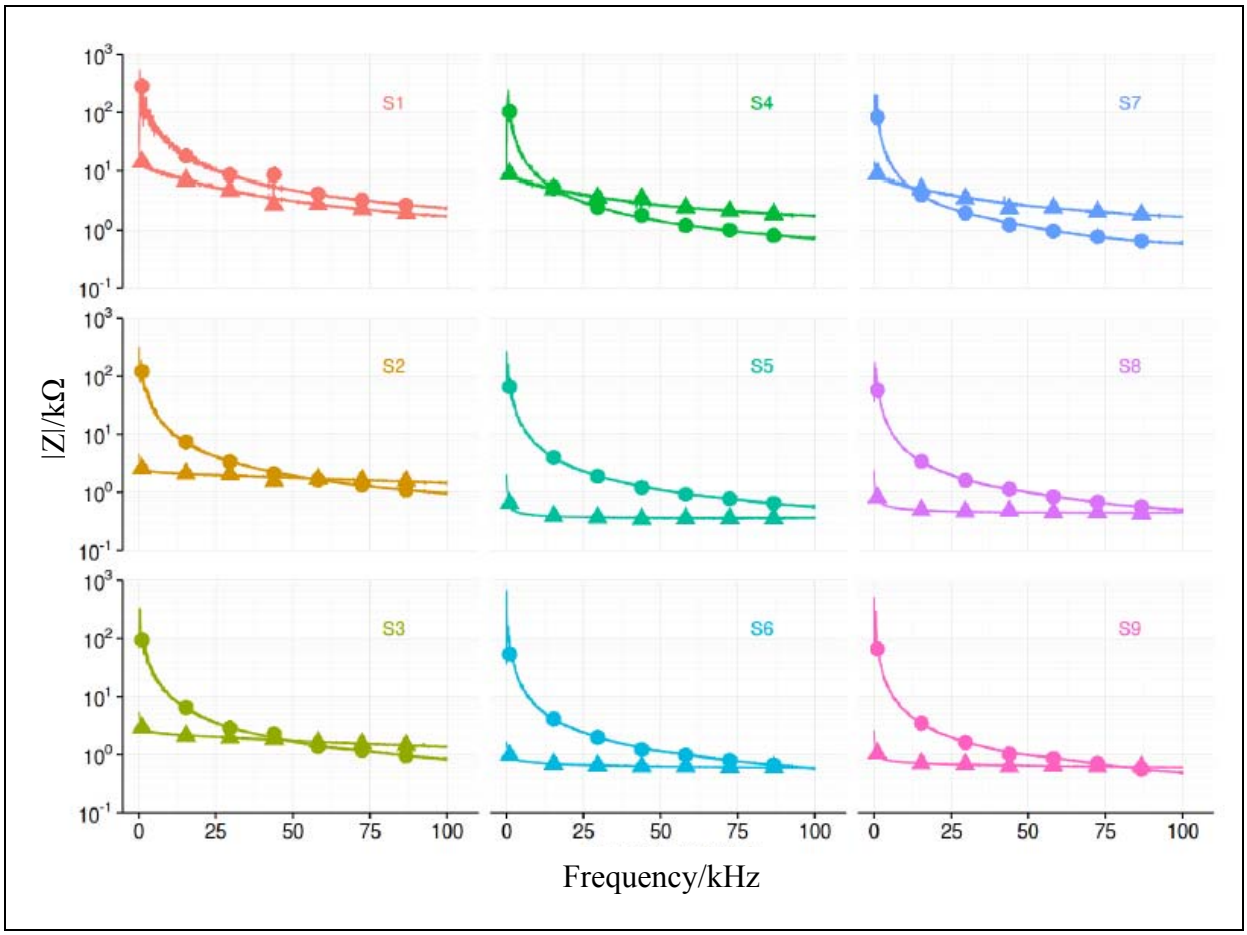

Figure 7: Impedance magnitude versus frequency before (circles) and after (triangles) electric pulses. Sectors 1-9 from a representative animal exposed to 200 V/cm pulses in the DEI group.

Comparing changes in impedance for each sector is complicated by the spatial differences in tissue impedance as seen in the before EF Nyquist curves in Figure 5A and impedance magnitude curves in Figure 6. To compare changes in impedance in different sectors before and after EF, the mean ratio of impedance magnitude after EF relative to before EF for DEI groups with field strengths of (A) 100 V/cm, (B) 150 V/cm, (C) 200 V/cm, and (D) 250 V/cm is shown in Figure 7. For all field strengths shown in Figure 7, the mean ratio of impedance after EF relative to before EF is well below 1.0 for many frequencies. The range of frequencies corresponding to mean impedance magnitude ratios less than or equal to 1.0 increased with field strength. This mean ratio being below 1.0 can be easily explained by impedance being dominated by resistance

at low frequencies with the after EF resistance expected to be lower than that before EF due to new current pathways through cell membranes [36, 38]. However, the mean ratio of impedance magnitude after EF relative to before EF is greater than 1.0 at high frequencies in all sectors for both 100 V/cm and 150 V/cm and several sectors in 200 V/cm and 250 V/cm. Since impedance is inversely proportional to capacitance, a mean ratio of greater than 1.0 at high frequencies may be due to the capacitance after EF being lower than the capacitance before EF. The shape and value of the mean ratio of impedance magnitude after EF relative to before EF shown in Figure 7 is extremely different both qualitatively and quantitatively. First, the 100 V/cm samples (Figure 7A) had a much smaller range of frequencies in which the mean ratio was less than 1.0 than the 250 V/cm group (Figure 6D). Second, the general shapes of the 100 V/cm curves (Figure 6A) for each sector were overtly different from those of the 250 V/cm 300 curves (Figure 6D) with the exception of sectors S4 and S7. These differences may be explained by the presence of cell death in the 250 V/cm group as indicated by the reduced luciferase expression levels shown in Figures 3 and 4 as well as observed tissue damage in these animals. However, the mean ratio curves for sectors S4 and S7 for the 250 V/cm group were similar in shape and value to those at the lower field strengths.

Figure 7B shows the mean ratio of impedance magnitude for all frequencies after EF relative to before EF for all animals in the 150 V/cm group while Figure 7C shows analogous data for the animals treated with 200 V/cm. The 15 shape of the mean ratio of impedance magnitude after EF relative to before EF is similar for the 150 V/cm and 200 V/cm groups while the values for the 200 V/cm group are generally less than those of the 150 V/cm group. In addition, the range of frequencies in which the mean ratio is less than 1.0 is greater for the 200 V/cm group relative to the 150 V/cm group. These differences may be explained by increased luciferase expression

levels in the 200 V/cm group relative to the 150 V/cm group indicating more successful DNA uptake as shown in Figures 3 and 4. Differences in the shape and the range of frequencies corresponding to a mean impedance magnitude ratio less than 1.0 between sectors may be due to unequal exposure of sectors to electric fields, a result of sector spacing, pulse timing, and/or pulse sequence. A consistent pattern in these values began to emerge as field strength increased which implied a possible influence of electrode geometry and electrode reuse on the electric field conditions each sector experienced.

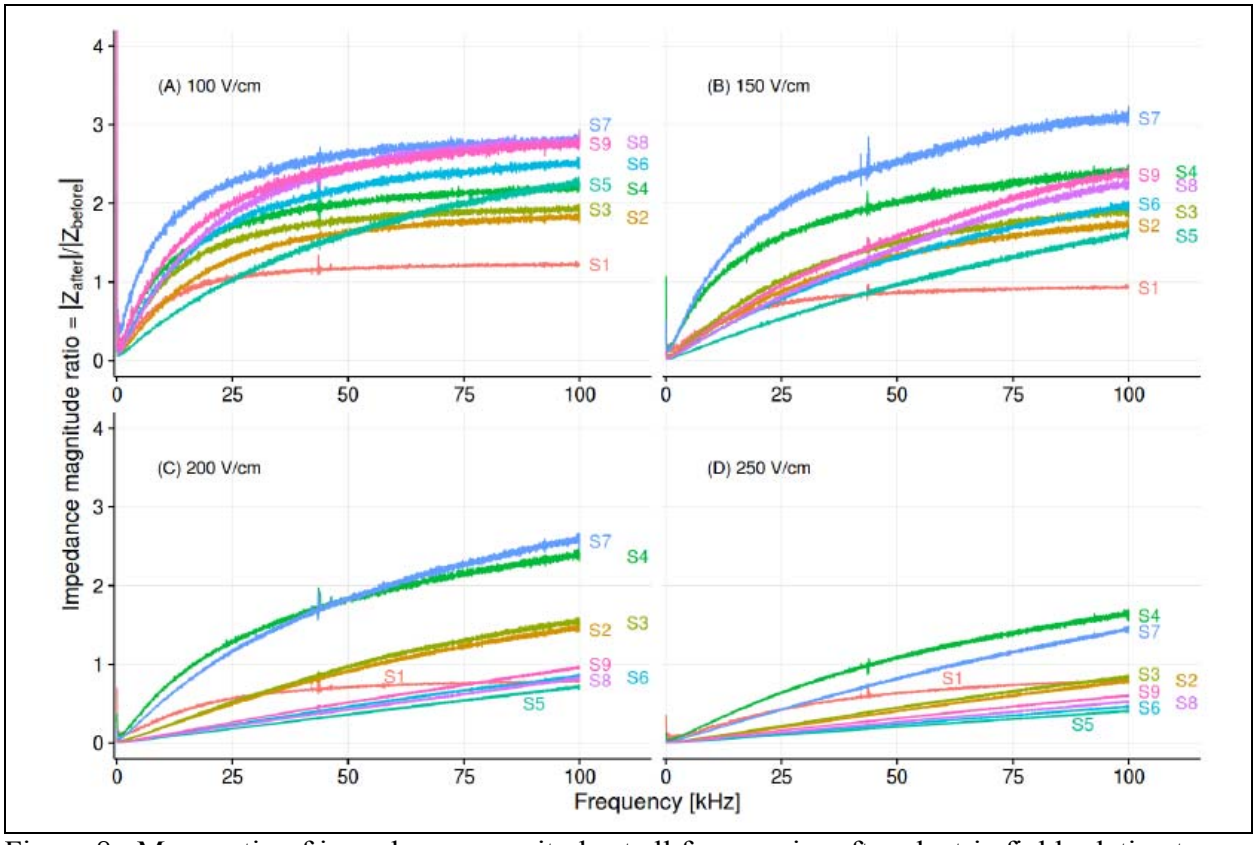

Figure 8: Mean ratio of impedance magnitude at all frequencies after electric field relative to before electric field pulses. DEI groups with field strengths of (A) 100 V/cm, (B) 150 V/cm, (C) 200 V/cm, and (D) 250 V/cm, (N=12).

The mean ratio of impedance magnitude after electric field (EF) relative to before EF data presented in Figure 7 cannot be directly correlated with the luciferase luminescence data presented in Figures 3 and 4 as the biological response of each sector cannot be extracted from the overall

biological response due to the spatial resolution limitations of the Xenogen measurement. However, the mean overall ratio of impedance magnitude for all nine sectors and frequencies for all DEI groups (twelve animals per group) presented in Figure 8 allow for direct comparison to the biological response data in Figures 3 and 4. Both sets of data are measures of overall / average response throughout the entire regions of tissue affected by the gene electrotransfer protocols tested. Similar to the results discussed in Figure 7, Figure 8 shows both the mean ratio of impedance magnitude and number of frequencies in which the ratio less than 1.0 increases with increasing field strength. Although the mechanism of DNA uptake during gene electrotransfer and its effect on the impedance spectra of tissue after experiencing an electric field is not well understood, the mean overall ratio of impedance magnitude presented in Figure 8 can be used as a template to generate a desired level of gene delivery when combined with the gene expression data presented in Figures 3 and 4. For example, since the 200 V/cm group demonstrated the maximum level of gene expression in this study, the 200 V/cm mean overall impedance magnitude ratio 16 curve presented in Figure 8 may be used as a target to generate optimum gene expression in a four by four pulsing gene electrotransfer protocol.

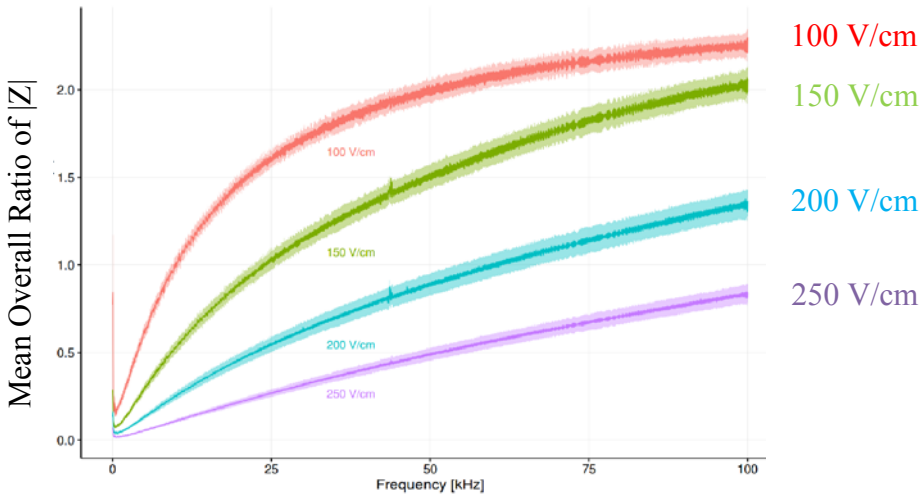

Figure 9: Mean overall ratio of impedance magnitude over all nine sectors at all frequencies after electric field relative to before electric field for all DEI groups (N=12).

4.4 Conclusion

The current state-of-the-art for optimizing in vivo gene electrotransfer through membrane permeabilization in different tissues has historically employed a trial and error approach. The goal of this study was to determine whether changes in tissue impedance correlate with biological responses and thus indicate successful membrane permeabilization and subsequent gene transfer. Experimental results showed a strong relationship between the change in impedance magnitude with both field strength and biological response indicating tissue impedance is an excellent indicator of membrane permeabilization and subsequent transfection. The effect of low voltage impedance measurements before and after the application of an electric field were also evaluated to identify any significant contribution to membrane permeabilization. Considering a 200 V/cm field strength was required to produce peak expression, it was not expected a 0.25 V/cm impedance interrogation field would significantly increase or improve DNA uptake. Experimental results showed this to be true as there was no statistically significant difference in the biological response between DE and DEI groups of the same field strength. Results also revealed differences in the mean ratio of after electric field relative to before electric field impedance magnitudes with respect to frequency between sectors. This may be due to an unequal stimulation of sectors by electric fields from adjacent sectors and the timing in which this occurs. The distribution of impedance magnitude after EF relative to before EF versus frequency revealed interesting differences between impedance changes in different sectors underscoring the significance of pulse timing and how this relates to membrane permeabilization kinetics. A deeper examination of pore kinetics may provide insight into the pulse timing and sequence necessary for producing controlled DNA uptake in all sectors.

This research correlated identified tissue response impedance to membrane permeabilization via gene expression. Future work will identify changes in dynamic electrical parameters to be used in optimizing gene electrotransfer algorithms in an attempt to target and maintain the distribution of the ratio of impedance magnitudes after EF relative to before EF versus frequency within a desired range similar to the 200 V/cm group shown in Figure 6C. Parameters such as field strength, pulse number, frequency, and duration will be considered. This may obviate protracted trial and error methods and allow for the desired level of gene delivery obtained per application. Future efforts will also attempt to identify the impedance change that correlates with irreversible permeabilization and subsequent cell death.

CHAPTER 5: SPECIFIC AIM II: IMPEDANCE CONTROLLED GENE ELECTROTRANSFER[2]

5.1 Introduction

The basis for integrating impedance measurements into GET stems from the need to measure and control the response of cells to EF pulses so that targeted delivery can be achieved consistently and maximally. In theory, as additional pathways for current increase in a conducting volume, resistance to current flow through this volume decreases. When considering a volume of tissue treated with EF pulses, if impedance is reduced after exposure to EFs and no significant change is assumed to have occurred with respect to the conductivity of the fluids comprising the matrix or extracellular compartments, new conductive pathways must be present in plasma membranes through cells to account for the reduction in impedance. Furthermore, the dry surface electrodes in non-galvanic contact with tissue used in this study prevented electrochemical reactions at the electrodes and subsequent generation of ions that would have affected conductivity of extracellular fluid.

It has been hypothesized that pulsed electric fields induce rearrangement of cell membrane phospholipids after dielectric breakdown creating porous discontinuities in the membrane that function as new current pathways through cells. These pathways account for the reduced impedance seen in tissue after exposure to EF pulses. This is necessary because tissue-to-tissue differences in chemical microenvironment and tissue architecture confer an anisotropic quality to

[2] Portions of this chapter will be submitted for publication in *Bioelectrochemistry*.

tissue causing it to respond uniquely to EF pulses. As a result, a unique number of pulses is required to generate target impedance and corresponding permeability in each treated region of tissue. Fixed pulse number protocols do not account for differences in tissue architecture and thus create a nonhomogeneous profile of permeability across treatment regions. Additionally, open loop fixed pulse protocols do not provide an optimum number of pulses nor do they measure tissues response to pulsed electric fields. Impedance measurements present an ideal method for addressing the shortcomings of open loop methods due to its label free, rapid, low voltage nature, which have previously been shown not to affect delivery [56]. Ultimately, this may enhance electric field mediated gene delivery and provide for more controlled methods by utilizing closed loop feedback control to drive EF pulsing instead of empirically derived open loop protocols. It is also possible that this method may be universally applied to all tissues significantly contributing to more consistent and controlled gene delivery in any electrode accessible tissue. It was expected that reductions in membrane permeability could indicate when the membrane permeability necessary for pDNA uptake are present. It is still unknown whether pDNA uptake occurs directly via electrodiffusion through transient pores created when membranes become hyperpolarized during EF exposure or whether EF pulses stimulate or upregulate a biological response similar to endocytosis that mediates transfection as recently purported [87]. Regardless, increases in membrane permeability would occur during both proposed phenomena during which additional conductive pathways would arise.

5.2 Methods

5.2.1 Hardware

Instrumentation hardware (Figure 1) for generating electric fields was comprised of thirty-two (32) isolated solid state relays contained within a National Instruments (NI) SCXI-1163R

module housed in a NI SCXI-1000 chassis. A NI SCXI-1600 USB Data Acquisition and Control Module (200 kS/s) was used to control the isolated solid-state relay module. Half of the relays were connected to the positive terminal while the other half sixteen relays were grounded to the high voltage power supply (Glassman High Voltage Inc., PS/EW02R300-115). Waveforms for analyzing impedance were generated from a National Instruments (NI) USB-6361 multifunction input/output card that generated a multi-frequency sine analog voltage reference signal buffered by a unity gain high-bandwidth amplifier (Linear Technology LT1358) rated to drive capacitive loads. The differential voltage across and current flowing through the tissue was buffered (LT1359) and measured by a pair of instrumentation amplifiers (LT1995) before being recorded by the analog input channels of the USB-6361. The reference signal generation and voltage/current measurements were sampled at a frequency of 1 MHz. Tethering the high voltage field generator and the impedance analyzer into a single composite device allowed for both EF pulses and impedance measurement execution with the same multielectrode array. This was critical as it minimized error in impedance measurement associated with movement of or a break in electrode contact with skin. The relays used to disconnect and connect the high voltage pulse delivery system and the low voltage impedance spectroscope allowed for switching times as fast as 50 ms after each high voltage pulse. A series of high-voltage reed relays (Cynergy3 DAT71210) were used to accomplish switching. A custom NI Labview 2013 application was installed and used on a laptop to control all devices.

5.2.2 Applicator and Pulsing Sequence

Each GET pulse, impedance pulse, and impedance measurement was performed with a multielectrode array (MEA) applicator (Figure 10A and B) in direct static contact with the treatment region for the duration of the GET protocol. The electrode array was constructed with

sixteen gold-plated, flat bottom electrodes 0.54 mm in diameter (100039-025-958, Interconnect Devices). The 4x4 square array had an 8.0 mm side length and 2.5 mm center-to-center spacing between electrodes. Electrodes were 8.75 mm long and contained depressible spring loaded tips to ensure good contact with tissue regardless of topology. With depressible to allow tips to maintain firm contact with tissue surface. The square geometry and equal spacing between electrodes created nine 2.5 mm by 2.5 mm square spaces referred to as sectors. Figure 9B shows a treatment region schematic consisting of the MEA superimposed over an intradermal pDNA injection (dashed circle), numeric labeling used to identify individual electrodes (1-16), and treatment sectors (S1-S9). Two pulsing regimes were used to evaluate the utility of tissue impedance changes to optimize gene electrotransfer efficiency: a fixed pulse number regime and an impedance guided dynamic pulsing regime.

Figure 10: Image of multielectrode array(left) and (center), schematic of electrodes (1-16) with sector labels (S1-S9) (right).

The first pulsing regime used a fixed number of 8 pulses per treatment sector that progressed sequentially from S1 to S9. These treatment groups received pDNA injections, electric pulses, and impedance measurements (DEI groups) before EF pulsing began and after pulsing in each sector. DEI treatments began with sequential impedance measurements, as described above, in all sectors to establish baseline skin impedance. Following initial impedance measurements,

EF pulsing began in sector 1 with the following example pattern: two 150 ms DC pulses from each positive potential electrode 1 and 5 to negative potential electrode 2 and 6 for a total of 4 vertical pulses followed by two 150 ms DC pulses from each positive electrode 1 and 2 to negative potential electrode 5 and 6 for a total of 4 horizontal pulses. Impedance measurements were made using the same pattern after vertical EF pulsing and after horizontal EF pulsing finished for a total of 8 1 V AC pulses. After the last horizontal impedance in S1, EF pulsing began in S2 followed by the same impedance pulsing pattern as above. This pattern continued from S3 - S9 in the same manner. Prepulsed baseline impedance was measured horizontally and vertically in all sectors, using the pattern above before pulsing began in S1. This pulsing regime was referred to as 4x4 pulsing where each sector received a total of 8 pulses, four horizontal and four vertical.

The second pulsing regime (impedance guided pulsing) did not use a fixed number of pulses. EF pulsing continued in each sector until a predetermined impedance drop was attained relative to baseline impedance. Interpulse impedance measurements were taken to evaluate response of tissue to EF pulses. To assess precision and accuracy of hardware and the affect closed loop control had on DNA delivery, two relative impedance change values were evaluated: 80% and 95%. Pulsing advanced sequentially through treatment sectors after a predetermined change (80% or 95%) in each sector impedance was attained. The duration and interval of a single pulse was identical in both DEI and DEIF pulsing regimes however the number of pulses and time between advancement to each sector was different in DEIF groups as pulse number was guided by change in tissue impedance. Because the pulse number was unique in all feedback groups, the total time required for a complete protocol in a single animal varied as well as the times for corresponding sectors between animals. A single EF pulse was generated by a DC power supply with a duration of 150 ms and interval of 500 ms between pulses.

5.2.3 Treatment

In this study white, mixed sex BALB/c mice (Charles Rivers) 8-10 weeks of age were used. Forty-eight hours before treatment the right flank of each animal was shaved. Animals were shaved at this time point to allow healing of any minor abrasions that occasionally occur from clipping that might affect baseline impedance levels. Immediately prior to treatment, animals were placed in an induction chamber under continuously supply of 2.5% isoflurane/97.5% oxygen mixture (Caliper Life Sciences). Once completely anesthetized, animals were removed and attached to a standard scavenged nose cone under the same 2.5% isoflurane/97.5% oxygen mixture resting on a temperature controlled warming pad where they remained throughout pDNA injection the remainder of treatment.

Eleven different treatment groups were established to compare the efficacy of different field strengths with either fixed or dynamic EF pulsing protocols to enhance the delivery of luciferase encoding plasmid. A control group received neither a pDNA injection nor exposure to applied EF pulses. To evaluate baseline uptake of pDNA that occurs without EF pulse exposure a second treatment group received an intradermal pDNA injection only (DO). Nine treatment groups received intradermal pDNA injections and one of three different EF pulsing regimes in combination with one of three different field strengths. Of these nine groups, three treatment groups received a pDNA injection followed by exposure to a fixed number of pulsed electric fields of either 100 V/cm, 150 V/cm, or 200 V/cm with impedance measurements taken before, during, and after pulses (DEI). The six remaining groups received an intradermal pDNA injection followed by impedance controlled pulsation at a field strength of 100 V/cm, 150 V/cm, or 200 V/cm that continued until treatment sector impedance dropped by either 80% or 95% (DEIF). In DEIF groups, impedance measurements were taken before pulses to establish a baseline impedance

and after pulses to measure the change in impedance. pDNA was administered as an intradermal bolus injection with a 1 cc syringe and a 30-gauge needle (BD). Each injection contained 100 μg of gWiz Luciferase pDNA (Aldevron) in phosphate buffered saline, in an injection volume of 50 μl.

5.2.4 Biological Response, Quantification, and Statistical Analysis

Successful transfection in treatment groups resulted in expression of luciferase reporter gene. All treatment groups exhibited reductions in impedance after pulsed electric fields were applied, a surrogate for increased membrane permeability. Generally, radiance increased as impedance decreased. The amount of transfection present in each animal was determined from the detection of photons emitted by the luciferase-catalyzed reduction of injected luciferin substrate. Luciferase enzyme was the protein product of the delivered reporter gene. As the number of transfected cells or the number of reporter gene constructs delivered to a single cell increased, the concentration of luciferase increased. To quantify radiance each animal was anaesthetized, as described above. Once anaesthetized each animal received a 200 μl intraperitoneal injection of D-Luciferin at 15 mg/mL (Gold Biotechnology Inc.). After injection, animals were kept anaesthetized, on a warming pad in a Xenogen IVIS 200 series imaging system (Caliper Life Sciences) for 15 minutes to allow transport of luciferin to the treatment site and for luminescence to reach a maximum. At fifteen minutes, radiance (photon/s) was measured over a 10-second exposure time. This procedure was used to collect luciferin radiance 2, 4, 7, 10, and 14 days post treatment. Upon collection of data at all time points the mean radiance and standard error of the means for each group was calculated. Statistical significance between groups was determined using a single-tailed Students t-test at a 95% significance level.

5.3 Results

5.3.1 Gene Expression

Figure 11 shows UV/VIS images of luciferin luminescence (photons/s) in a representative animal from each DEI, DEIF, and DO group 10 days post treatment. Observable differences in the amount of delivery and area of successfully treated tissue between treatment groups were apparent. Both luciferin luminescence and area of transfected tissue generally increased with electric field strength and stop impedance in all groups. Image A in Figure 11, shows an animal that received a DNA injection only where luciferase expression was minimal as expected [88]. All DEIF groups (images C, D, F, G, I, and J) under feedback control showed marked increases in transgene expression above fixed pulse DEI (images B, E, and H) and the DO group. Impedance based feedback groups not only showed the same dose response to field strength but also showed luciferin luminescence increased as targeted impedance drop increased. Measurable expression of luciferase in the DO group was expected, as there is typically some uptake of plasmid by cells at the injection site more than likely associated with the shearing of cell membranes with the hypodermic needle during injection. Radiance of control group animals that did not receive DNA injections or exposure to EF fields was also measured to establish baseline luminescence of healthy untreated tissue and found to be relatively negligible (not shown).

Figure 12 shows mean luciferin luminescence data (photons/s) for all DO, DEI, and DEIF groups 2, 4, 7, 10, and 14 days post treatment. Luciferin luminescence reached a maximum in all groups either by day 7 or 10 and began to approach background levels by day 14. Luminescence levels for DO and DEI groups remained relatively level throughout the duration of the experiment starting at day 2 compared to DEIF groups. The DO group exhibited lowest luciferin luminescence throughout the entire experiment. In contrast to DO and DEI (non-feedback groups), all DEIF

groups showed a steep increase in luminescence beginning at day 4 that was not present in DEI and DO groups. As expected, mean radiance and luciferase expression levels generally increased with field strength indicating an electric field mediated effect on delivery associated with field strength alone that contributed to increased permeability. However, DEIF groups showed a marked increase in expression over DEI and DO groups when targeted relative impedance drops were used to guide EF pulse number. This confirmed impedance was an acceptable surrogate for permeability. Therefore, controlling GET pulse number to target relative impedance reductions also allowed for the controlled targeting of membrane permeability leading to enhanced DNA delivery.

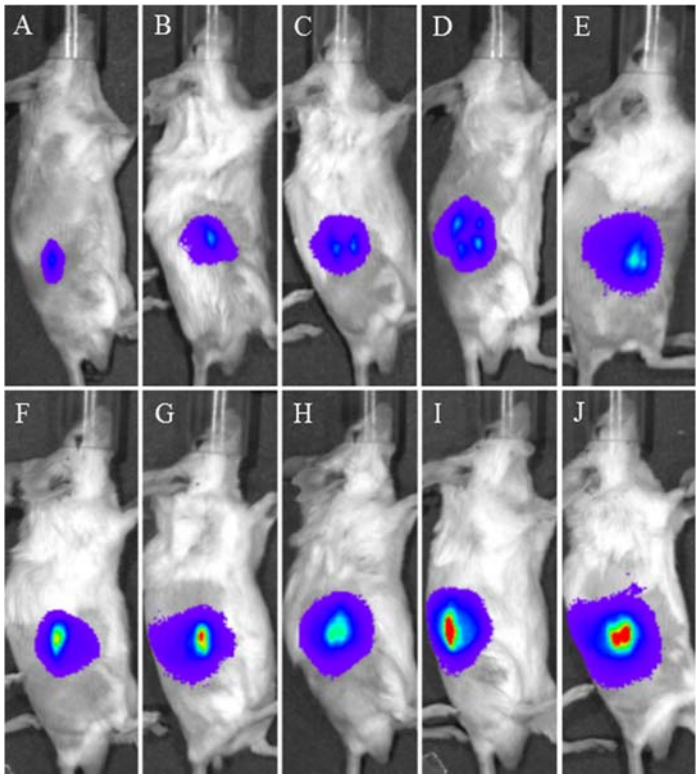

Figure 11: Xenogen images of representative animals. (A) DO group (B) 100 V/cm DEI group (C) 150 V/cm DEI group (D) 200 V/cm DEI group (E) 100 V/cm DEIF group at 95% (F) 150 V/cm DEIF group at 95% (G) 150 V/cm DEIF group at 80% (H) 100 V/cm DEIF group at 80% (I) 200 V/cm group at 80% (J) 200 V/cm DEIF group at 95%.

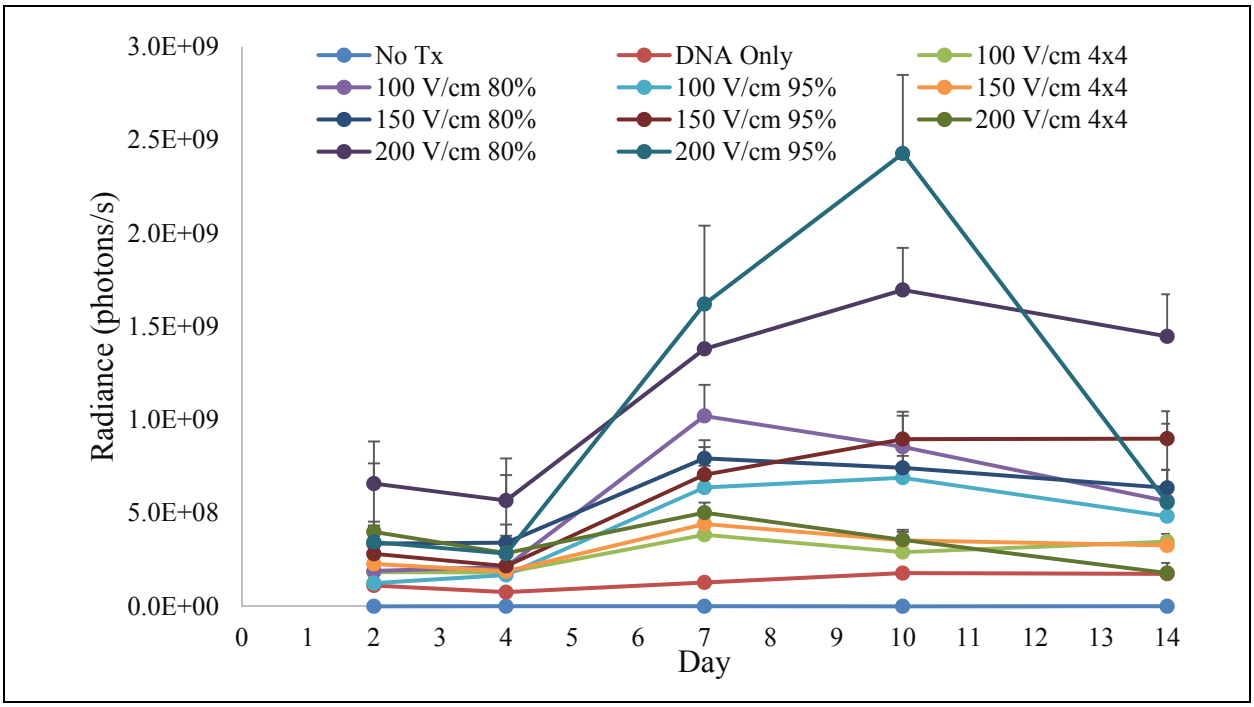

Figure 12: Mean luciferin luminescence for all groups 2, 4, 7, 10, and 14 post treatment.

Table 2: Mean luciferin luminescence for all groups at 2, 4, 7, 10, 14, and 30 days post treatment.

	Mean Luciferase [x 10^8 photon/sec]				
Group	Day 2	Day 4	Day 7	Day 10	Day 14
DEI-100 V/cm	1.83*	1.81*	3.84**	2.9	3.47*
DEI-150 V/cm	2.3	1.88*	4.41**	3.82*	3.3
DEI-200 V/cm	4.0	2.44*	5.02*	3.57*	1.8
DEIF-100 V/cm at 80%	1.89*	2.12*	10.21**	8.55*	5.6
DEIF-100 V/cm at 95%	1.2	1.68*	6.37**	6.9*	4.83*
DEIF-150 V/cm at 80%	3.36*	3.41*	7.93**	7.42*	6.35*
DEIF-150 V/cm at 95%	2.82**	2.16**	7.06**	8.96**	8.98**
DEIF-200 V/cm at 80%	6.58**	5.67**	13.8**	20.62**	14.47*
DEIF-200 V/cm at 95%	3.45**	2.82**	16.2**	24.28**	5.58*

* sig. at $p<0.05$; **sig. at $p < 0.01$ compared to injection alone.

Table 2 shows the one tailed student t-test p values ($\alpha = 0.05$) comparing DEI and DEIF group mean radiance to the DO group. At day 7 all DEI and DEIF groups exhibited statistically higher mean radiance relative to DO group. Peak mean radiance relative to the DO group was highest for all DEI and DEIF groups by day 7 or 10. Figure 12 shows the greatest relative

expression levels was produced with 200 V/cm field strength pulses in DEIF groups targeting 80% and 95% stop impedances which exhibited statistically higher 11.6 (p value = 0.005) and 13.7 (p value = 0.006) fold increases in mean radiance relative to DO group at day 10. Radiance in these DEIF groups remained statistically higher than DO group for fourteen days post treatment. Comparison of 200 V/cm DEIF groups targeting 80% and 95% impedance reduction with the non-feedback 200 V/cm DEI group showed statistically greater radiances in DEIF groups that was 5.2 and 6.8 fold higher respectively at day 10. The statistically enhanced transfection present in the 200 V/cm DEIF groups suggests impedance may accurately quantify the relative changes in membrane permeability associated with electric pulse stimulation. In theory, a reduction in tissue impedance indicates the presence of new conductive pathways in tissue. Within the epidermis and dermis cell membranes act as the primary barriers to current flow, therefore decreases in impedance may indicate when new current pathways through these barriers are present. These results support that forcing reductions in membrane impedance with EF pulses as a method for ensuring maximum DNA transfection occurs consistently during GET. Although the 200 V/cm DEIF 95% stop impedance group showed a higher mean radiance than the 200 V/cm DEIF 80% stop impedance group, they were not statistically different. Considering the magnitude of the inherent variability in the biological response data, it was expected that increasing sample size might provide for a statistical difference in delivery between the DEIF groups targeting 80% and 95% reductions in tissue impedance. Increases in radiance were seen in lower field strength feedback groups relative to the DO group, although to a lesser degree. The 100 V/cm DEI and DEIF groups targeting 8%0 and 95% impedance reduction exhibited mean radiances 3.0, 8.0, and 5.0 fold higher relative to the DO group respectively at day 10. The 150 V/cm DEI and DEIF groups targeting 80% and 95% impedance reduction exhibited greater mean radiances that were

3.5, 6.2, and 5.6 fold higher relative to the DO group respectively. Again, in these lower field strength groups, mean radiance of 80% and 95% DEIF groups of the same field strength were not statistically different.

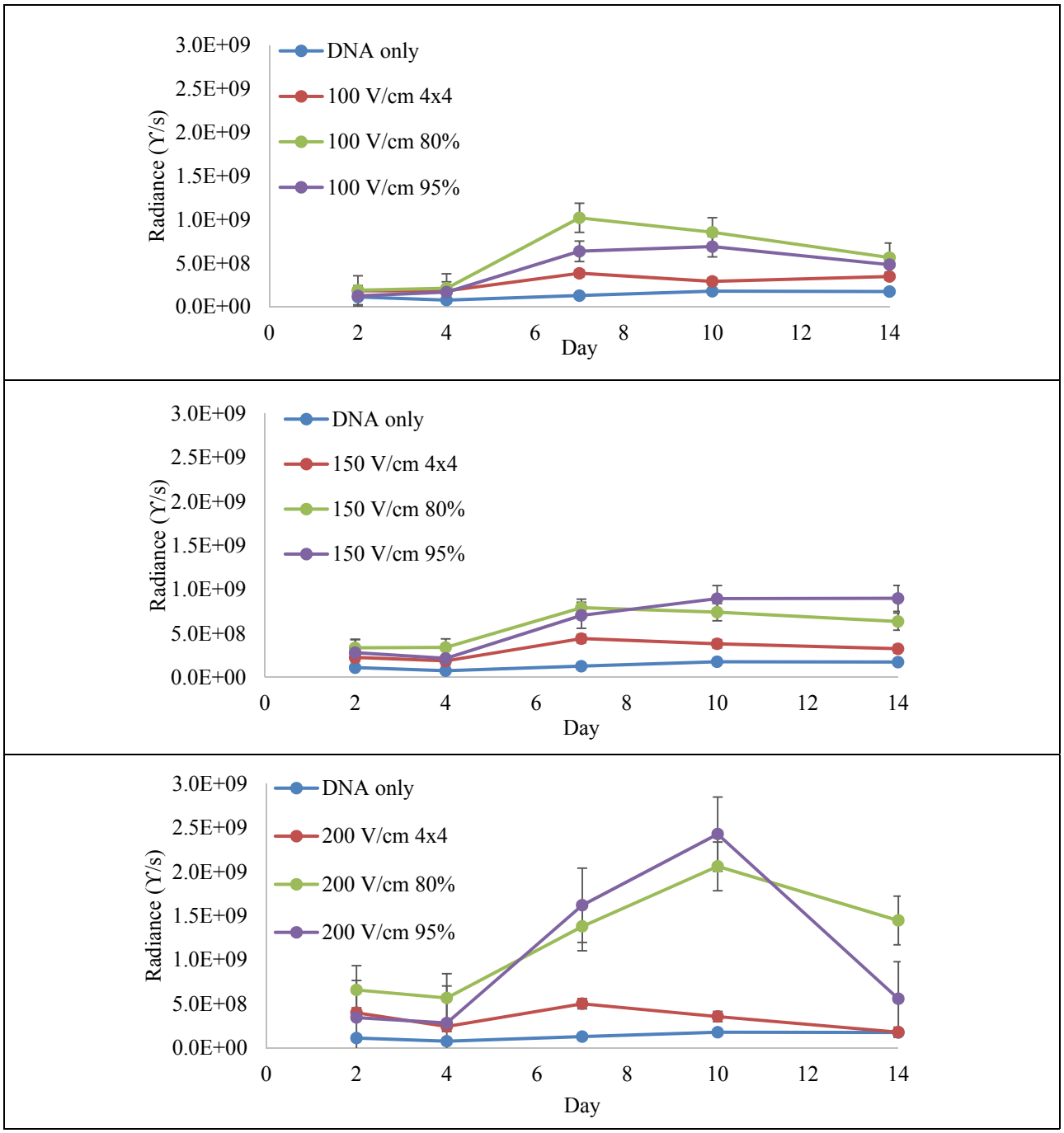

Figure 13: Mean luciferin luminescence at days 2, 4, 7, 10, and 14 days post treatment for DEI and DEIF groups. (A) 100 V/cm (B) 150 V/cm and (C) 200 V/cm.

To assess the effect of permeability associated with 80% and 95% stop impedances on delivery, the contribution of field strength to delivery must be held constant. Figure 13 shows radiance versus time for DEI and DEIF groups that received EF pulses of the same field strength. All DEIF groups exhibited statistically higher mean radiance when compared to DEI groups of the same field strength where $\alpha = 0.05$. Mean radiance of 100 V/cm DEIF groups targeting 80% and 95% stop impedances (Figure 13A) were 3.0 (p value = 0.041) and 2.4 (p value = 0.025) fold higher relative to 100 V/cm DEI group respectively at day 10. Mean radiance of 150 V/cm DEIF groups targeting 80% and 95% stop impedances (Figure 13B) were 2.1 (p value = 0.043) and 2.5 (p value = 0.024) fold higher relative to 150 V/cm DEI group respectively at day 10. Mean radiance of 200 V/cm DEIF groups targeting 80% and 95% stop impedances (Figure 13C) were 5.2 (p value = 0.012) and 6.8 (p value = 0.011) fold higher relative to 200 V/cm DEI group respectively at day 10. However, there was no statistical difference in mean radiance between any 80% and 95% feedback groups of the same field strength. Considering mean radiance in all 95% DEIF groups was higher than 80% DEIF groups of the same field strength, it is expected further testing with larger sample sizes may reveal there is a statistical difference between these groups. These increases in mean radiance between feedback groups and non-feedback groups of the same field strength underscore the potential utility of impedance spectroscopy to enhance gene delivery during GET. The lower field strength, 100 V/cm and 150 V/cm, 80% and 95% feedback groups on average produced respective radiances 2.4 and 2.3 fold higher than the non-feedback group of the same field strength. The 200 V/cm feedback groups on average produced radiances 6.3 fold higher than the non-feedback 200 V/cm group. This suggests the membrane permeability resulting from EF stimulation was dependent on both field strength and relative change in impedance. Targeting a higher relative impedance reduction near 99% may provide for statistically enhanced

delivery above the 80% DEIF groups. The significantly higher delivery in DEIF groups indicates the utility of interpulse impedance measurements to evaluate cell response to EF pulses. This information is ideal for use in optimizing EF pulse number to achieve the membrane permeability necessary for ensuring DNA uptake upon every application of a GET protocol.

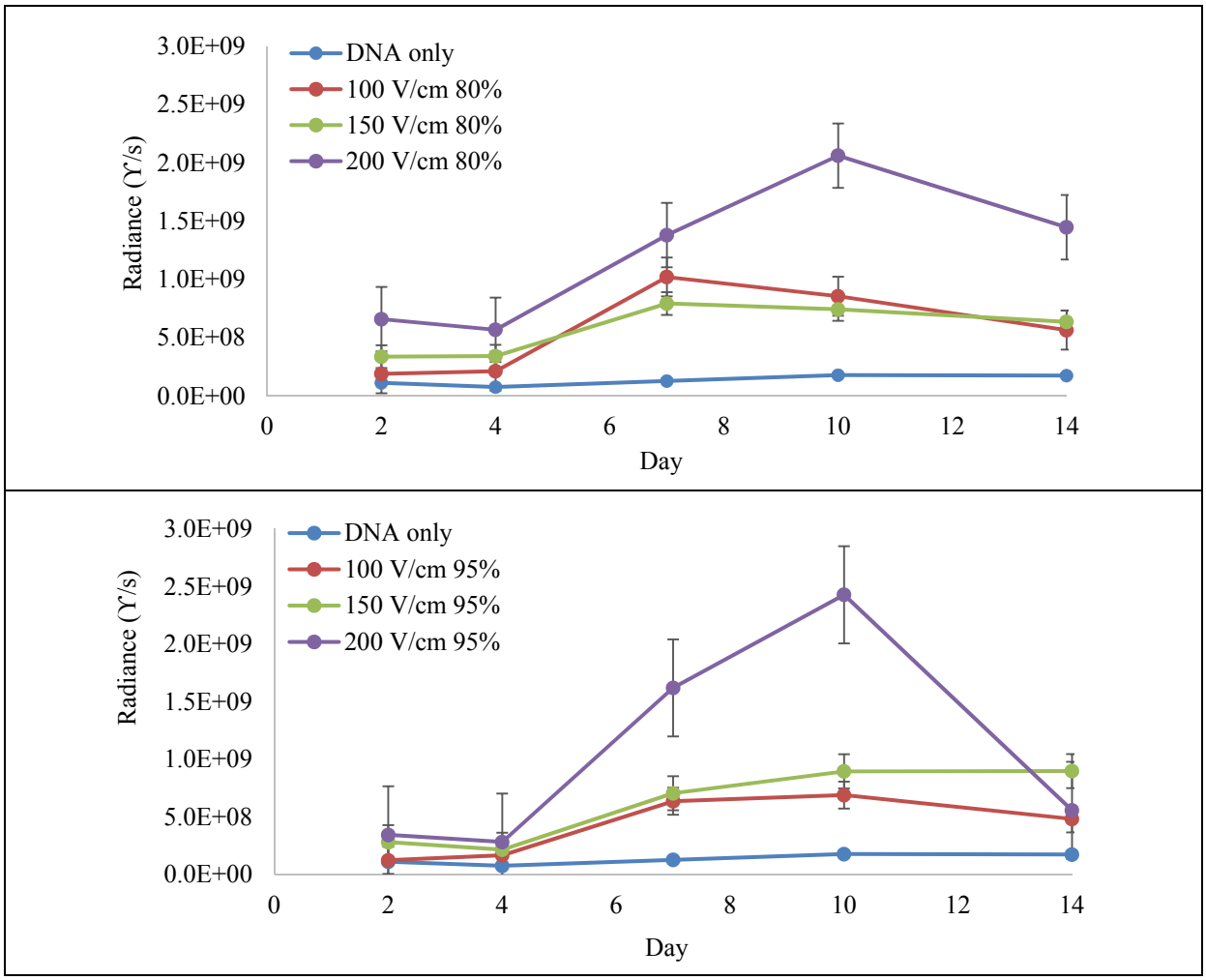

Figure 14: Mean luciferin luminescence at days 2, 4, 7, 10, and 14 days post treatment for 100 V/cm, 150 V/cm, and 200 V/cm DEIF groups. Stop impedances of (A) 80% and (B) 95%.

To assess the effect of field strength on delivery in feedback groups, the contributions to permeability associated with 80% and 95% stop impedances to delivery must be held constant. Figure 14 shows the change in radiance over time for DEIF groups targeting the same stop impedance but with different field strength pulses. Because impedance was expected to indicate

membrane permeability, it was logical to expect that tissues with relatively equal reductions in impedance would have roughly equal permeabilities however this was not the case. In DEIF groups targeting an 80% impedance reduction, pDNA delivery was not statistically different between 100 V/cm and 150 V/cm DEIF groups. However, radiance in the 200 V/cm, 80% DEIF group was greater than the radiance in the 100 V/cm and 150 V/cm 80% DEIF groups. This result was also present in the 95% DEIF groups. Figure 14A shows the 200 V/cm, 80% DEIF group radiance was 2.4 (p value = 0.041) and 2.8 (p value = 0.027) fold higher than the 100 V/cm and 150 V/cm 80% DEIF groups at day 10 respectively. Figure 14B shows the 200 V/cm, 95% DEIF feedback group radiance was 3.5 (p value = 0.018) and 2.7 (p value = 0.029) fold higher than the 100 V/cm and 150 V/cm 95% DEIF groups at day 10 respectively. These groups targeted the same reduction in impedance, a measurement of cellular response to the electric field, but exhibited differences in pDNA indicating the quality of permeability may be field strength dependent. The quality of membrane permeability refers to the number and size of membrane discontinuities contributing to new current pathways and changes in impedance. For example, a greater number of permeabilized regions of membrane with smaller diameters could provide an equal quantity of current through a cell as a fewer number of permeabilized regions with larger diameters. Models have been suggested that predict the rate of evolution, diameter, and number of membrane discontinuities are a function of electric pulse duration and magnitude [89] [90]. This data supports these models; the quality of membrane permeability may be dependent on field strength and an integral component of GET that warrants consideration. If this was the case and these transient pores facilitated transfection then regions of the membrane that become permeabilized must remain permeable long enough for DNA transport to occur. In addition, these permeabilized regions must also be large enough for supercoiled DNA to translocate through these permeabilized

regions. Investigating the quality of membrane permeability may be possible to resolve with more advanced spectroscopic techniques but was beyond the scope of this investigation. The results in Figure 14 could also be explained by a different GET mechanism. Other researchers have proposed that GET occurs because of an active cellular/biological response that is induced by electric field stimulation where the strength of the electric field determines the magnitude of the response [67]. This purportedly involves pDNA binding to cell membranes followed by endocytosis-like uptake. Regardless of the mechanism, Figure 15 results imply the quality of permeability is a critical variable that effects DNA delivery.

5.3.2 Pulse Number, Electrode Effects, and Stop Impedance

Although tissue architecture between the same regions in different animals or organisms has the same overall structure with respect to cell types and matrix components there exists variation between the geometric distributions of these entities essentially creating unique anisotropic microenvironments that respond differently to EF pulses [91]. It has been shown that even cell morphology can significantly affect electric properties of tissue [92]. Skin Hydration was another factor that contributed to tissue architecture and chemistry that in turn affected how tissues responded to electric field stimulation. Certain pathologies, general health status and exterior air humidity have been shown to affect stratum corneum thickness [93] [94]. The impact of these factors on electrical properties of treated skin were evident in all DEIF groups. The number and distribution of pulses was unique for all animals in DEIF groups, a result of anisotropic tissue architecture, chemical makeup of treated skin, electrode reuse, and pulse sequence. These factors underscored the need for the integration of feedback control mechanisms in GET methods. This was apparent in animals that received the identical treatment conditions where the same treatment sectors required a different number of pulses. As expected differences between pulse

number in animals receiving identical treatment conditions were significantly smaller than differences between animals in other groups. Variations in sector pulse number and total pulse number between animals of the same group where treatment occurred on different days was identified as a possible inconsistency in experimental setup or GET execution. This resulted in an inflation of sector pulse number and total pulse number in the first four animals in each treatment group. The twelve animals in each treatment group were broken into three separate experiments in groups of four where animals 1 through 4 were treated separately on a different day than animals 5 through 12, which received treatment on the same day. This may explain the obvious variation in the number of pulses required to reach targeted stop impedances in each sector between the first four animals and animals 5 through 12 in each group. Differences in experimental setup involving different electrode tips, fouling of electrodes, and or differences in protocol execution such as electrode contact quality between experiments performed on separate days may have been the source of this variation. However, the pulse number trends per animal in the inflated groups (animals 1-4) mirrored the same trends in animals 5 through 12.

The pulse number required to reach or exceed the target stop impedance as previously mentioned was expected to be a function of differences in tissue architecture, and electrode contact quality. However, experimental results also revealed a distinct pattern in the distribution of electric pulses each treatment sector required when pulsing was driven by impedance changes. This pattern was consistent in all feedback groups and was a function of 2 electrode design/protocol aspects: electrode geometry and pulse sequence progression through the electrode array. With respect to electrode geometry, the extension of electric fields from sectors being directly pulsed into adjacent sectors and the reuse of common electrodes shared between adjacent sectors contributed to patterns in the ease with which impedance was lowered in some sectors relative to

others. During GET pulses, electric fields were not strictly contained within the treatment sectors but also extended into adjacent sectors. It appeared that fringe fields generated by GET pulses in upstream sectors increased the permeability in adjacent downstream sector tissue, which decreased impedance in downstream sectors further from baseline before being directly pulsed. As a result, the number of pulses required to reach the targeted stop impedance was reduced in downstream sectors and in sectors where electrode reuse was greatest. This pattern in pulse number was generally consistent throughout all DEIF groups but became less prevalent as field strength increased. The reuse of common electrodes in treatment sectors provided for a significant cumulative effect in most downstream sectors. For example, at least one of the 4 electrodes defining sector 5 was used in every pulse prior to being pulsed directly. As a result, sector 5 consistently required the fewest number of pulses in all feedback groups and exhibited the greatest reduction in impedance of all sectors in all groups. In contrast, the first sector (S1) to receive pulsing generally required more pulses than other sectors because tissue in this sector was the first to be pulsed and therefore effects associated with electrode reuse or neighboring sector pulses was not present. The time and distance between indirect and direct pulses was another critical factor contributing to the collective effect of the electrode array geometry and pulse progression on patterns in sector impedance. The duration between indirect and direct pulses in a sector was longer in lower field strength groups because they required a greater number of pulses compared to the 200 V/cm groups which required a significantly fewer number pulses. Effects associated with this were most apparent in the reduced change in impedance seen in sectors 1, 4, and 7. This may have allowed impedance to relax more before direct pulsing therefore reducing the impact of fringe fields in these sectors.

Table 3 shows the mean pulse number per sector and total pulse number for each animal in the 100 V/cm field strength DEIF group targeting a stop impedance of 80%, reported with peak radiance for each animal. Considering the central location of sector five and because it is the only sector that shared at least one electrode during every pulse, it was expected it would correlate best with gene delivery success. Table 3 shows sector 5 received the fewest mean number of pulses or was tied for the fewest number of pulses in all animals with a group mean of 4 pulses. The number of pulses required in sector 5 was the least variable with a standard deviation of 2. These results reinforced the effect upstream pulses and electrode reuse had on reducing membrane permeability in downstream sectors. The reuse of upstream electrodes common to sector 5 may have initiated the permeabilization mechanism and reduced impedance in this sector before receiving direct pulsing accounting for the observed reduction in pulses. Pulse number was greater for sectors in the corners of the array (S1, S3, S7, and S9) where corner electrode reuse was the lowest. This resulted in these sectors receiving the most pulses, requiring a mean of 24 pulses between. Sectors 2, 4, 6, and 8 formed a second tier of sectors that generally required an intermediate mean number of 8 pulses. In this treatment group, corner sector 7 required a mean of 24 pulses, the most of any sector, which was also the most variable with a standard deviation of 14 pulses. The maximum number of pulses in each sector was 40; therefore, it was assumed that sectors that received 40 pulses might have not achieved stop impedance. For this group, the mean total number of pulses was 93 with a standard deviation of 60. The high variability in the total pulse number exhibited in this group was more than likely a result of differences in the setup and execution of experiments occurring on different days. There also appeared to be no correlation between total pulse number and radiance, supporting that differences in tissue architecture contribute to pulse number requirements, but it is impedance changes and permeability that more closely indicate magnitude

of delivery. Evidence of closed loop pulsing to compensate for electrode geometry was consistently supported by the disparity of required pulses between peripheral and central sectors.

Table 3: Sector pulse number, total pulse number, and peak radiance per animal in 100 V/cm DEIF group targeting 80% stop impedance. Red sectors received maximum number of pulses.

Animal	S1	S2	S3	S4	S5	S6	S7	S8	S9	Total Pulse #	Peak Radiance
1	18	6	24	12	6	20	40	34	40	200	1.59E+08
2	20	8	16	22	6	14	40	34	20	180	1.31E+08
3	12	4	18	18	2	8	40	34	20	162	1.14E+08
4	16	10	16	28	6	10	40	2	4	132	2.20E+08
5	24	4	6	2	2	2	6	2	2	50	3.31E+09
6	2	2	2	2	2	2	20	2	2	36	6.01E+08
7	2	2	2	4	2	4	4	2	8	30	4.93E+08
8	2	2	2	4	2	2	20	2	2	38	4.22E+08
9	4	4	6	12	2	4	12	4	6	54	3.08E+09
10	6	8	10	6	4	4	34	4	16	92	1.80E+09
11	2	2	14	4	2	2	20	2	10	58	1.09E+09
12	14	10	16	14	6	4	14	2	2	82	8.87E+08
$\bar{x}$	10	5	11	11	4	6	24	10	12	93	1.03E+09
σ	8	3	7	9	2	6	14	13	13	60	1.12E+09

Table 4: Sector pulse number, total pulse number, and peak radiance per animal in 100 V/cm DEIF group targeting 95% stop impedance. Red sectors received maximum number of pulses.

Animal	S1	S2	S3	S4	S5	S6	S7	S8	S9	Total Pulse #	Peak Radiance
1	40	40	36	40	2	24	40	40	40	302	6.56E+08
2	40	40	40	40	20	40	40	40	40	340	1.53E+08
3	40	40	40	40	18	40	40	40	32	330	1.69E+08
4	40	40	40	40	12	40	40	40	40	332	1.88E+08
5	22	6	8	4	2	4	40	2	6	94	9.39E+08
6	32	4	20	14	2	4	40	12	16	144	4.87E+08
7	8	4	4	8	2	6	40	6	10	88	4.43E+08
8	16	6	18	16	2	2	16	4	6	86	1.58E+08
9	26	34	40	40	8	10	40	12	14	224	2.00E+09
10	40	6	26	18	4	6	40	14	14	168	1.85E+09
11	40	16	40	18	14	14	40	8	40	230	1.12E+09
12	32	10	22	36	8	12	40	16	36	212	6.93E+08
$\bar{x}$	31	21	28	26	8	17	38	20	25	213	7.38E+08
σ	11	17	13	14	7	15	7	16	15	98	6.38E+08

Table 4 shows mean pulse number per sector and total pulse number for each animal in the 100 V/cm field strength DEIF group targeting a stop impedance of 95%, reported with peak radiance for each animal. Again, sector 5 required the fewest number of pulses in every animal with a group mean of 8 pulses. This was evidence of the effect upstream pulses had on reducing membrane permeability in downstream sectors. The reuse of upstream electrodes common to sector 5 initiated the permeabilization mechanism and reduced impedance in this sector before being directly pulsed. However, because stop impedance was increased more pulses were needed in each sector compared to the 80% stop impedance group of the same field. Table 4 indicates a large number of sectors received the maximum number of 40 pulses and may not have or were very near reaching targeted impedance reduction. The lower field strength in this group was unable to generate the permeability needed to produce a 95% reduction in impedance in all sectors. Table 4 shows generally eight out of nine sectors in the first four animals were near or did not reach the stop impedance accept for the centrally located sector 5, evidence of possible differences in experimental setup. This was not the case in animals 5 through 12. Additionally, sector 7 in all but one animal in this group required 40 pulses indicating this sector was most resistant to the electrode effects associated with electrode reuse, indirect pulses, and electric pulse progression. Sector 7's resistance to these effects prevented any marked impedance reduction before being directly pulsed. Again, pulse number was greatest for corner sectors of the array (S1, S3, S7, and S9) where electrode reuse was the lowest. These sectors required a mean of 31 pulses. Sectors 2, 4, 6, and 8 again formed the second tier of sectors requiring an intermediate number of pulses with a mean of 21 pulses. Electrode reuse was higher in these groups thus, they required fewer direct pulses. The mean total number of pulses for this group was 213 with a standard deviation of 98, a mean increase of 120 pulses compared to the DEIF 80% stop impedance group of the same field

strength. Again, variability was due to differences in experimental setup and execution that occurred between two separate experiments as well as differences in tissue architecture between animals. Table 4 shows many sectors received the maximum number of pulses indicating the minimum targeted impedance and corresponding permeability was not achieved in many sectors. Therefore, it was expected that GET delivery was not homogeneous throughout all treatment sectors in these animals. As a result, this protocol would not have been considered successful based on the possible lack of achieving targeted impedance reduction in all sectors even though delivery and transgene expression was greater than the DEI group of the same field strength. In the future, to ensure target impedance and a permeability is homogeneous in all sectors the maximum number of pulses must be increased when using 100 V/cm pulses to target a 95% reduction in tissue impedance.

Table 5 shows mean pulse number per sector and total pulse number for each animal in the 150 V/cm DEIF group targeting a stop impedance of 80%, reported with peak radiance for each animal. The mean pulse number per sector in this group was significantly lower in all sectors when compared to lower field strength groups. This was result of the increased field strength applying a greater force on ions so that cell membrane charging and potential increased a greater amount per pulse causing dielectric breakdown and permeabilization to occur more quickly. Many animals required only 2 pulses in every sector except for sector 7. This low pulse requirement was also a result of a reduction in the rate at which pulsing advancement though sectors. These faster advancing sequences enhanced the permeabilizing effects of indirect pulsing in downstream sectors because the impedance in downstream sectors had less time to decay before being directly pulsed. Table 5 shows sector 5 required a mean of only 2 pulses, the fewest in every animal, supporting the effect electrode reuse and indirect pulsing had on reducing membrane permeability

in downstream sectors. Pulse number was still greater for sectors in the corners (S1, S3, S7, and S9) of the array and sector 4 where indirect pulsing and corner electrode reuse was lower. This resulted in these sectors requiring more pulses with a mean of 7 pulses. Sectors 2, 6, and 8 generally formed the second tier of sectors that required an intermediate mean number of 3 pulses. However this mean number of was much closer to the mean number of pulses in the centrally located sector 5 indicating electrode effects at this higher field strength and lower stop impedance were less prevalent. This also meant differences in treatment sector permeabilities were less variable. This protocol was considered successful because all sectors in all animals having achieved targeted impedance reduction and corresponding permeability.

Table 5: Sector pulse number, total pulse number, and peak radiance per animal in 150 V/cm DEIF group targeting 80% stop impedance. Red sectors received maximum number of pulses.

Animal	S1	S2	S3	S4	S5	S6	S7	S8	S9	Total Pulse #	Peak Radiance
1	6	2	14	8	2	4	20	4	6	66	1.03E+09
2	6	6	8	6	2	2	26	2	20	78	1.50E+09
3	14	4	6	10	2	6	40	2	8	92	1.68E+09
4	16	8	10	20	2	2	4	4	10	76	3.85E+08
5	4	2	2	2	2	2	4	2	2	22	2.04E+09
6	2	2	2	2	2	2	6	2	2	22	1.27E+09
7	2	2	2	2	2	2	12	2	2	28	1.21E+09
8	2	2	2	2	2	2	2	2	2	18	6.57E+08
9	2	2	2	2	2	2	4	2	2	20	2.06E+09
10	2	2	8	6	2	2	12	2	8	44	1.04E+09
11	2	2	2	4	2	2	4	2	6	26	1.09E+09
12	2	4	8	2	2	2	4	2	2	28	3.07E+08
$\bar{x}$	5	3	6	6	2	3	12	2	6	43	1.19E+09
σ	5	2	4	5	0	1	12	1	5	27	5.71E+08

Table 6 shows mean pulse number per sector and total pulse number for each animal in the 150 V/cm field strength DEIF group targeting a stop impedance of 95%, reported with peak radiance for each animal. Mean pulse number per sector increased in all animals when compared to the lower 80% stop impedance group of the same field strength. Targeting a higher 95% stop

impedance required more pulses of the same field strength to reduce tissue impedance to a greater degree. Even though the targeted change in impedance was increased, fewer animals had sectors that required maximum number of pulses or did not reach stop impedance when compared to the lower 100 V/cm field strength group with the same stop impedance. As expected, sector 5 received the fewest mean number of pulses in every animal with a group mean of 3 pulses with low variability as shown by a standard deviation of 1. This was evidence of the effect electrode reuse and upstream pulses had on reducing membrane permeability in downstream sectors. Pulse number was still greater for sectors in the corners of the array (S1, S3, S7, and S9) and sector 4 where corner electrode reuse was the lowest. This resulted in these sectors receiving more pulses, requiring a mean of 20 pulses. Sectors 2, 6, and 8 generally formed the second tier of sectors that required an intermediate mean number of pulses with a mean of 7 pulses. In contrast to the lower 80% stop impedance, DEIF group of the same field strength there was greater variation in pulse number in peripheral sectors. This greater number of pulses was a result of the increase in targeted reduction in impedance that amplified differences in tissue architecture and electrode effects. Sectors 1 and 7 required the greatest number of pulses with means of 28 and 25 respectively. In order to reduce impedance to 95%, a greater number of pulses was required as compared to the 80% group at the same field strength. Table 6 shows 150 V/cm field strength pulses were strong enough to achieve the targeted impedance reduction within 40 pulses in most animals. Excluding animals 1 through 4, all treated tissue in animals 5 through 12 achieved the targeted impedance reduction and corresponding membrane permeability leading to delivery that was more homogeneous across sectors. Even though delivery in this group was statistically greater than the DEI group at 150 V/cm, this protocol was not considered successful because the impedance and permeability in many sectors did not reach targeted values due to pulse number limitations.

Maximum pulse number must be greater than 40 when targeting 95% stop impedance with 150 V/cm electric pulses to ensure targeted permeability is achieved in all sectors when using this electrode and protocol. However, the distribution of pulses between low and high electrode use sectors showed this feedback method was able to compensate for electrode geometry and pulse sequence effects.

Table 6: Sector pulse number, total pulse number, and peak radiance per animal in 150 V/cm DEIF group targeting 95% stop impedance. Red sectors received maximum number of pulses.

Animal	S1	S2	S3	S4	S5	S6	S7	S8	S9	Total Pulse #	Peak Radiance
1	40	10	24	40	6	18	40	4	28	210	1.6E+09
2	40	18	26	40	2	4	38	4	16	188	1.7E+09
3	40	24	26	10	2	6	40	4	20	172	3.5E+08
4	40	12	32	40	4	10	40	6	20	204	2.2E+08
5	32	2	16	8	2	2	14	2	8	86	2.2E+09
6	12	2	6	8	2	2	2	2	2	38	1.2E+09
7	8	6	4	4	2	4	6	4	6	44	1.9E+09
8	40	6	12	8	2	6	16	6	4	100	4.3E+08
9	14	10	14	10	2	2	36	4	8	100	1.6E+09
10	16	4	16	12	2	4	8	2	10	74	1.4E+09
11	36	24	26	2	2	2	14	2	2	110	6.0E+08
12	14	12	8	6	2	4	40	6	16	108	4.8E+08
$\bar{x}$	28	11	18	16	3	5	25	4	12	120	1.26E+09
σ	13	8	9	15	1	5	16	2	8	60	6.8E+08

Table 7 shows mean pulse number per sector and total pulse number for each animal in the 200 V/cm field strength DEIF group targeting a stop impedance of 80%, reported with peak radiance for each animal. The increased field strength in these animals significantly reduced the mean number of pulses per sector to the lowest values of any DEIF group. This trend supports the premise that higher field strength pulses charged cell membranes more quickly by moving more charge with a fewer number of pulses. More charges were moved because of the greater force imposed on each ion by the higher magnitude electric fields in the extracellular and intracellular compartments. As a result, membrane permeability also increased when membranes were charged

to a greater degree because the breakdown potential of the lipid bilayer was exceeded by a greater extent in a shorter period. The mean number of pulses in all sectors was 2 or 3. The effect of upstream pulses on lowering impedance in downstream sectors was not assessable because the protocol required each sector receive at least one pulse regardless of the impedance drop that occurred before direct pulsing. By the time pulsing advanced to sector 5, it was likely that impedance had been reduced by 80% due to electrode reuse and indirect pulses, but one pulse was still required in the protocol as a practical safeguard to ensure delivery occurred. 200 V/cm pulses abolished the resistance of sector 7 to impedance reductions at this lower stop impedance requiring a mean of 3 pulses. The highest 200 V/cm field strength electric pulse may be a better choice for cutaneous GET as it was able to generate targeted impedance reductions in all sectors within a fewer number of pulses with less variability. The permeability associated with the 80% impedance reduction achieved in all treatment sectors in all animals in this group likely accounted for the 6-fold increase in radiance relative the DEI group of the same field strength. Radiance in this group was also the second highest (12 fold) relative to the DO group. As a result, this protocol was considered successful and identified that the permeability associated with a targeted minimum impedance reduction of 80% achieved with 200 V/cm electric pulses was of a different quality than lower field strength groups targeting the same impedance reduction.

Table 8 shows mean pulse number per sector and total pulse number for each animal in the 200 V/cm field strength DEIF group targeting a stop impedance of 95%, reported with peak radiance for each animal. A minimal overall increase in pulses was required to achieve target stop impedances when compared to the lower 80% stop impedance group of the same field strength. Sectors 2, 5, 6, and 8, where electrode reuse was higher, required the fewest number of pulses, a mean of 3, to reach the 95% stop impedance compared to other sectors. This continued to support

the effect upstream pulses had on reducing membrane permeability in downstream sectors. Corner sectors 1, 3, 7, and 9, as well as sector 4, where electrode reuse was lower, required a mean number of 8 pulses. Table 8 shows 200V/cm field strength pulses were strong enough to achieve the targeted impedance reduction within 40 pulses in all sectors. Because of this, it was expected the targeted impedance reduction and corresponding membrane permeability was achieved in all sectors. This protocol was the most successful and identified that the permeability associated with a minimum impedance reduction of 95% achieved with 200 V/cm electric pulses was of a different quality than lower field strength groups targeting the same impedance reduction. This quality was responsible for the 7 fold increase in expression relative to the 200 V/cm DEI group. Although radiance in this group was not statistically greater than the 200 V/cm, 80% stop impedance DEIF group, it is expected that a greater sample size would show the permeability associated with 95% impedance reduction does produce a statistically greater amount of delivery.

Table 7: Sector pulse number, total pulse number, and peak radiance per animal in 200 V/cm DEIF group targeting 80% stop impedance. Red sectors received maximum number of pulses.

Animal	S1	S2	S3	S4	S5	S6	S7	S8	S9	Total Pulse #	Peak Radiance
1	2	2	2	2	2	2	4	2	2	20	3.7E+09
2	4	2	4	4	2	2	4	2	4	28	4.7E+09
3	4	2	4	6	2	2	6	2	4	32	2.5E+09
4	4	2	2	4	2	2	4	2	2	24	1.4E+09
5	2	2	2	2	2	2	2	2	2	18	4.3E+09
6	2	2	2	2	2	2	2	2	2	18	3.2E+09
7	2	2	2	2	2	2	2	2	2	18	7.4E+08
8	2	2	2	2	2	2	2	2	2	18	6.5E+08
9	2	2	2	2	2	2	2	2	2	18	1.8E+09
10	4	2	4	2	2	2	2	2	2	22	2.0E+09
11	2	2	2	2	2	2	2	2	2	18	7.7E+08
12	2	2	2	2	2	2	2	2	2	18	2.6E+08
$\bar{x}$	3	2	3	3	2	2	3	2	2	21	2.2E+09
σ	1	0	1	1	0	0	1	0	1	5	1.5E+09

Table 9 shows the mean total pulse number per group, and the mean peak radiance for the six DEIF groups. In feedback groups with EF pulses of the same field strength, the mean total number of pulses increased with targeted stop impedance. The mean total pulse number in the 100 V/cm DEIF groups increased from 93 to 213 when stop impedance was increased from 80% to 95%. Similarly, the mean total pulse number in the 150 V/cm DEIF groups increased from 43 to 120 when stop impedance was increased from 80% to 95%. Lastly, the mean total pulse number in the 200 V/cm DEIF group increased from 11 to 21 when stop impedance was increased from 80% to 95%. Interestingly, there was a roughly 50% reduction in the mean total pulse number when stop impedance was increased from 80% to 95% in groups of the same field strength indicating a possible linear relationship may exist within this range of excitation. The differences in pulse number between animals in the same group and animals of the same field strength targeting different stop impedances can be explained. For animals in the same group, when keeping field strength constant each pulse exerted the same force on intra and extra cellular ions. However, differences in tissue architecture and ion concentration effected the number of pulses required to move the roughly same amount of ions needed charge membranes to the same degree in order to attain the targeted stop impedance. This accounted for the variation in pulse number required to reach the same target impedance drop in animals of the same group. For animals in different stop impedance groups of the same field strength, it was expected that after ions had charged the cell membrane in response to EF pulses, the transmembrane potential in a portion of membrane exceeded the breakdown potential inducing permeabilization. Therefore, tissues targeting the same impedance drop should have roughly similar degrees of membrane permeability across sectors with correspondingly similar radiances. When stop impedance was increased, more pulses were required to move more ions to increase the membrane potential over a greater area of

the cell, which may have led to a greater amount of delivery as was indicated by a greater reduction in impedance. When holding stop impedance constant and comparing groups of different field strengths, mean total pulse number decreased with field strength again supporting the presence of an EF dose response. Table 9 shows that in feedback groups targeting a stop impedance of 80% the mean total pulse number was 93, 43, and 21 for 100 V/cm, 150 V/cm and 200 V/cm EF pulse strengths respectively. In DEIF groups targeting a stop impedance of 95%, mean total pulse number was 213, 120, and 51 for 100 V/cm, 150 V/cm and 200 V/cm EF pulse field strengths respectively. The reduction in pulse number can be explained. A greater field strength pulse imposed a greater amount of force on ions inside and outside the cell therefore moving more ions and charging a greater degree of membrane to a higher membrane potential. Ultimately, as the membrane continued to charge the breakdown voltage was eventually exceeded, inducing permeability within a fewer number of pulses. This was shown in Table 9 where total pulse number decreased by roughly 50% for every 50 V/cm increase in field strength.

Table 8: Sector pulse number, total pulse number, and peak radiance per animal in 200 V/cm DEIF group targeting 95% stop impedance. Red sectors received maximum number of pulses.

Animal	S1	S2	S3	S4	S5	S6	S7	S8	S9	Total Pulse #	Peak Radiance
1	28	2	8	12	2	2	28	4	6	92	1.5E+09
2	20	2	6	8	2	2	8	4	6	58	4.7E+09
3	8	4	10	2	2	2	14	2	4	48	2.4E+09
4	40	12	8	12	2	4	36	2	8	124	3.9E+09
5	6	2	2	6	2	2	2	2	2	26	7.6E+09
6	2	2	2	2	2	2	2	2	2	18	4.3E+09
7	10	2	4	6	2	2	4	2	2	34	1.7E+09
8	6	2	4	4	2	2	2	2	2	26	4.4E+08
9	10	2	6	12	2	2	6	2	2	44	2.7E+09
10	8	2	4	8	2	2	6	2	6	40	Deceased
11	10	4	4	8	2	2	4	2	2	38	1.1E+09
12	20	4	2	10	2	6	12	2	2	60	Deceased
$\bar{x}$	14	3	5	8	2	3	10	2	4	51	3.0E+09
σ	11	3	3	4	0	1	11	1	2	30	2.1E+09

It was expected that animals, which achieved the same impedance reduction per sector, should have had generally equal amounts of membrane permeability regardless of field strength and corresponding radiances that were also roughly equal, however this did not occur. Mean radiance of the 200 V/cm, 80% and 95% stop impedance DEIF groups was significantly greater than lower field strength groups targeting the same impedance reduction. In groups targeting an 80% stop impedance, the 200 V/cm field group mean peak radiance was 2.4 and 2.8 fold greater than the 100 V/cm (p value = 0.041) and the 150 V/cm group (p value = 0.027). In groups targeting a 95% stop impedance, the 200 V/cm field group mean radiance was 3.5 and 2.7 fold greater than both the 100 V/cm (p value = 0.018) and the 150 V/cm group (p value = 0.029). This was an unexpected yet insightful result that implied field strength must still be one of the critical variables, along with impedance reduction, responsible for producing the quality of permeability optimum for DNA delivery. Field strength may determine the quality of membrane permeability with respect to the number and diameter of permeabilized sites. Higher field strengths may produce a fewer number of larger discontinuities within the membrane, whereas lower field strength pulses may induce a greater number of smaller membrane discontinuities while each case still produces similar changes in impedance. This difference in the quality of permeability may allow for greater direct transport of DNA or stimulated uptake of DNA by the cell. Regardless of the mechanism, the quality of membrane permeability created by 200 V/cm electric pulses was significantly different from that created by the lower by 100 V/cm and 150 V/cm pulses and was critical in enhancing DNA uptake.

Another variable to consider that may account for differences in the radiance of different field strength groups targeting the same stop impedance was the change in membrane permeability that occurred in sectors after direct pulsing caused by the exposure to overlapping fields in

downstream sectors. The unmeasured change in impedance occurring in sectors already pulsed was not known. It was highly likely that impedance in earlier pulsed sectors continued to decrease below the target stop impedance because of exposure to overlapping fields from adjacent downstream sectors and electrode reuse. This may have contributed to an increase in radiance. For example, it was highly likely that the actual impedance change experienced by sector 5 at the end of the protocol was greater than the target stop impedance because of pulsing in adjacent downstream sectors 6, 7, 8, and 9. Considering this, it was likely that sector 9 was the only sector to have achieved targeted stop impedance and all other sectors would attain a final reduction in impedance that was greater than the stop impedance achieved by direct pulsing. The protocol evaluated in this study could be described as having targeted a minimum change in impedance in treatment sectors. Regardless, optimizing pulse number to target a minimum impedance reduction in all sectors still contributed to significantly higher pDNA delivery. Additional work must be done to identify the best stop impedance, and to develop an electrode design or different pulsing pattern with fewer elements that confound what is occurring in treated sectors.

Table 9: Mean total pulse number and mean peak radiance per treatment group.

Field Strength + Stop Impedance	Mean Total Pulse #	Mean Peak Radiance
100 Vcm + 80%	93	1.0E+09
150 Vcm + 80%	43	1.2E+08
200 Vcm + 80%	21	2.2E+09
100 Vcm + 95%	213	7.4E+08
150 Vcm + 95%	120	1.3E+09
200 Vcm + 95%	51	3.0E+09

Limitations in spatial resolution of radiance measurements precluded the analysis of the effect the number of applied pulses had on the radiance in each sector. As a result, peak animal radiance versus total pulse number was used to establish whether a correlation existed between total pulse number and radiance. To evaluate this, peak radiance of each animal in each group was plotted versus the total number of pulses that animal received. Differences in metabolic status

resulted in peak radiance occurring at different time points for different animals. Therefore, selecting peak radiance regardless of the day it occurred accounted for this and was necessary to capture any correlation between these two variables. Figure 15 shows peak radiance per animal versus total pulse number for all DEIF groups. With a sample size of N=12, Figure 15 shows there was no apparent relationship between pulse number and peak radiance in any DEIF group as was evident by the low coefficient of determination (R^2) between these two variables in all groups. The DEIF group receiving the lowest field strength EF pulse of 100 V/cm targeting the lowest stop impedance of 80% had an R^2 value of 0.2236 that was the greatest of any group. The 100 V/cm at 95%, 150 V/cm at 80% and 95%, and the 200 V/cm at 80% groups had respective R^2 values of 0.0414, 0.0018, 0.0860, and 0.1258. The lowest R^2 of 0.0014 was present in the DEIF group receiving the greatest field strength pulse of 200 V/cm targeting the greatest stop impedance of 95%, which had an R^2 value of 0.0014. This group also exhibited the greatest mean radiance of any group. All DEIF groups exhibited a generally random distribution of peak mean radiance versus total pulse number with low coefficient of determination values indicating no relationship between pulse number and pDNA delivery within the stop impedance and field strengths evaluated.

Observation of animals immediately, 24 hours, and 48 hours after GET protocol showed no observable tissue damage in any DEI or DEIF groups. All DEIF groups exhibited excellent safety profiles, there was no evidence of necrosis or scabbing similar to what occurred in DEI fixed pulsing groups that received 72, 250 V/cm pulses. There was an inherent element of safety in all feedback groups. Animals that received a high number of pulses necessary to achieve targeted stop impedances were exposed to relatively lower field strength pulses (e.g. 100 V/cm) and animals exposed to relatively higher field strength pulses (200 V/cm) received a lower number of

pulses. The aim of GET was to reversibly permeabilize cells and not trigger apoptosis or irreversibly permeabilize cells (necrosis). Gene transfer and protein production only occur in viable cells. Seeing statistically higher gene delivery in animals in the DEIF groups targeting 80% and 95% reduction in impedance, agrees with exhibited safety profiles in these groups; more cells were reversibly versus irreversibly permeabilized therefore more DNA was delivered to a greater population of viable cells which lead to greater reporter gene expression. Moreover, this indicates the impedance reductions evaluated were effective at reversibly permeabilizing cell membranes to a degree that facilitated gene delivery without reducing cell viability. However, reductions in impedance greater than 95% near 100% may reduce expression levels because of lowered viability. It is likely that once the relative impedance drop exceeds a certain percent, a majority of cells will be irreversibly permeabilized negatively affecting DNA delivery. Greater stop impedances must be evaluated to determine this.

A primary reason for integrating feedback control into GET was to develop a method that could generate homogeneous permeability across all treatment sectors to control and enhance gene delivery. The ability to control cell membrane permeability ensures the conditions necessary for targeted of gene delivery could be created. Open loop methods lack the means necessary to ensure the same amount of permeability is created in all treatment sectors. As a result, delivery of DNA cannot be ensured. Additionally, fixed pulsing protocols do not compensate for differences in tissue architecture and therefore have no way of quantifying the degree of membrane permeability in tissue. This results in sub optimal permeability and the inability to discern whether gene delivery was successful. Closed loop GET methods that incorporate impedance based feedback provide a way to compensate for the variability in delivery associated with tissue anisotropy and

determine whether the conditions for facilitating DNA delivery have been created by electric pulses in tissue.

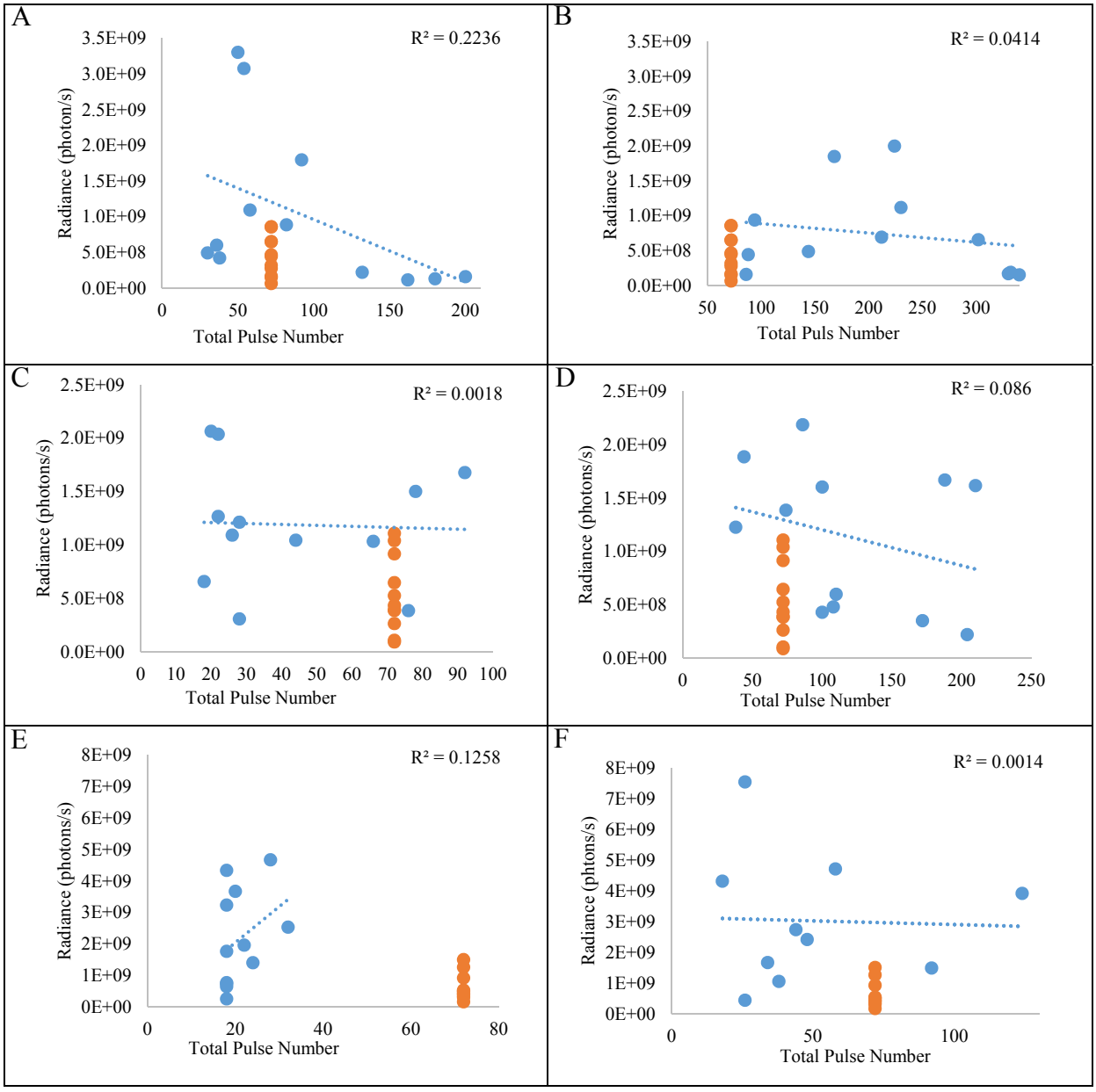

Figure 15: Mean peak radiance vs total pulse number for each DEIF group. (A) 100 V/cm, 80% (B) 100 V/cm, 95% (C) 150 V/cm, 80% (D) 150 V/cm, 95% (E) 200 V/cm, 80% (F) 200 V/cm, 95%. Orange markers represent DEI groups of same field strength.

The utility of the impedance-based feedback and the MEA to generate near homogeneous tissue permeability in a treatment region is shown in Figure 16. The box plots in Figure 16 show the variability in percent impedance reduction in treatment sectors in all groups as a function of

field strength and stop impedance. Significant differences in the percent reduction of impedance were present between sectors that were treated with an open loop GET protocol using a fixed number of 72 pulses. This variability was markedly reduced when impedance based feedback control was used to drive pulse number. Reduced variability in feedback groups validated the ability of this method to control and target permeability across all sectors which lead to enhanced gene delivery. All feedback groups showed statistically greater mean radiance compared to non-feedback groups of the same field strength. Furthermore, the 200 V/cm feedback groups had the lowest variability in impedance drop per sector and exhibited the greatest mean transgene expression. Figure 16 shows that variability in impedance drop decreased as field strength increased in DEI and DEIF groups. In theory, higher field strengths fully charge the membrane faster therefore, even without feedback it was expected that higher field strength groups would show less variability and overall greater impedance drops in all sectors. This data also shows variability in impedance drop decreased as stop impedance increased in DEIF groups. Variability was lower in these groups because the minimum allowable range impedance drop was reduced. The 80% impedance drop groups allowed a 20% range in impedance reduction whereas the 95% stop impedance groups allowed 5% range in impedance reduction. Electrode effects associated with indirect pulsing and electrode reuse were also consistent through DEIF groups but were minimized in groups receiving higher field strength pulses and higher stop impedances, again a result of smaller allowable range in impedance reduction. Electrode effects were apparent in impedance drop patterns within columns of the electrode array that agreed with pulse number trends. Sectors 1, 4, and 7 at the top of the left, central, and right columns always exhibited the smallest drop in impedance relative to same column sectors. These sectors were most resistant to reductions in impedance associated with electrode reuse and indirect pulses and required a greater

number of pulses. Because pulse sequence advanced away from these sectors the immediate indirect pulses, prior to sectors 4 and 7 occurred at a greater distance two sectors away in sectors 3 and 6. The effect of this indirect pulse on sectors 4 and 7 was therefore minimal. The central sectors 2, 5, and 8 within these columns exhibited the greatest reduction in impedance while bottom sectors 3, 6, and 9 exhibited intermediate reductions in impedance within these columns. Before pulsing advanced to a central or bottom row sector the two lower left and right electrodes in the sector above were pulsed, as a result the top half of the adjacent downstream sector was also pulsed. For example, the upper two electrodes (2 and 6) in sector 2 were used during pulsing in sector 1 before direct pulsing in sector 2 began. These indirect pulses initiated reductions in impedance in the sectors below it. This occurred in sectors 2 and 3 in the left column, sectors 5 and 6 in the center column, and sectors 8 and 9 in the right column, and accounted for their larger drops in impedance. This was most apparent in 100 V/cm and 150 V/cm DEI groups where the percent reduction in impedance was more variable and overall lower especially in sectors 1, 4, and 7 relative to other sectors. Many sectors in these groups did not attain target impedance drop due to protocol restraints in the pulse number maximum. Some of these sectors required more than the maximum allowable twenty pulses and therefore either did not achieve targeted stop impedance or were very near it. Sector 5 still showed the greatest impedance reduction of all sectors in all groups. Most important, Figure 16 validates that tissue permeability can be controlled when pulse number is guided by changes in impedance. The variability in tissue impedance was greatly reduced when feedback methods were integrated into GET. Interestingly, the right column of sectors (S7, S8, and S9) generally showed lower reductions in impedance relative to other columns in DEI groups. The 200 V/cm DEI group exhibited the least variable and greatest percent reduction in impedance across sectors of any group, a result of the 72 pulses each animal received which

was roughly 40% fewer pulses than the 200 V/cm 95% DEIF group. In this non-feedback group, all downstream sectors 2, 3, 5, 6, 8, and 9 had minimal variability in impedance reduction that were near all 99%. Upstream sectors 1, 4, and 7 showed smaller reductions in impedance with slightly greater variability relative to other sectors. The significantly lower expression levels, relative lack of variability in all sectors, and the near maximum (99%) decrease in impedance in the 200 V/cm non-feedback group, indicated these animals were overpulsed. It was likely that overpulsed tissues had a large percentage of cells that were irreversibly permeabilized which left a reduced number of viable transfected cells to express the reporter gene. Although necrosis and visible tissue damage was not present in this group, these conditions were considered excessive especially when comparing expression levels of other feedback groups to the lower expression levels in this group. This indicates a fine line exists between the optimum impedance reduction and membrane permeability needed for maximum DNA delivery versus the impedance reduction present in overpulsed tissue.

Figure 16 shows the variability of the mean percent change in impedance was markedly reduced in all treatment sectors in DEIF groups relative to DEI groups. The impedance drops in these groups were forced to the minimum stop impedance set point in most animals. Some of the sectors in lower field strength groups that required the maximum number of 20 pulses did not achieve target impedance drops. Electrode effects associated with electrode reuse and indirect pulses were still evident as mentioned previously. Sectors 1, 4, and 7, like the DEI groups, still exhibited the smallest drop in impedance relative to same column sectors. Again, this was due to minimal reductions in impedance associated with electrode reuse and indirect pulses. The impedance drop in bottom sectors 3, 6, and 9 was slightly lower in magnitude compared to the respective sectors 2, 5, and 8 above them. This was consistent in all DEIF groups. Variability in

percent impedance drop was lower in all sectors as target stop impedance and field strength increased. The 200 V/cm DEIF group targeting a 95% reduction in impedance, exhibited the least variability in impedance change between sectors. The reduced variability in impedance reduction shown in DEIF animals verifies that the device and protocol used were capable of controlling and targeting minimum impedance drops in tissue to produce roughly similar membrane permeability in cells across all sectors. The greatest amount of gene delivery was achieved in the 200 V/cm (highest field strength) feedback group targeting the greatest reduction in sector impedance (95%). This was followed by the 200 V/cm group targeting 80% impedance reduction. The data shows that integrating feedback control into GET allowed for targeted reductions in tissue impedance to be achieved, which compensated for differences in tissue architecture. Considering lower field (100 V/cm and 150 V/cm) feedback groups also produced radiances that were statistically greater than the 200 V/cm non-feedback group, it is likely that the near 100% impedance drops present in the 200 V/cm DEI group lead to sub optimal DNA uptake as a result of overpulsing in some sectors and underpulsing in others. Because the 200 V/cm DEI group impedance reduction was near 100% in each sector it is likely that the optimum impedance reduction for DNA delivery lies within a small range greater than or equal to 95% and less than or equal to 99%. The differences in radiance of different field strength groups targeting the same stop impedance, as supported by Figure 14, implies there was as an element of quality to the permeability that may be a function of the number and size of permeabilized regions in the cell membrane. The highest field strength created the quality of permeability optimum for DNA delivery. Two hundred V/cm electric pulses targeting a 95% reduction in impedance produced the greatest mean pDNA delivery with the least variable impedance drops. Therefore, these parameters generated the quality and magnitude of membrane permeability best suited for DNA delivery. It is important to note that the reported impedance

drop in each sector was measured when the pulsing sequence had advanced to that sector. This does not indicate the final impedance reduction generated in sectors only the minimum reduction in impedance. Additional reductions in impedance in upstream sectors caused by indirect pulses and electrode reuse in downstream sectors already having achieved target stop impedance were present but not measured.

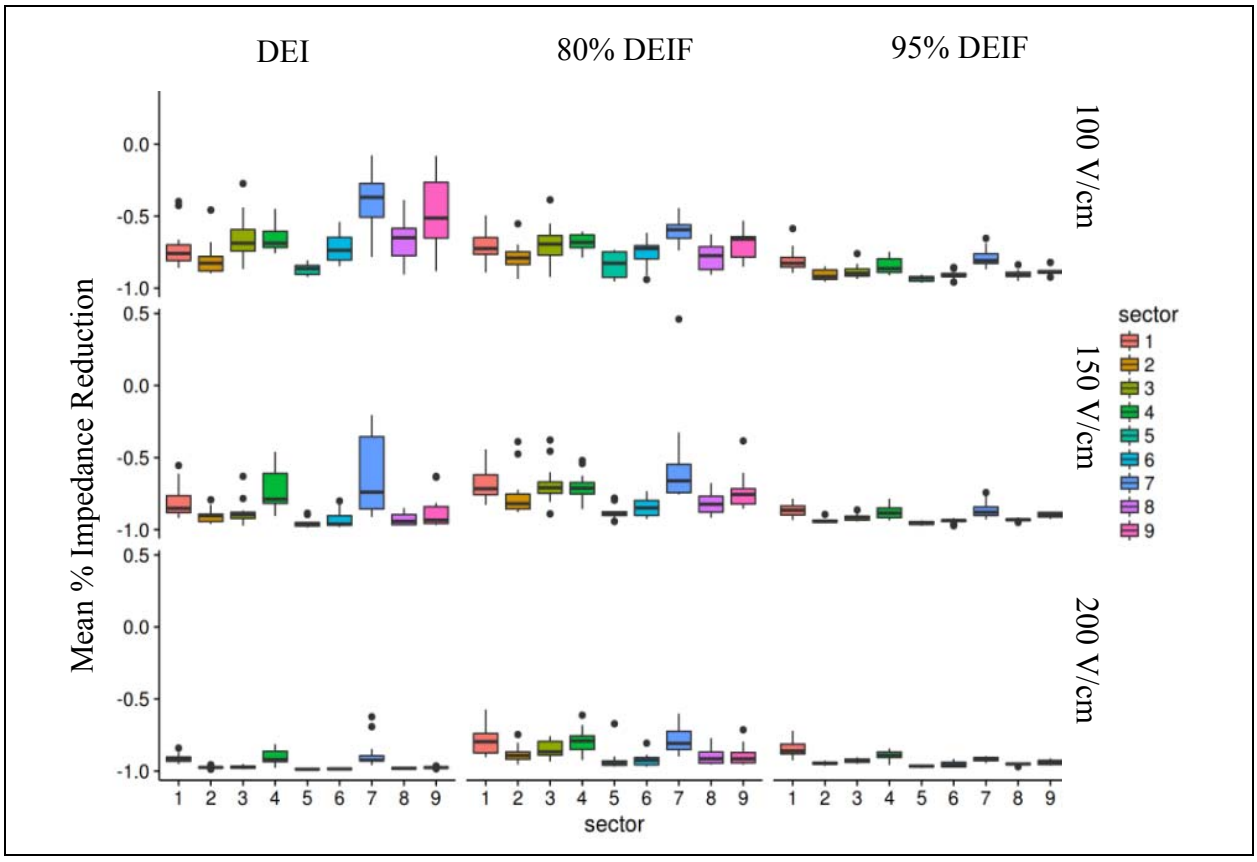

Figure 16: Mean percent impedance change box plots versus sectors 1, 2, 3, 4, 5, 6, 7, 8, and 9 for all DEI and DEIF groups.

The major difference between DEIF groups and the DEI groups of the same field strength was not only the total number of pulses but in the distribution of pulses over sectors. All animals in DEI groups received 72 pulses as compared to the 21 and 51 respective mean total number of pulses required in the 80% and 95%, 200 V/cm feedback groups. Table 8 shows that in sectors where electrode reuse was higher fewer pulses were required. For example, sectors 2, 5, 6, and 8

required a mean number of 3, 2, 3, and 2, pulses respectively to achieve a 95% reduction in impedance. Peripheral sectors 1, 4, and 7, where electrode reuse and indirect pulsing effects were lower, required a mean of 14, 8, and 10 pulses to achieve a 95% stop impedance. Only 4.2% (27 out of all 648 sectors in feedback animals) required the 8 pulses DEI groups received which has been an accepted optimum number of pulses used in many open protocol approaches. This underscores the need to provide the dose of electric field exposure commensurate with tissue architecture that also compensates for electrode geometry to generate a non-lethal degree of permeability that is optimum for DNA uptake. There is no single number of pulses considered optimum. The results from these feedback groups and the reduced number of pulses they required indicate the reduced expression in the DEI group was more than likely caused by overpulsing. More importantly, closed loop pulsing that was based on targeted impedance drops eliminated overpulsing. In DEI groups, fixed pulse number and electrode effects resulted in suboptimal responses to electric fields and variable permeabilities across sectors; however, the impedance guided pulse number in DEIF groups was able to account for these effects as well as tissue anisotropy and ensure a targeted permeability was achieved across sectors. The feedback controlled pulsing ensured targeted permeability was achieved in all sectors, maximizing the population of cells primed for DNA uptake and significantly increased gene expression in all feedback groups.

5.3.3 Impedance Spectroscopy

Assuming that tissue is roughly comprised of components with resistive (intra/extracellular fluid and transmembrane pores) and capacitive (lipid membrane) nature some qualitative implications can be made with respect to what is happening physiologically during GET if these biologic structures are treated as electric components. Passive membrane capacitance has been

proposed to have frequency dependent relaxation mechanisms within the 1 kHz to 100 MHz range referred to as β dispersions [95]. Therefore, impedance measurements over this range of frequencies can provide quantitative information about tissue components that have these relaxation mechanisms. A simplified circuit model was used to describe the electrical characteristics of the epidermis comprised of a resistance in series with a resistor in parallel with a capacitor, referred to as Randle's circuit (Figure 17). However to account for any non-ideal charge storage behavior a constant phase element was substituted for the capacitor. Where R_s represents the resistance exterior to cells comprised of the extracellular fluid matrix and the stratum corneum. R_m represents the resistance of permeabilized regions of plasma membranes and the C_{dl} characterizes the charge storage behavior of plasma membranes. Generally, at higher frequencies within the dispersion zone, capacitive reactance contributes more to the magnitude of impedance as current is shunted to charge the membrane. This pathway is the least resistive due to the increased rate of current oscillations and the reduced amount of charge stored on membranes. Conversely, at lower frequencies, resistive components contribute most to the magnitude of impedance where the capacitor (cell membranes) acts as an open circuit and current is shunted through leaks and permeabilized regions of membranes. Therefore, high frequency impedance norms describe the cumulative capacity of cell membranes within in the treated volume to store charge and low frequency impedance norms describe the movement of current through leaks and permeabilized regions of cell membranes. The skin, including the layers of the epidermis, dermis, hypodermis, and deep layers of muscle were all assumed to have no inductive components. This agreed with the semicircular shape of impedance spectra exhibited by all animals in all groups. This incomplete semicircle was a result of the range of frequencies used to collect impedance data.

Nyquist plots were used to assess the relative magnitudes of these different mechanisms to better understand what occurred at the cellular level during GET.

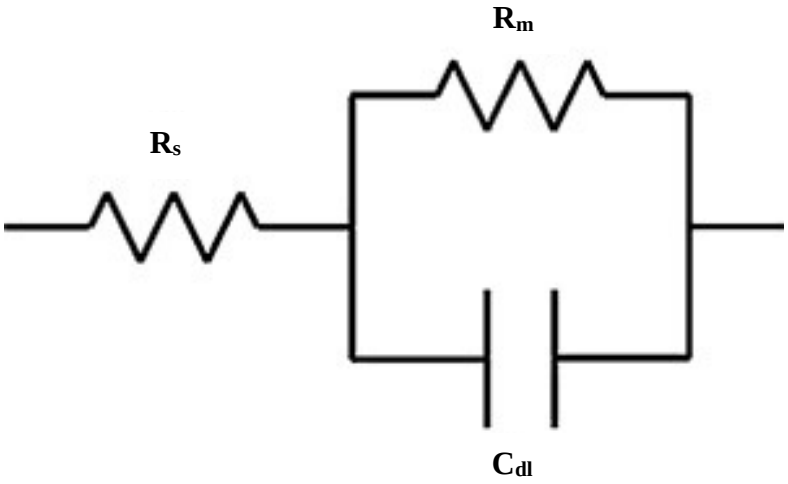

Figure 17: Epidermis circuit model.

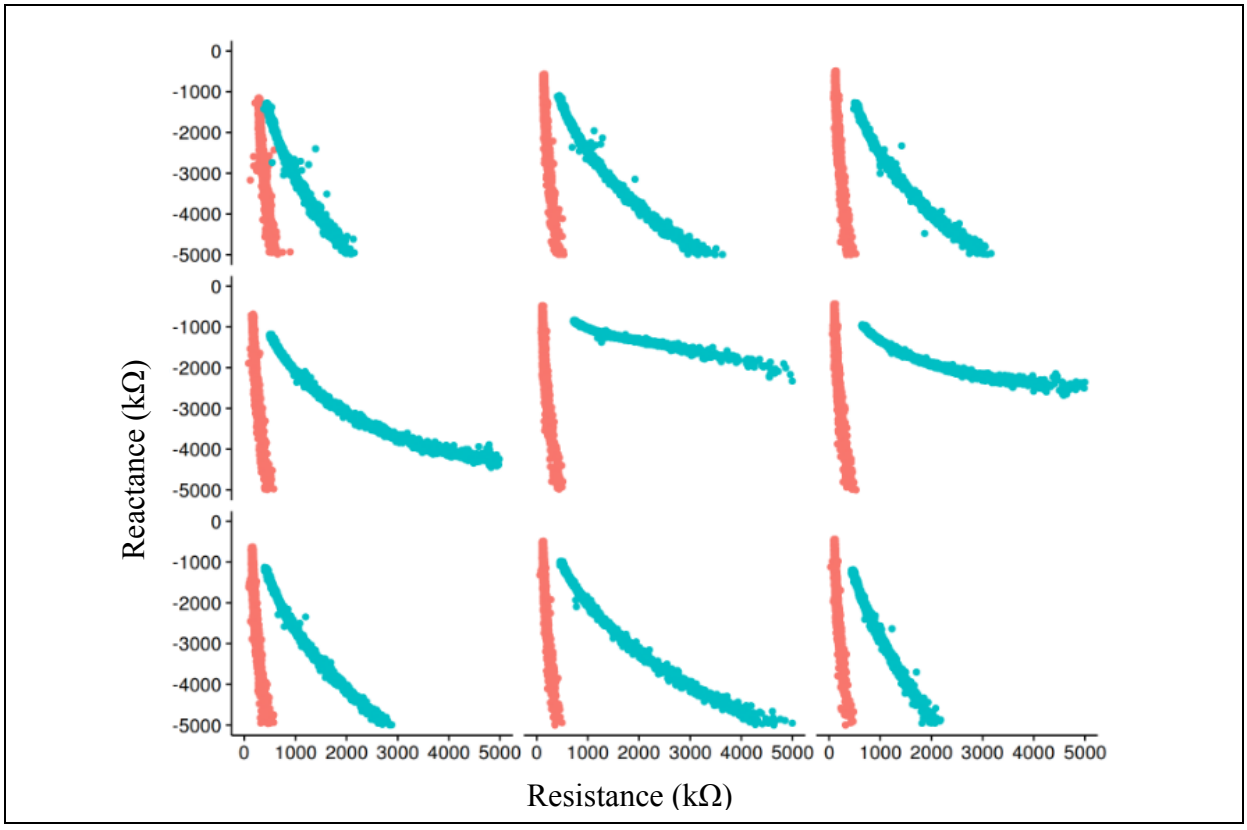

Figure 18: 100 V/cm DEI group, single animal Nyquist plots for each sector before (orange) and after (blue) pulsing.

A change in the permeability of tissue due to EF pulses was confirmed by differences in before and after electric field pulsing Nyquist curves in all groups. As field strength and stop impedance increased, these differences became larger and more obvious. Figure 18 shows Nyquist plots for all sectors in a representative animal before and after EF pulses in the 100 V/cm DEI group where each sector received a fixed number of 8 pulses for a total of 72 pulses over the duration of the protocol. Differences in before Nyquist curves between sectors was a function of variations in tissue properties and measurement noise, again supporting the need for feedback control to account for the unique tissue architecture of each treatment region. The after Nyquist curves show a marked decrease in the magnitude and shape of impedance loci relative to skin that had not yet received EF pulses. In Figure 18, before pulsing (orange) Nyquist plots were semicircular in shape confirming the RC nature of cells in tissue that was also in series with an additional resistance represented by the positive horizontal shift of the Nyquist trace. The horizontal shift present in all before and after Nyquist plots likely represented the resistance of the stratum corneum and extracellular fluid residing in the interstitial compartments around cells. However, the magnitude of the extracellular compartment resistance was considered negligible relative to the stratum corneum resistance. The same semicircular shape indicative of parallel RC nature was present in the after EF pulse Nyquist plots (blue) however, major reductions in resistance and reactance were present resulting in a flattened and horizontally compressed Nyquist signature. The reduction in resistive and reactive components validated that the opposition to current flow through tissue was decreased after pulsing and that new current pathways were present. Because the short 150 ms duration of GET pulses were not expected to contribute to any significant change in the conductivity of the interstitial compartments prior to a permeabilization event, these new current pathways were expected to exist through cell membranes because of the

permeability induced by electric fields. Additionally, all after pulsing Nyquist plots in all treatment groups exhibited positive horizontal shifts relative to before pulsing Nyquist plots. This shift implied an increase in the stratum corneum resistance was present after pulsing. Current flow through tissue during GET pulses increased the temperature of the semi-solid phase stratum corneum causing an increase in its resistance. This agreed with the increase in temperature of tissue sensed by fingertips that supported the MEA during execution of the GET protocol. A change in the shape of Nyquist traces represented a change in the charge storage capability of membranes and the charge transfer through them. The increased permeability of cell membranes induced by pulsed electric fields indicated the conditions proposed for the GET mechanism were initiated. This was supported by the significantly enhanced radiance of all treatment groups relative to the DO group. Electrode effects were pronounced in non-feedback groups relative to feedback groups especially at higher field strengths where they were marked. Evidence of electrode reuse, indirect pulsing, and pulse sequence effects were present in differences in after Nyquist plots usually between the lower right quadrant of the array (sectors 5, 6, 8, and 9) and the remaining sectors especially sectors 1, 4, and 7. In sectors 5, 6, 8, and 9, the reduction in both resistance and reactance was significantly greater as can be seen by the flattened and compressed after pulsing Nyquist curves. Relatively shorter and flatter after Nyquist curves identify treatment regions where tissue was permeabilized more by EF pulses. Figure 18 shows this in the 100 V/cm DEI group after Nyquist curves of sectors 2, 5, 6, and 8 which had lower resistance and reactance values across all frequencies compared to other sectors. Figure 16 also confirms this, supporting these sectors as consistently having the greater mean impedance reduction compared to other sectors. Sector 7 consistently appeared to have the lowest reduction in impedance and was expected to have the lowest degree of permeability and gene delivery. Considering all treatment

sectors in this group received the same number of pulses, the consistent pattern in the differences between after Nyquist plots for the bottom right quadrant of sectors and the top row and left column of sectors indicated an unequal exposure of treatment regions to electric fields. The permeabilizing effects induced by electric fields were not balanced equally across all sectors due to electrode reuse and pulse sequence effects, and to a much lesser extent tissue architecture. The lower radiance in this group confirms this and indicates the limitations of open loop GET methods. The concomitant flattening and reduction in real and imaginary components of impedance do indicate a significantly decreased time constant in all sectors. A decrease in the RC time constant indicated the time required to charge the capacitive membrane was decreased because of a reduction in membrane integrity.

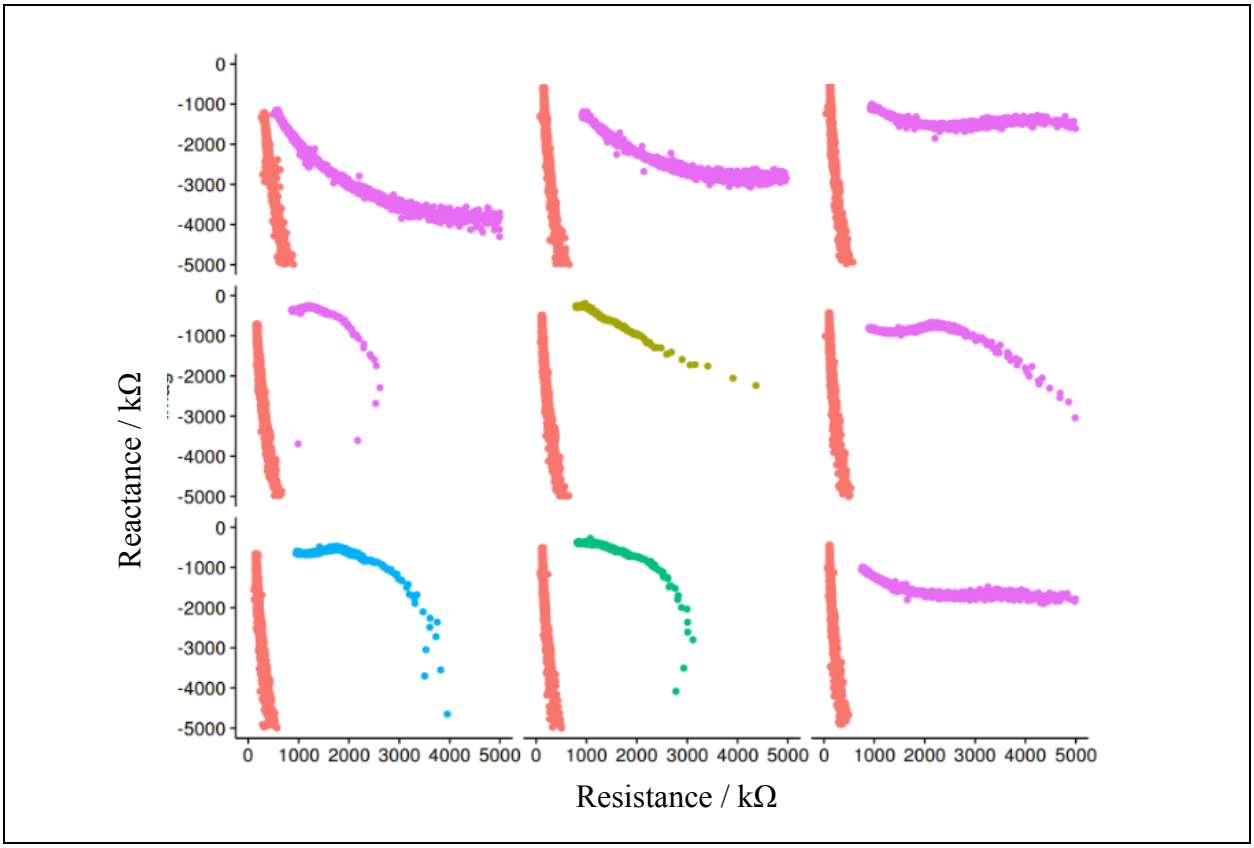

Figure 19: 100 V/cm, 95% DEIF group, single animal Nyquist plots for each sector before (orange) and after pulsing.

Nyquist plots from the 100 V/cm field DEIF group targeting a 95% stop impedance shown in Figure 19, provide evidence of a more homogenous reduction in impedance across all sectors when minimum impedance reductions were targeted with a closed loop protocol. The 100 V/cm DEIF group targeting 80% stop impedance exhibited similar Nyquist plots (not shown) however magnitudes of impedance loci were slightly greater as expected due to the lower stop impedance that was targeted. The after Nyquist traces in Figure 19 show a greater reduction in impedance loci at all frequencies in all sectors compared to the non-feedback group of the same field strength shown in Figure 18. This indicated permeability in the 95% DEIF group was greater than the DEI group of the same field strength. Differences in post EF pulsing impedance Nyquist plots between sectors associated with electrode effects and tissue anisotropy were reduced relative to the DEI group but still present. Sectors in the left column and top row of the array still exhibited smaller reductions in impedance loci at all frequencies when compared to the lower right quadrant of sectors. The shape and magnitude of impedance spectra for these peripheral sectors remained semicircular whereas the impedance spectra for the lower right quadrant of sectors appeared to be roughly linear and almost horizontal. This implies the degree and quality of permeability was different between these groups of sectors. The reduced values of resistance and reactance in the lower right quadrant of sectors at all frequencies does imply that permeability was greatest in these sectors therefore it is expected delivery was also greater in these sectors. Furthermore, the linear impedance spectra exhibit a very low, near horizontal slope indicating reactance or capacitance changed very little in magnitude with frequency. In other words, the reactance and capacitance were roughly constant due to membrane permeability reaching a near maximum. A linear impedance spectrum with a slope approaching zero over a small range of resistances may be the strongest evidence of high permeability and DNA uptake. Using feedback to target a specific

impedance drop reduced electrode effects and accounted for differences in tissue architecture ensuring a greater minimum permeability was achieved in more sectors. This feedback approach ensured tissue in all sectors was permeabilized to a greater degree, which significantly enhanced transfection. Targeting a minimum impedance reduction of at least 80% and 95% with 100 V/cm electric pulses resulted in respective 3.0 and 2.4 fold increases in radiance over the non-feedback group of the same field strength.

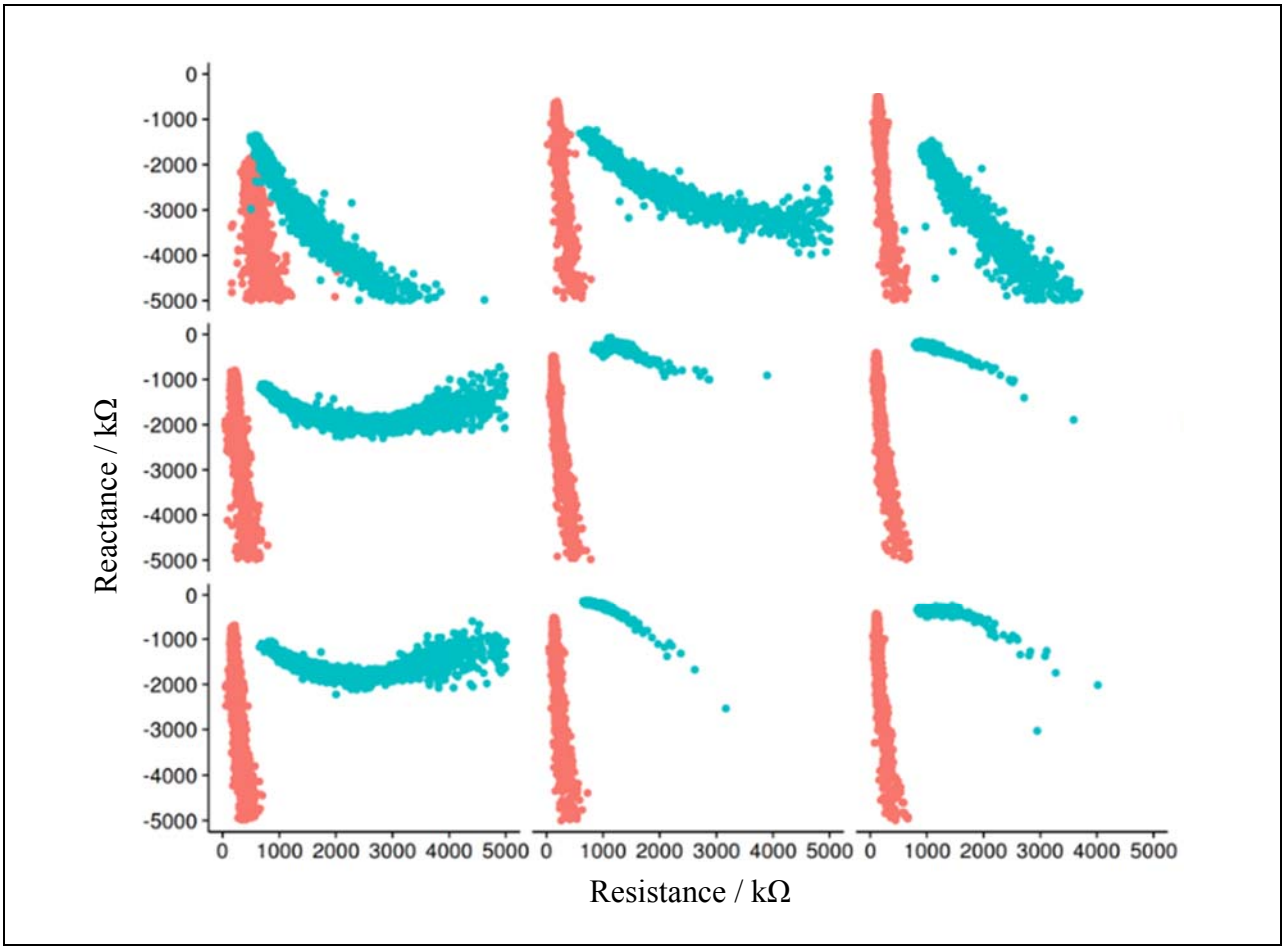

Figure 20: 150 V/cm DEI group, single animal Nyquist plots for each sector before (orange) and after (blue) pulsing.

Figure 20 shows the before (orange) and after (blue) pulsing Nyquist plots for all sectors for a representative animal from the 150 V/cm DEI group. All sectors exhibited significant reductions in impedance loci at all frequencies, however the reduction in after pulsing (blue)

Nyquist plots in the lower right quadrant of sectors was markedly greater than other sectors. The shape of impedance spectra between these groups of sectors was also very different implying the degree and quality of permeability was also different. Considering all treatment sectors in this group received the same number of pulses, the marked differences between the permeability present in these two groups of sectors indicated an unequal exposure of treatment regions to field conditions which was even greater than what was seen in the 100 V/cm DEI group. The permeabilizing effects induced by electric fields were not balanced equally across all sectors due to electrode geometry and tissue anisotropy. This was further exacerbated by greater field strengths. The lower mean radiance of this group supports this and indicated the limitations to delivery that are present in open loop GET methods where targeted minimum permeability across sectors cannot be ensured. The after electric field pulsing impedance loci were reduced in all sectors and but only semicircular in shape for sectors in the upper row and left column in the array (S1, S2, S3, S4, and S7). The retained semicircular shape in these peripheral sectors indicated the phase angle of the impedance in tissue in these sectors was still dependent on frequency more than likely because membrane integrity remained relatively intact compared to the lower right quadrant of sectors. The after Nyquist plots for the lower right hand quadrant of sectors 5, 6, 8, and 9 were significantly different in shape with large reductions in resistance and reactance values indicating the degree of permeability was greater in these sectors. Reactance in these sectors varied over a small range compared to resistance because the membrane capacitance became stable. These sectors exhibited roughly linear impedance spectra showing that reactance in these sectors did not change appreciable with frequency. Measurement noise was also reduced in these sectors; a possible result of preferential current pathways that were established after changes in permeability became less variable with each pulse. As permeability in these sectors became stable so too did

current pathways resulting in a reduction in measurement variability. The lower expression of this non-feedback group relative to the 150 V/cm feedback groups indicated this combination of impedance spectra did not reflect the degree or quality of permeability that were optimum for DNA uptake. The presence of two different types of permeability in this group make it difficult to assess which impedance spectra correlated with optimum DNA uptake.

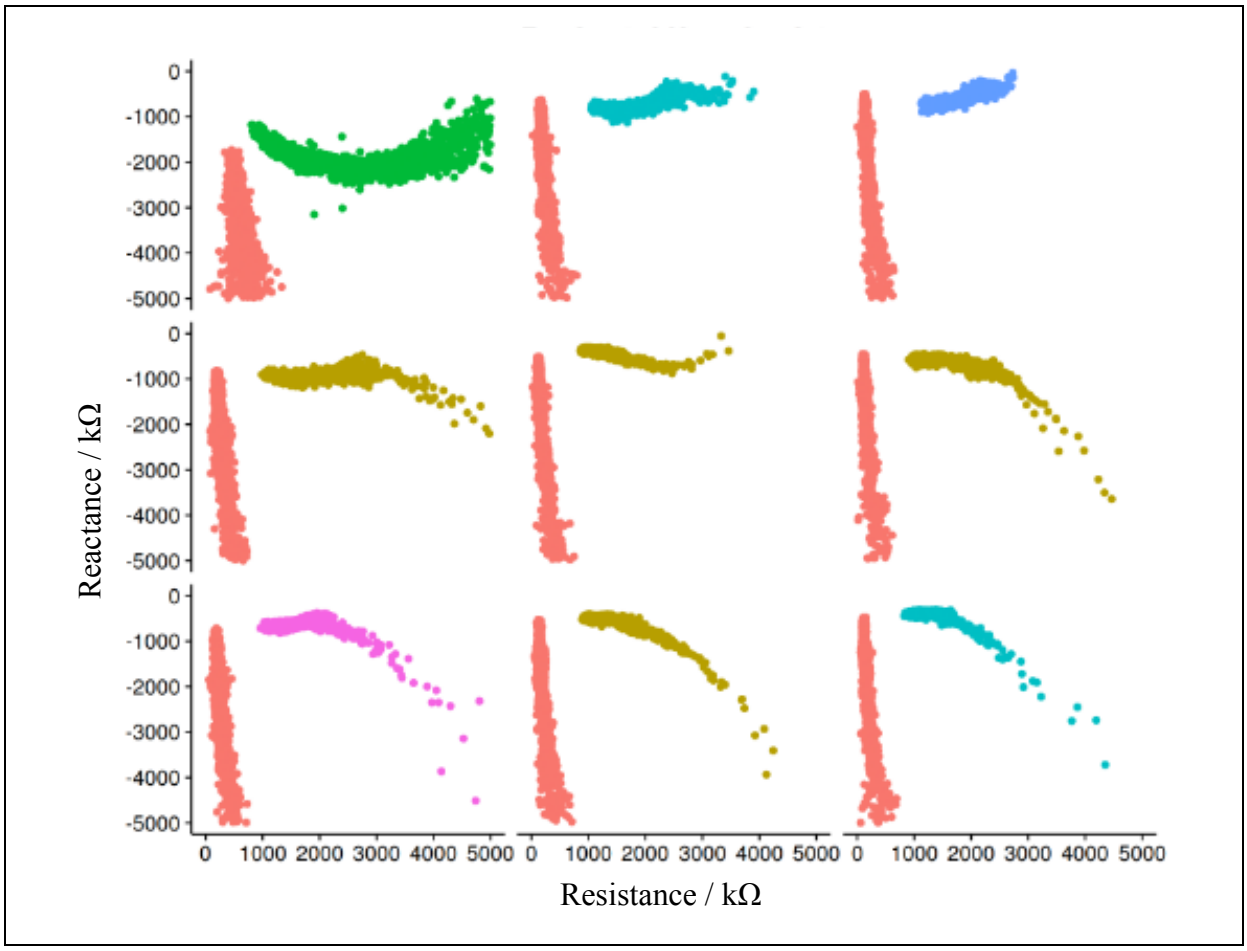

Figure 21: 150 V/cm, 95% DEIF group, single animal Nyquist plots for each sector before (orange) and after pulsing.

Figure 21 shows the before and after Nyquist plots for all sectors in a representative animal from the 150 V/cm DEIF group targeting a 95% impedance reduction. Like the 100 V/cm, 95% DEIF group this group also showed more homogeneous impedance reductions across all sectors however, impedance loci were reduced a greater extent in more sectors. The 150 V/cm DEIF

group targeting 80% stop impedance exhibited similar Nyquist plots (not shown) with respect to shape and homogeneity of impedance changes however magnitudes of impedance loci were slightly greater due to the lower targeted stop impedance. The after Nyquist traces in Figure 21 show a greater reduction in impedance loci at all frequencies in all sectors compared to the non-feedback group of the same field strength (Figure 20) which indicated the permeability in the 95% DEIF group after pulsing was greater than the DEI group of the same field strength. Differences in after EF pulsing impedance spectra between sectors associated with electrode effects and tissue anisotropy were minimized but still present. Peripheral sectors 2, 3, 4, and 7 (top row and left column of sectors) exhibited impedance spectra that were the same shape as those of the lower right quadrant of sectors. This was evidence that the closed loop method was able to compensate for electrode reuse and tissue architecture. More importantly, this indicated that using a closed loop protocol to target a minimum reduction in impedance of 95% in all sectors with 150 V/cm electric pulses generated a consistent degree of permeability in 8 out of 9 sectors. This was a significant improvement over the 100 V/cm 95% stop impedance group that showed only 4 out of 9 sectors had marked increases in tissue permeability. The greater reduction in impedance loci in 8 of 9 sectors compared to the 150 V/cm non-feedback group was expected to have contributed to the greater DNA delivery seen in in this group. Sector 1 was the only sector with a semicircular after pulsing impedance spectra. Sectors 2 through 9 all had roughly linear spectra with slopes near zero indicating reactance and capacitance of tissues in these sectors changed very little with frequency. It was expected that the reactance and cumulative membrane capacitance in these 8 sectors was more than likely near its lowest and stable achievable value respectively. The quality and degree of permeability in sectors 2 through 9 was near the optimum for DNA uptake accounting for the 2.3 fold increase in pDNA delivery seen by this group relative to the non-

feedback group of the same field (150 V/cm). The indicative of the impedance spectra that correlate with enhanced DNA uptake.

Figure 22 shows before (orange) and after (blue) electric field pulsing impedance spectra from a representative animal in the 200 V/cm DEI group. Significant differences in the permeability present after pulsing between the top row of sectors and remaining sectors indicate the impact electrode effects and tissue architecture had on delivery. The open loop method used in this group did not compensate for these effects and as a result the permeability between sectors was not homogeneous. These effects were concentrated in all downstream sectors in the central and bottom rows of the array. The top row of sectors exhibited significantly smaller reductions in impedance loci relative to lower sectors. Impedance spectra in sectors 2, 3, 5, 6, 8, and 9 exhibited reactance values that were near zero and roughly constant relative to the range and magnitude of resistance values. The after Nyquist plots for these sectors may be indicative of over pulsed tissue considering the low mean radiance exhibited by this group. Sector 5 impedance spectrum shows resistance and reactance were almost constant as frequency changed relative to the before pulsing spectrum. Permeability in this sector and in sectors with similar impedance spectra may have been near maximum and signified irreversible permeability in a large portion of cells. This was a result of over pulsing in the bottom two rows of sectors. The remaining population that had not been irreversibly permeabilized contributed to the reduced radiance seen in Figure 12. Even though this group showed statistically higher radiance relative to the DO group, these impedance spectra represent suboptimal permeability when compared to the 80% and 95% feedback groups of the same field that exhibited 5.8 and 6.8 fold increases in radiance relative to this group respectively. Interestingly, the sectors exhibiting these large reductions in resistance and impedance also had an equally noticeable reduction in measurement variability or noise. This may be another dimension

of impedance spectra indicative of the quality of the permeability created by pulses. The statistically lower expression of this non-feedback group relative to the 200 V/cm feedback groups indicate this combination of impedance spectra did not reflect the degree or quality of permeability optimum for DNA uptake.

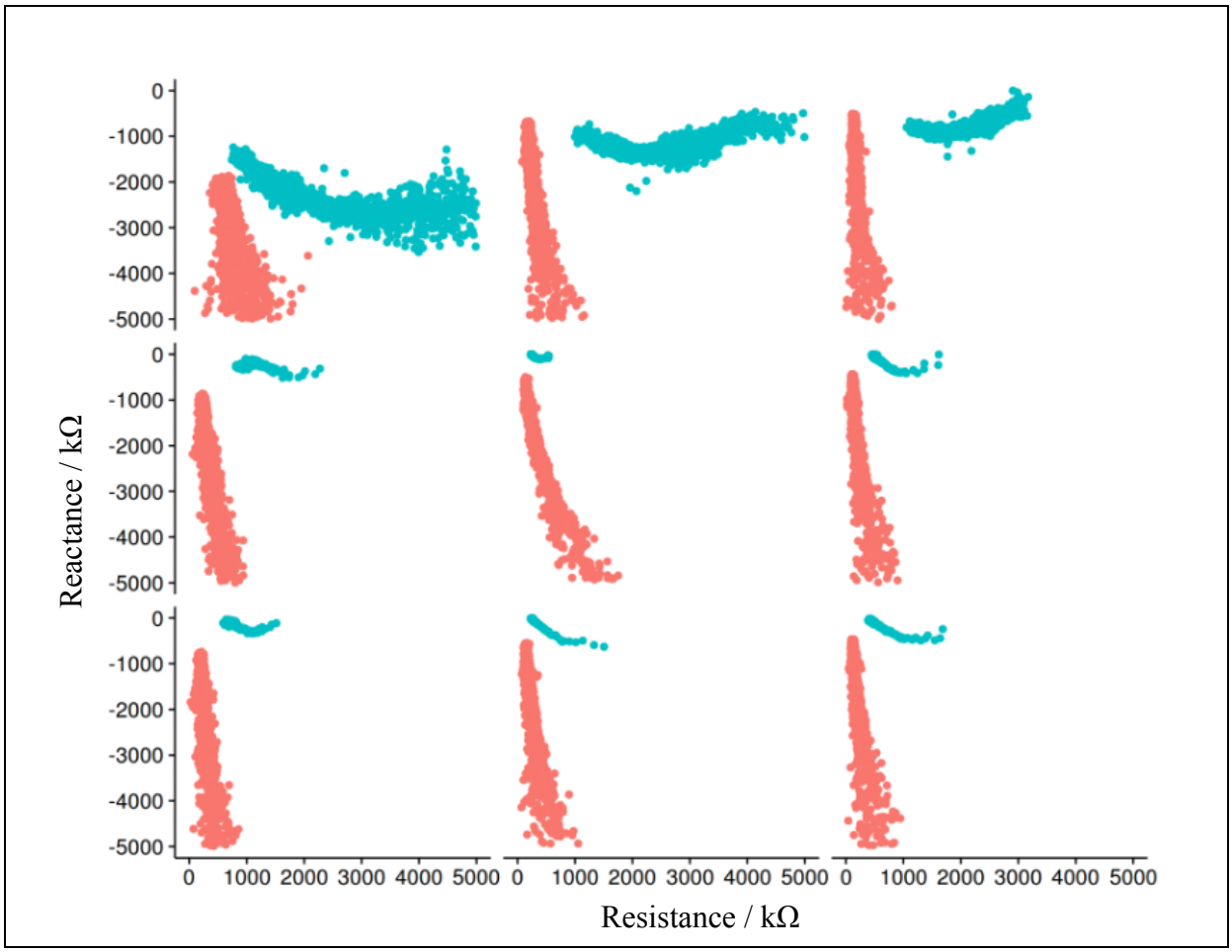

Figure 22: 200 V/cm DEI group, single animal Nyquist plots for each sector before (orange) and after (blue) pulsing.

Figure 23 shows before (orange) and after electric field pulsing impedance spectra from a representative animal in the 200 V/cm, 95% stop impedance DEIF group. Like the other DEIF groups, this group also showed more homogeneous impedance reductions across all sectors. Impedance spectra for the 200 V/cm 80% DEIF group (not shown) exhibited slightly greater resistance and reactance values at lower frequencies and generally more sectors retained after

pulsing impedance spectra with semicircular shape. The 200 V/cm, 95% DEIF group generally exhibited more sectors with linear or near horizontal impedance spectra. Electrode reuse, indirect pulsing, and pulse sequence effects were less prevalent as shown by the very similar impedance spectra in 8 of 9 sectors. The peripheral sectors 2, 3, 4, and 7 (top row and left column of sectors) exhibited impedance spectra that were near the same shape and magnitude as those of the lower right quadrant of sectors, evidence that electrode reuse and sequence effects were minimal but not absent. The impedance spectra of these peripheral sectors showed greater resistance values at low frequencies relative to other sectors indicating permeability of membranes in these regions of tissue was also relatively lower. Figure 23 shows sector one was the only sector with a relatively semicircular after pulsing impedance spectra. Sectors 2 through 9 all had roughly linear spectra with slopes approaching zero indicating reactance of tissue in these sectors changed very little with frequency and was more than likely near its lowest achievable value before a significant portion of cells were irreversibly permeabilized. At this point, the available area of membranes to store charge was near constant. The quality and degree of permeability in sectors 2 through 9 was near the optimum for DNA uptake accounting for the statistically greater 6.8 fold increase in DNA delivery seen by this group relative to the non-feedback group of the same field (200 V/cm). Given the high radiance and the general similarity of impedance spectra in all sectors in this group, it is likely that spectra with this shape and magnitude may be indicative of the degree and quality of impedance that correlates best with enhanced DNA uptake.

At first glance, comparison of impedance spectra from the 200 V/cm DEI and 200 V/cm, 95% DEIF groups revealed almost no discernable difference between impedance loci in corresponding sectors. However, closer analysis of these spectra revealed subtle differences were present. The difference in resistance values from the lowest and highest frequency data points in

the impedance spectra provide a qualitative measure of the cumulative resistance in tissue associated with charge transfer through membranes. If a larger range of frequencies had been used to capture the complete dispersion mechanism under investigation, the resulting impedance spectra would more than likely have had two loci where reactance values were zero. The difference in the real coordinates (resistance) between these points on the complex plane quantifies the cumulative resistance of charge transfer through cell membranes or R_m from Figure 17 in tissue - a direct measurement of membrane permeability. However, because these points were not attained within the frequencies that were used, this value can be estimated by comparing the magnitude of the difference in resistance between the real coordinates of the impedance loci for the highest and lowest frequency impedance loci of each spectra. This value qualitatively describes the degree of horizontal compression of impedance spectra. It can be used to compare the transmembrane charge transfer resistance (R_m) in corresponding sectors between groups. Given that the horizontal compression of the impedance spectra was greater in corresponding sectors of the 200 V/cm DEI group relative to the 200 V/cm DEIF group targeting 95% impedance reduction, it was expected that R_m was lower in 200 V/cm DEI group sectors which. This represented a degree of membrane permeable that was less resistive or permeable to current flow. For example, the R_m represented by the compression of impedance spectra similar to that in sector 5 of Figure 22 may be too great and represent a very low R_m indicative of irreversible permeability. Overall, the cumulative transmembrane charge transfer resistance in sectors of the 200 V/cm DEIF, 95% group in Figure 23 was greater relative to spectra in corresponding sectors of the 200 V/cm DEIF group. However, without spatial resolution in radiance data, it was difficult to determine which spectra and R_m was optimum for transfection. This also underscored the fine line that exists between irreversible permeability and permeability that is optimum for DNA uptake. Moreover, these differences were

only exploitable when impedance based feedback was used to guide the number of applied electric pulses which, in the process, validated the utility of this method.

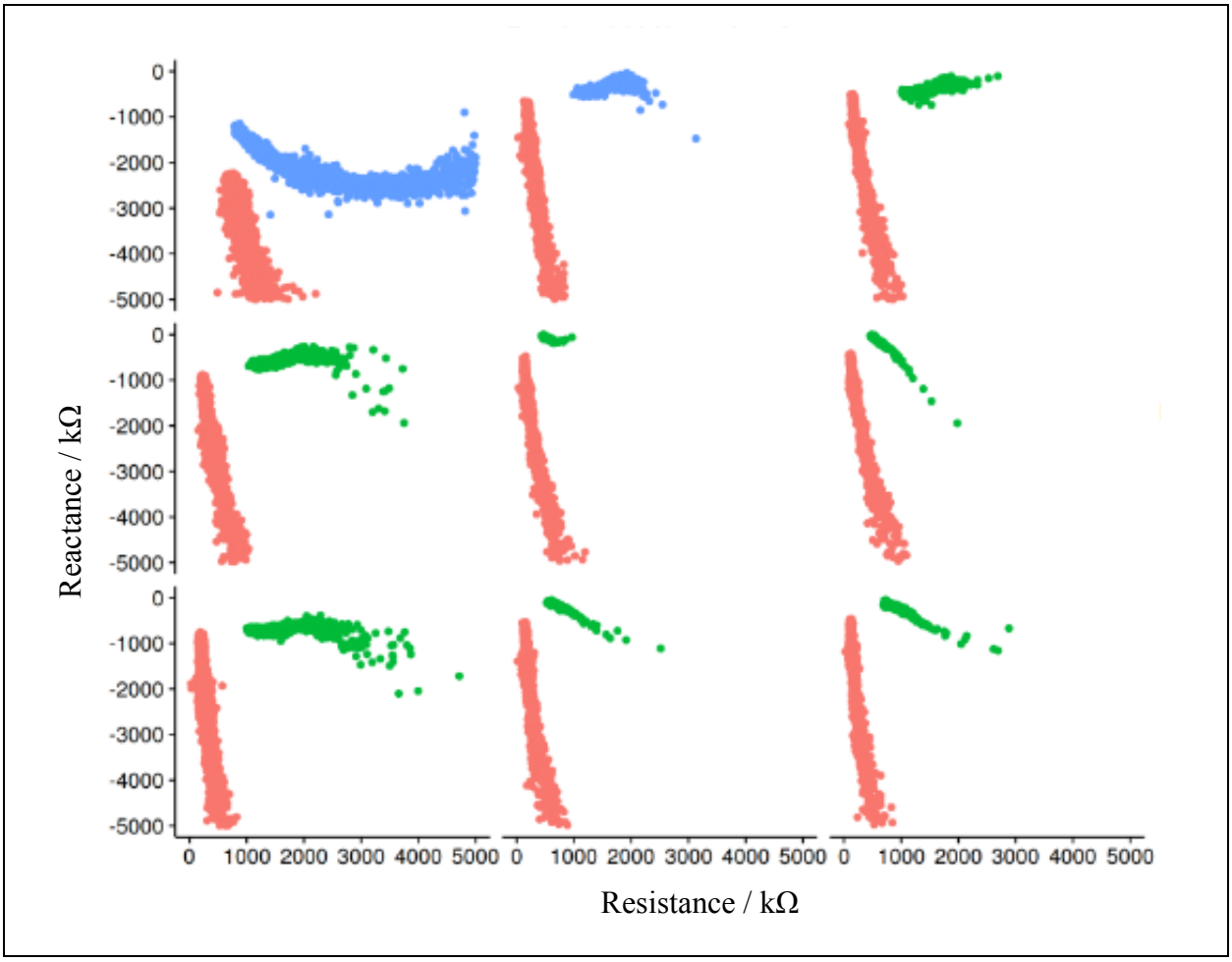

Figure 23: 200 V/cm, 95% DEIF group, single animal Nyquist plots for each sector before (orange) and after pulsing.

To help define the upper limits of permeability it was necessary to evaluate spectra from a group with conditions that induced tissue damage where irreversible permeability had been created. Figure 24 represents after pulsing Nyquist plots in a representative from the 250 V/cm DEI (non-feedback) group that received 8 EF pulses per sector animal and showed tissue damage at the treatment site with significantly low expression levels. This field strength was considered to irreversibly permeabilize tissues when used in non-feedback protocols where 72 pulses were administered. Irreversibly permeabilized sectors exhibited linear after pulsing Nyquist plots with

reactance magnitudes that were near zero at all frequencies. The permeability in animals of this group was near maximum because a large portion of cells had been irreversibly permeabilized. The magnitude and shape of these impedance spectra were indicative of the degree and quality of impedance that correlated best with irreversible permeability and should be avoided.

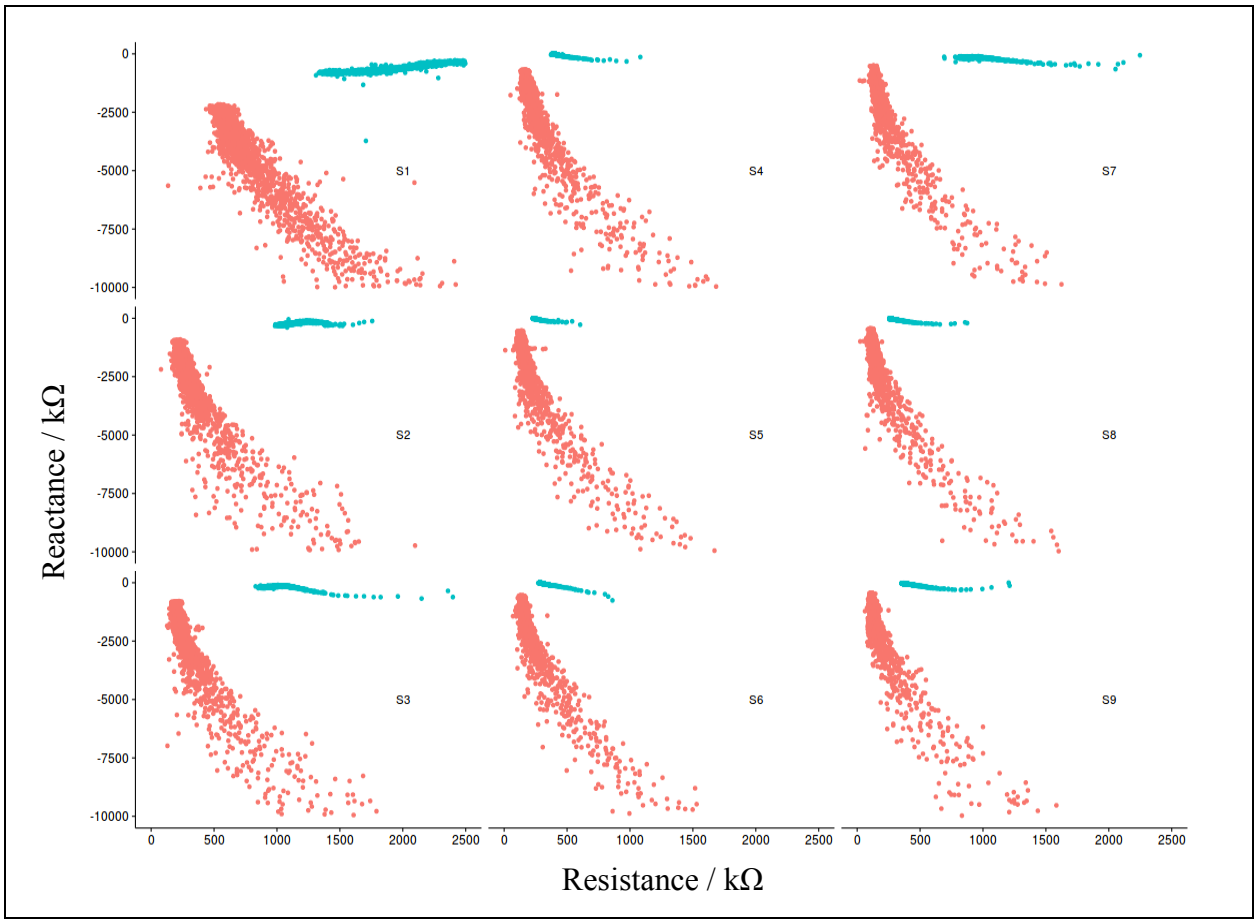

Figure 24: Before pulsing (orange) and after pulsing (blue) Nyquist plots for a representative animal from the 250 V/cm DEI group, 8 pulses per sector.

5.4 Conclusion

The motivation of this work was to investigate the utility of a closed loop GET method to control tissue permeability during electric field exposure for delivering gene constructs to cells *in vivo*. This is not practiced by the current state of the art. It was expected that targeting relative changes in tissue permeability with pre and interpulse impedance measurements, had the potential to ensure the conditions necessary for maximum gene delivery were created. This could enhance

the biological response and reliability of this method. This study showed that 200 V/cm pulsed electric fields targeting a 95% reduction in tissue impedance produced mean transgene expression levels that were 6.8 fold greater than open loop methods and 13.7 fold greater than non-electric field mediated pDNA injection only. Furthermore, the quality of permeability induced by electric fields was evidently dependent on the field strength and critical for increasing delivery. Feedback groups targeting the same reduction in tissue impedance with different field strengths showed that permeability induced by the highest electric field strength (200 V/cm) delivered more pDNA than other lower field strength groups. The impedance spectra and relatively attenuated expression exhibited by open loop protocol groups revealed the hindering effects of the multielectrode array, anisotropic tissue architecture, and fixed pulsing on gene delivery. When impedance-based feedback was used to guide pulse number to target a reduction in impedance, these effects were significantly minimized and almost abolished. As a result, in feedback groups, treatment sectors were subjected to the unique amount of electric field exposure necessary to account for differences in tissue architecture and electrode/protocol associated effects. This generated homogenous degrees of permeability across all sectors of treated tissue, not present in open loop methods, which contributed to significant increases in gene delivery. Not only did this feedback based GET method enhance delivery, but it also proved this approach may be universally applied to a near infinite number of electrode geometries because of its ability to account for tissue architecture and effects associated with multielectrode designs. These two discoveries should make significant contributions to the field and help advance GET methods to an even more widely accepted space in clinical medicine where it can be used to improve the quality of life of many.

CHAPTER 6: DISCUSSION AND FUTURE DIRECTIONS

6.1 Discussion

Electric field mediated gene delivery has gained popularity as a result of its ability to deliver nucleic acid constructs rapidly and with relatively high transfection efficiencies. The non-viral nature of these electric field based methods has engendered great interest as they have highly preferable safety profiles when compared to viral based delivery. However, the current state of the art utilizes empirically derived parameters that do not monitor cell/tissue responses to electric pulses, indicate if delivery was successful, target degree of permeability, or optimize electric pulse parameters in real time. This open loop approach does not account for anisotropic tissue architecture or compensate for electrode design/protocol effects that result in variable and sub therapeutic delivery efficiencies. This work showed that to ensure targeted transfection efficiencies can be achieved consistently closed loop methods need to be developed that optimize pulsing parameters in real time to apply the unique dose of electric field stimulation needed to achieve a desired level of membrane permeability. The electrical nature of GET and required hardware conveniently positions this method to incorporate other electric based controls that can be used to ensure gene delivery occurs. Impedance spectroscopy provided a way to quantify the transient permeability created in cell membranes after electric field exposure making it ideal for use as feedback control variable.

The device constructed for these experiments integrated a custom software controlled, dual mode capability high voltage/low voltage pulsing system, tethered to a multielectrode array

applicator. The 32 solid-state relays with 50 ms switching times allowed low voltage impedance chirps to measure impedance almost instantaneously after high voltage GET pulses. Custom software utilized a Fast Fourier Transform (FFT) to transform time dependent voltage and current waveforms into the frequency domain for calculating baseline and post pulse tissue impedance.

Treatment groups were formed to evaluate impedance-based feedback to optimize pulse number for achieving either 80% or 95% impedance drops in each treatment sector. The magnitude of impedance reduction was expected to indicate the degree of permeability in cell membranes, ensure roughly homogenous delivery across sectors, and significantly enhance gene delivery. Experiments conducted in animals showed reporter gene expression increased with field strength up to 200 V/cm and with target stop impedance. The 200 V/cm feedback groups targeting 95% and 80% impedance drops showed 14 and 11 fold increases in radiance relative to injection alone respectively, and 7 and 5 fold increases in radiance relative to the non-feedback group of the same field strength respectively. These results confirmed the use of impedance based feedback control to enhance gene delivery.

It was expected that impedance might indicate changes in the available current pathways or permeability present in tissue associated with electric pulses. This followed the logic that as impedance decreased additional pathways for current through cell membranes would also increase. Therefore, a reduction in impedance indicated an increase in membrane permeability and the mechanism responsible for the uptake of genetic constructs by cells had been initiated. Results supported this reasoning however, it there was a fine difference between optimum membrane permeability/impedance drop and irreversible permeabilization. Although visible cell death or tissue damage was not visible the significantly lower radiance levels in the 200 V/cm non feedback group indicate the 72 pulses these animals received created overpulsed responses in some sectors

where irreversible membrane permeability was present and underpulsed responses in others sectors. This resulted in reduced gene delivery relative to DEIF groups that was still statistically greater than DNA injection only groups. In comparison, animals that received the same field strength (200 V/cm) and a mean total of 101 pulses where pulses were varied to target 95 % reductions in treatment sector impedance, exhibited a 6.8 fold increase in radiance relative to the 200 V/cm DEI group. This proved that impedance based feedback could guide pulse number to compensate for electrode and pulse sequence effects and anisotropic tissue architecture. All DEIF groups exhibited a variable distribution of pulses across sectors to provide the unique amount of electric field exposure to each sector necessary for inducing a targeted permeability optimum for pDNA uptake.

Experimental results showed that by controlling pulse number to target a desired impedance drop across all sectors, an optimum degree of membrane permeability could be achieved to enhance DNA uptake. This validates the utility of impedance-based feedback in GET methods to increase gene delivery when compared to open loop methods.

6.2 Future Directions

Although gene delivery was improved in GET protocols employing feedback control, statistical power was hindered by inherent variability in biological response data and small sample sizes. In order to establish statistically different delivery profiles between feedback groups targeting 80% and 95% exposed to the same EF pulse strength, a larger sample size is needed. The method for calculating impedance drop in these experiments used the baseline mean value impedance magnitude from 1 kHz to 3 kHz for normalization. This low frequency interval generally characterizes the resistive components of the cells and tissue. Using relative changes in high frequency intervals of the impedance magnitude may provide more insight into the status of

the membrane and therefore provide for better control when targeting a desired membrane permeability. This may be a better feedback variable as it may more accurately describe the cumulative charge storage capacity of cell membranes in tissue which may correlate better with delivery and the relative degree of membrane permeability present after each pulse.

The electrode design and pulse sequence pattern used in this study did not expose sectors to an equal amount of electric field stimulation when a fixed pulse number was used in each sector. Effects associated with electrode reuse and the indirect exposure of sectors to fields in upstream/downstream sectors clouded the exact impedance changes associated with direct pulses in a sector. Because of this, the minimum relative impedance change was known instead of the final relative sector impedance change. More experiments need to be done that pulse and measure in only one sector while monitoring reporter gene expression to identify the true impedance reduction and spectra that correlates with maximum transgene expression.

The probing depth of the electric fields generated by the 2 mm spacing used in the MEA requires further validation. The impedance spectra collected were assumed to provide information within the region of tissue where volume of pDNA was injected. This was never confirmed. Other possible impedance measurement techniques should also be explored that incorporate passive sensing electrodes not responsible for injecting current into tissue.

Future work should utilize impedance-based feedback to investigate the mechanism of action occurring in gene electrotransfer. To remove the confounding effects of extracellular matrix components and an infinitely large set of cell/tissue architecture configurations, impedance spectroscopy must be adapted to single cell analysis *in vitro*. This may shed much needed light onto a disputed mechanism and more importantly advance the state of the art to allow the potential of gene-based medicine to be realized. Finally, the culmination of this litany of proposals and

recommendations would be the assessment of closed loop GET methods to consistently induce clinically relevant outcomes.

REFERENCES

[1] C. C. Trosko JE, "An Integrative Hypothesis Linking Cancer, Diabetes and Atherosclerosis-The Role of Mutations and Epigenetic Changes," *Medical Hypothesis,* vol. 6, no. 5, pp. 455-468, 1980.

[2] P. Galvez, A. Ruiz and B. Clares, "The future of new therapies in clinical medicine," *Medicina Clinica,* vol. 137, no. 14, pp. 645-649, 2011.

[3] S. Liu and K. Maeyama, "Gene Therapy for Rheumatoid Arthritis," *Critical Reviews in Immunology,* vol. 36, no. 2, pp. 149-161, 2016.

[4] A. Bradshaw and A. Baker, "Gene therapy for cardiovascular disease: Perspectives and potential," *Vascular Pharmacology,* vol. 58, no. 3, pp. 174-181, 2013.

[5] M. Bertolaso, J. Olsson and A. Picardi, "Gene therapy and enhancement for diabetes (and other diseases): the multiplicity of considerations," *Diabetes-Metabolism Research and Reviews,* vol. 26, no. 7, p. 520524, 2010.

[6] S.-A. Shu, J. Wang and M.-H. e. a. Tao, "Gene therapy for Autoimmune Disease," *Clinical Reviews in Allergy & Immunology,* vol. 49, no. 2, pp. 163-176, 2015.

[7] D. O'Connor and N. Boulis, "Gene therapy for neurodegenerative diseases," *Trends In Molecular Medicine,* vol. 21, no. 8, pp. 504-512, 2015.

[8] Q. Shi, X.-L. Zhang and K.-R. Dai, "siRNA therapy for cancer and non-lethal diseases such as arthritis and osteoporosis," *Expert Opinion on Biological Therapy,* vol. 11, no. 1, pp. 5-16, 2011.

[9] I. Slivac, D. Guay and M. Manion, "Non-viral nucleic acid delivery methods," *Expert Opinion On Biological Therapy ,* vol. 17, no. 1, pp. 10-118, 2017.

[10] P. Lollini, F. Cavallo and P. Nanni, "The Promise of Preventitive Cancer Vaccines," *Vaccines,* vol. 3, no. 2, pp. 467-489, 2015.

[11] S. Pejawar-Gaddy and O. Finn, "Cancer Vaccines: Accomplishments and challenges," *Critical Reviews in Oncology Hematology,* vol. 67, pp. 93-102, 2008.

[12] D. Auci, D. Cecil, D. Herendeen, E. Broussard, J. Liao, G. Holt and M. Disis, Gene Therapy of Cancer: Translational Approaches from Preclinical Studies to Clinical Implementation, San Diego: Elsevier Academic Press Inc, 2014.

[13] D. Han, D. Weiner and J. Sin, "DNA Vaccines against Infectuous Cancer," *Biomolecules & Therapeutics,* vol. 18, no. 1, pp. 1-15, 2010.

[14] P. Bosze, "The first vaccine against cancer: the human papillomavirus vaccine," *Orvosi Hetlap,* vol. 154, no. 16, pp. 603-618, 2013.

[15] T. De Pas, M. Giovannini, M. Rescigno, C. Catania, F. Toffalorio, G. Spitaleri, A. Delmonte, M. Barberis, L. Spaggiari and P. Solli, "Vaccines in non-small cell lung cancer: Rationale, combination strategies and update on clinical trials," *Critical Reviews in Oncology Hematology,* vol. 83, no. 3, pp. 432-443, 2012.

[16] A. Mescher, Junqueira's Basic Histology Text & Atlas 12th. Ed., New York: McGraw Hill, 2010.

[17] N. Kashibuchi, Y. Hirari, K. O'Goshi and H. and Tagami, "Three-dimensional analyses of individual corneocytes with atomic force microscope; morpholgical chagnes related to age, location and to the pahtologic skin condition," *Skin Research and Technology,* vol. 8, pp. 203-211, 2002.

[18] J. Bouwstra, A. de Graaff, G. Gooris, J. Nijsse, J. Wiechers and A. van Aelst, "Water distribution and related morphology in human stratum corneum at different hydration levels," *Journal of Investigative Dermatology,* vol. 120, pp. 750-758, 2003.

[19] V. Lulevich, H. Yang, I. Rivkah and L. Gang-yu, "Single cell mechanics of keratinocyte cells," *Utramicroscopy,* vol. 110, pp. 1435-1442, 2010.

[20] A. Lee, J. King and T. Rogers, "A multiple-pathway model for the diffusion of drugs in skin," *Mathematical Methods in Biology,* vol. 13, p. 127, 1996.

[21] U. Birgersson, E. Birgersson, I. Nicander and S. Ollmar, "A methodology for extracting the electrical properties of human skin," *Physiological Measurment,* vol. 34, pp. 723-736, 2013.

[22] L. Hui and Y. Chen, "Tumor microenvironment: Sanctuary of the devil," *Cancer Letters,* vol. 368, no. 1, pp. 7-13, 2015.

[23] D. Fukumura and R. Jain, "Tumor microvasculature and microenvironmnet: Targets for anti-angiongenesis and normalization," *Microvasular Research,* vol. 74, no. 2-3, pp. 72-84, 2007.

[24] M. Martin, H. Wei and T. Lu, "Targeting microenvironment in cancer therapeutics," *Oncotarget,* vol. 7, no. 32, pp. 52575-52583, 2016.

[25] S. Amarnath, C. Mangus, J. Wang, F. Wei, A. He, V. Kapoor, J. Foley, P. Massey, T. Felizardo, J. Riley, B. Levine, C. June, J. Medin and D. Fowler, "the PDL1-PD1 Axis Converts Human T(H)1 Cells into Regulatory T Cells," *Science Translational Medicine,* vol. 3, no. 111, p. 111ra120, 2011.

[26] E. Arkhangelsky, Y. Sefi, B. Hajaj, G. Rothenberg and V. Gitis, "Kinetics and mechanism of plasmid DNA penetration through nanopores," *Journal of Membrane Science,* vol. 371, no. 1-2, pp. 45-51, 2011.

[27] D. Latulippe and A. Zydney, "Radius of Gyration of Plasmid DNA Isoforms From Static Light Scattering," *Biotechnology and Bioengineering,* vol. 107, no. 1, pp. 134-142, 2010.

[28] S. De Silva, M. A. Mastrangelo, L. T. Lotta, C. A. Burris, H. J. Federoff and W. J. Bowers, "Extanding the transposable payload limit of Sleeping Beauty (SB) using the Herpes Simplex Virus (HSV)/SB amplicon-vector platform," *Gene Therapy,* vol. 17, no. 3, pp. 424-431, 2010.

[29] S. Chira, C. S. Jackson, I. Oprea, F. Ozturk, M. S. Pepper, I. Diaconu, C. Braicu, L.-Z. Raduly, G. A. Calin and I. Berindan-Neagoe, "Progresses towards safe and efficient gene therapy vectors," *Oncotarget,* vol. 6, no. 31, pp. 30675-30703, 2015.

[30] A. Fischer and M. Cavazzana-Calvo, "Gene Therapy of Inherited Diseases," *Lancet,* vol. 9629, no. 371, pp. 2044-2047, 2008.

[31] Z. S. Guo, Q. Li, D. L. Bartlett, J. Y. Yang and B. Gang, "Gene transfer: The challenge of regulated gene expression," *Trends Mol Med,* vol. 14, no. 9, pp. 410-418, 2008.

[32] D. He and E. Wagner, "Defined Polymeric Materials for Gene Delivery," *Macromolecular Bioscience,* no. 15, pp. 600-612, 2015.

[33] G. Caracciolo and H. Amenitsch, "Cationic liposome/DNA complexes: from structure to interactions will cellular membranes," *Eur Biophys J,* no. 41, pp. 815-829, 2012.

[34] X.-X. Zhang, T. J. McIntosh and M. W. Grinstaff, "Functional lipids and lipoplexes for improved gene delivery," *Biochimie,* no. 94, pp. 42-58, 2012.

[35] T.-H. Wu, T. Teslaa, M. Teitell and P. Chiou, "Photothermal nanoblade for patterned cell membrane cutting," *Optics Express,* vol. 14, no. 6, pp. 23153-23160, 2010.

[36] R. Sun, M. Noble, S. Sun, S. Song and C. Miao, "Development fo therapeutic microbubbles for enhancing ultrasound-mediated gene delivery," *J Controlled Release,* vol. 182, pp. 111-120, 2014.

[37] J. Wyber, J. Andres and A. Demanuele, "The use of sonication for the efficient delivery of plasmid DNA into cells," *Pharmaceutical Research,* vol. 14, no. 6, pp. 750-756, 1997.

[38] J. O'Brien and S. Lummis, "Nano-bolistics: a method of biolistic transfection of cells and tissues using a gene gun with novel nanometer-sized projectiles," *BMC Biotechnology,* vol. 11, pp. 66-72, 2011.

[39] C. Plank, O. Zelphati and O. Mykhaylyk, "Magnetically enhanced nucleic acid delivery. Ten years of magnetofection-Progress and prospects," *Advanced Drug Delivery Reviews,* no. 63, pp. 1300-1331, 2011.

[40] A. Daud, R. DeConti, S. Andrews, P. Urbas, A. Riker, V. Sondak, P. Munster, D. Sullivan, K. Ugen, J. Messina and R. Heller, "Phase I trial of interleukin-12 plasmid electroporation in patients with metastatic melanoma," *J Clin Oncol.,* vol. 26, no. 36, pp. 5896-5903, 2008.

[41] S. Li, "Electroporation gene therapy: New developments in vivo and in vitro," *Current Gene Therapy,* vol. 4, no. 3, pp. 309-316, 2004.

[42] E. Neumann, M. Schaeffer-Ridder, Y. Wang and P. Hofschneider, "Gene transfer into mouse lymphoma cells by electroporation in high electric fields," *EMBO J.,* vol. 1, pp. 841-845, 1978.

[43] L. Mir, "Therapeutic perspectives of in vivo cell electropermeabilization," *Bioelectrochemistry,* vol. 53, pp. 1-10, 2001.

[44] M. Rols, C. Delteil, M. Golzio and Teissie, "Control by ATP and ADP of voltage-induced mammalian-cell-membrane permeabilization, gene transfer, and resulting expression," *Eur. J. Biochem,* vol. 254, pp. 382-388, 1998.

[45] R. Heller, M. Jaroszeski, A. Atkin, D. Moradpour, R. Gilbert, J. Wands and C. Nicolau, "In vivo gene electro injection and expression in rat liver," *FEBS Lett,* vol. 389, pp. 225-228, 1996.

[46] A. Titomirov, S. Suhkarev and E. Kistanova, "In vivo electroporation and stable transformation of skin cells of newborn mice by plasmid DNA," *Biochimica ET Biophysica Acta,* vol. 1088, no. 1, pp. 131-134, 1991.

[47] J. Escoffre, T. Portet, L. Wasungu, J. Teissie, D. Dean and M. Rols, "What is (still not) known of the mechanism by which electroporation mediates gene transfer expression in cells and tissues," *Mol Biotechnol,* vol. 41, pp. 286-295, 2009.

[48] J. Teissie, M. Golzio and M. Rols, "Mechanisms of cell membrane electropermeabilization: a minireview of our present (lack of?) knowledge," *Biophys Acta Gen Subj,* vol. 1724, pp. 270-280, 2005.

[49] B. Ferraro, L. Heller, Y. Cruz, S. Guo, A. Donate and R. Heller, "Evaluation of delivery conditions for cutaneous plasmid electrotransfer using a multielectrode array," *Gene Ther.,* vol. 18, pp. 496-500, 2010.

[50] L. Heller, M. Jaroszeski, D. Coppola, A. McCray, J. Hickey and R. Heller, "Optimization of cutaneous electrically mediated plasmid DNA delivery using novel electrode," *Gene Therapy,* vol. 14, pp. 275-280, 2007.

[51] J. Weaver and Y. Chizmadzhev, "Theory of electroporation: a review.," *Bioelectrochem Bioenerg,* vol. 41, pp. 135-160, 1996.

[52] M. Naumowicz and Z. Figaszweski, "Pore formation in lipid bilayer membranes made of phosphatidylcholine and cholesterol followed by means of constant current," *Cell Biochem Biophys,* vol. 66, pp. 109-119, 2013.

[53] A. Ivorra and B. Rubinsky, "In vivo electrical impedance measurements during and after electroporation of rat liver," *Bioelectrochemistry,* vol. 70, pp. 287-295, 2007.

[54] F. Clemente, P. Arpaia and C. Mann, "Characterization of human skin impedance after electrical treatment for transdermal drug delivery," *Measurement,* vol. 46, pp. 3494-3501, 2013.

[55] T. Garcia-Sanchez, M. Guitart, J. Rosell-Ferrer, A. Gomez-Foix and R. Bragos, "A new spiral microelectrode assembly for electroporation and impedance measurements of adherent cell layers," *Biomed Microdevices,* vol. 16, pp. 575-590, 2014.

[56] R. Atkins, T. Fawcett, R. Gilbert, A. Hoff, D. Brown, A. Llewellyn and M. Jaroszeski, "Impedance spectroscopy as an indicator for successful in vivo electric field mediated gene delivery in a murine model," *Bioelectrochemistry,* 2017.

[57] F. Duck, Physical porperties of tissue: a comprehensive reference book, London: Acadmeic Press, 1990.

[58] C. Gabrial, S. Gabriel and E. Corthout, "The dielectric properties of biological tissues: I. Literature survey," *Physics in Medicine and Biology,* vol. 41, pp. 2231-2249, 1996.

[59] L. Geddes, "The specific resistance of biological material - a compendium of data for the biomedical engineer and physiologist," *Med. Biol. Eng,* vol. 5, pp. 271-293, 1967.

[60] Aldevron, "gWiz High Expression Reporter Plasmids," [Online]. Available: http://www.aldevron.com/services/related-services/dnas/gwiz/. [Accessed 1 December 2016].

[61] E. Chang and J. Zabner, "Presicions Genomic Medicine in Cystic Fibrosis," *CTS-Clinical and Translational Science,* vol. 8, no. 5, pp. 606-610, 2015.

[62] T. Hamidi, A. Singh and T. Chen, "Genetic alterations of DNA methylation in human diseases," *Epingenomics,* vol. 7, no. 2, pp. 247-265, 2015.

[63] H. Kim, S. Won, C. Fabia, M. Kang, M. Szardenings and M. Shin, "Mitochondrial DNA Aberrations and Pathophysiological Implications in Hematopoietic Diseases, Chronic Inflammatory Diseases, and Cancers," *Annals of Laboratory Medicine,* vol. 35, no. 1, pp. 1-14, 2015.

[64] C. Yang and B. Chiang, "Inflammasomes and human autoimmunity: A comprehensive review," *Journal of Autoimmunity,* vol. 61, pp. 1-8, 2015.

[65] L. Zhang, E. Padron and J. Lancet, "The molecular basis and clinical significiance of genetic mutations identified in myelodysplastic syndromes," *Leukemia Research,* vol. 39, no. 1, pp. 6-17, 2015.

[66] M. Meacham, K. Durvasula, L. Degertekin and A. Federov, "Physical methods for intracellular delivery: practical aspects from laboratory use to industrial-scale processing," *Journal of Laboratory Automation,* vol. 19, pp. 10-18, 2014.

[67] C. Rosazza, A. Buntz, T. Rieb, D. Woll, A. Zumbusch and M.-P. Rols, "Intracelluar tracking of sinlge-plasmid dna particles after delivery by electroporation," *Molecular Therapy,* vol. 21, pp. 2217-2226, 2013.

[68] G. Grafstrom, P. S. L. Engstrom and B. Persson, "99mTc-DTPA Uptake and Electrical Impedance Measurements in Verification of In Vivo Electropermeabilization Efficiency in Rat Muscle," *Cancer Biotherapy & Radiopharmaceuticals,* vol. 21, no. 6, pp. 623-635, 2006.

[69] S. Laufer, S. Solomon and B. Rubinsky, "Tissue characterization using electrical impedance spectroscopy data: a linera algebra approach," *Physiological Measurement,* vol. 33, pp. 997-1013, 2012.

[70] D. Dean, D. Ramanathan and R. S. R. Machado, "Electrical impedance spectroscopy study of biological tissues," *Journal of Electrostatics,* vol. 66, pp. 165-177, 2008.

[71] R. Davalos, B. Rubinsky and O. DM, "A Feasibility Study for Electrical Impedance Tomography as a Means to Monitor Tissue Electroporation for Molecular Medicine," *IEEE Transactions on Biomiedical Engineering,* vol. 49, no. 4, pp. 400-403, 2002.

[72] T. Garcia-Sanchez, A. Azan, I. Leray, J. Rosell-Ferrer, R. Bragos and L. Mir, "Interpulse multifrequency electrical impedance measurements during electroporation of adherent differentiated myotubes," *Bioelectrochemistry,* vol. 105, pp. 123-135, 2015.

[73] Y. Granot, A. Ivorra, E. Maor and B. Rubinsky, "In vivo imaging of irreversible electroporation by means of electrical impedance tomography," *Physics in Medicine and Biology,* vol. 54, pp. 4927-4943, 2009.

[74] I. Zampaglione, M. Arcuri, M. Cappelletti, G. Ciliberto, G. Perretta, A. Nicosia, N. La Monica and E. Fattori, "In vivo DNA gene electro-transfer: a systematic analysis of different electrical parameters," *The Journal of Gene Medicine,* vol. 7, pp. 1475-1481, 2005.

[75] S. Hacein-Bey-Abina, C. von Kalle, M. Schmidt, F. Le Deist, N. Wulffraat, E. McIntyre, I. Radford, J.-L. Villeval, C. Fraser, M. Cavazzna-Calvo and A. Fischer, "A serious adverse event after successful gene therapy for x-linked severe combined immunodeficiency," *New England Journal of Medicine,* vol. 348, p. 255256, 2003.

[76] J. Demeulemeester, J. De Rijck, R. Gijsbers and Z. Debyser, "Retroviral integration: Site matters: Mechanisms and consequences of retroviral integration site selection," *Bio Essays: news and reviews in molecular, cellular and developmental biology,* vol. 37, pp. 1202-1214, 2015.

[77] C. Thomas, A. Ehrhardt and M. Kay, "Progress and problems with the use of viral vectors for gene therapy," *Nature reviews. Genetics,* vol. 4, pp. 346-358, 2003.

[78] D. Lee, K. Upadhye and P. N. Kumta, "Nano-sized calcium phosphate (CaP) carriers for non-viral gene delivery," *Materials Science Engineering,* vol. 177, no. 3, pp. 289-302, 2012.

[79] M. C. Woodle and P. Scaria, "Cationic liposomes and nucleic acids," *Curr Opin Colloid Interface Sci,* vol. 2, pp. 241-41, 2001.

[80] A. Federov, E. King, J. Anderson, D. Karpilow and W. Ilsley, "Different delivery methods-different expression profiles," *Nat. Methods,* vol. 2, pp. 241-41, 2005.

[81] R.-Y. Huang, P.-H. Chiang, W.-C. Hsiao, C.-C. Chuang and C.-W. Chang, "Redox-sensitive polymer/SPIO nanocomplexes for efficient magnetofection and MR imaging of human cancer cells," *J Surfaces and Colloids,* vol. 31, no. 23, pp. 6523-6531, 2015.

[82] U. Pliquett, R. Joshi, V. Sridhara and K. Schoenback, "High electrcial field effects on cell membranes," *Bioelectrochemistry,* vol. 70, pp. 275-282, 2006.

[83] A. Ivorra, B. Al-Sakere, B. Rubinsky and L. Mir, "In vivo electrical conductivity measurements during and after tumor electroporation: conductivity changes reflect treatment outcomes," *Physics in Medicine and Biology,* vol. 54, pp. 5949-5963, 2009.

[84] M. Leguebe, A. Silve, L. Mir and C. Poignard, "Conducting and permeable states of cell membranes submitted to high voltage pulses: Mathematical and numerical studies validated by the experiments," *Journal of Thoeretical Biology,* vol. 360, pp. 83-94, 2014.

[85] M. Pavlin and D. Miklavcic, "Theoretical and experimental analysis of conductivity, ion diffusion, and molecular transport during cell electroproation - relation between short-lived and long-lived pores," *Bioelectrochemistry,* vol. 74, pp. 38-46, 2008.

[86] S.-L. Tsai and M.-H. Wang, "24 h observation of single HeLa cells by impedance measurments and numverical modeling," *Sensors and Actuators B: Chemical,* vol. B229, pp. 225-231, 2016.

[87] C. Rosazza, H. Deschout, A. Buntz, K. Braeckmans, M.-P. Rols and A. Zumbusch, "Endocytosis and Endosomal Trafficking of DNA after Gene Electrotransfer In Vitro," *Molecular Therapy - Nucleic Acids,* vol. 5, p. e286, 2016.

[88] M. Lucas, M. Jaroszeski, R. Gilbert and R. Heller, "In vivo electroporation using an exponentially enhanced pusle: A new waveform," *DNA Cell Biol,* vol. 20, pp. 183-188, 2001.

[89] K. Smith, J. Neu and W. Krassowska, "Model of Creation and Evolution of Stable Electropores for DNA Delivery," *Biophysical Journal,* vol. 86, pp. 2813-2826, 2004.

[90] W. Krassoska and P. Filev, "Modeling Electroporation in a Single Cell," *Biophysical Journal,* vol. 92, pp. 404-417, 2007.

[91] S. Huclova, D. Erni and J. Frohlich, "Modelling and validation of dielectric properties of human skin in the MHz region focusing on skin layer morphology and material composition," *Journal of Physics D: Applied Physics,* vol. 45, p. 025301, 2012.

[92] S. Huclova, D. Erni and J. Frohlich, "Modelling effective dielectric properties of materials containing diverse typese of biological cells," *Journal of Physics D: Applied Physics,* vol. 43, p. 365405, 2010.

[93] J. Sato, M. Yanai, T. Hirao and M. Denda, "Water content and thickness of the stratum corneum contribute to skin surface morphology," *Archives of Dermatological Research,* vol. 292, pp. 412-417, 2000.

[94] C. Silva, D. Topgaard, V. Kocherbitov, J. Sousa, A. Pais and E. Sparr, "Stratum corneum hydration: Phase transformations and monility in stratum corneum, extracted lipids and isolated corneocytes," *Biochimica et Biophysica Acta,* vol. 1768, pp. 2647-2659, 2007.

[95] H. Schwan, "Electrical properties of tissues and cells," in *Advances in Biological and Medical physics*, vol. 5, Acad. Press, 1957, pp. 147-209.

APPENDIX A: COPYRIGHT PERMISSION

A.1 Elsevier Copyright Permission

Below is permission for the use of Chapter 4, which was accepted for publication in Bioelectrochemistry and is currently in press.

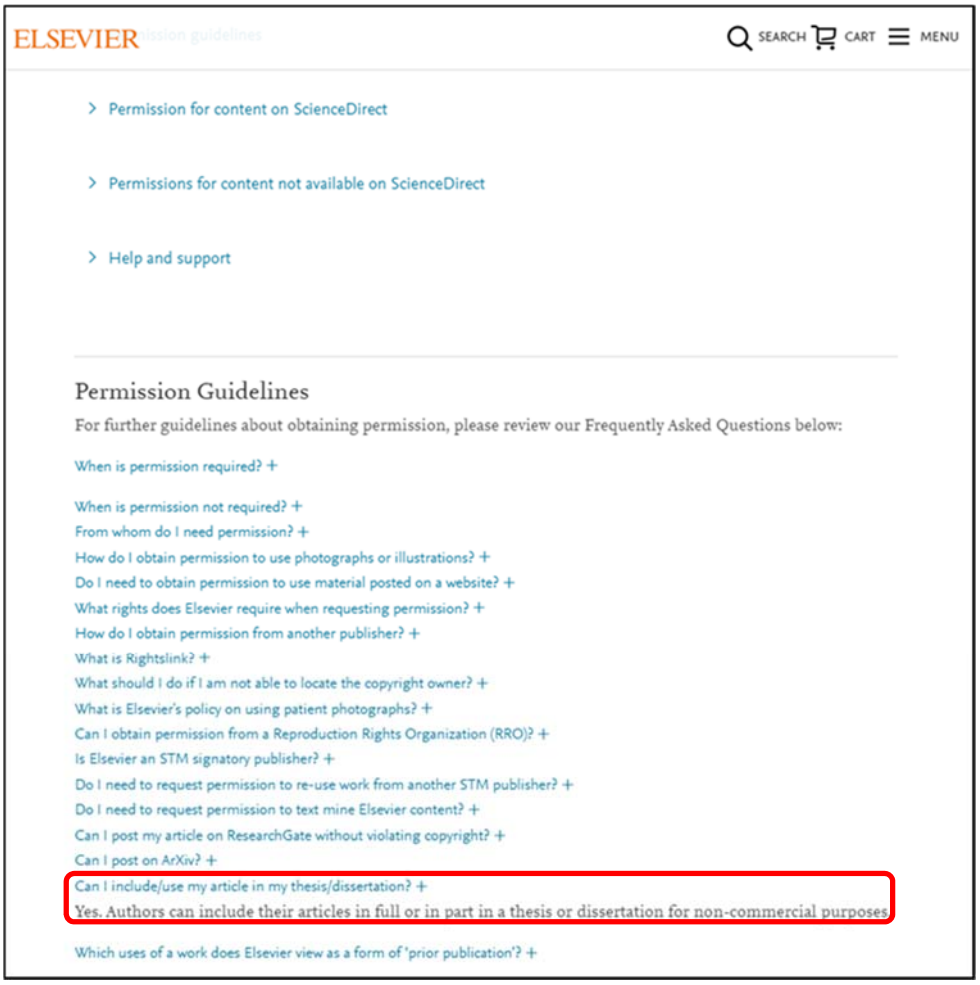

ELSEVIER SEARCH CART MENU

> Permission for content on ScienceDirect

> Permissions for content not available on ScienceDirect

> Help and support

Permission Guidelines

For further guidelines about obtaining permission, please review our Frequently Asked Questions below:

When is permission required? +

When is permission not required? +
From whom do I need permission? +
How do I obtain permission to use photographs or illustrations? +
Do I need to obtain permission to use material posted on a website? +
What rights does Elsevier require when requesting permission? +
How do I obtain permission from another publisher? +
What is Rightslink? +
What should I do if I am not able to locate the copyright owner? +
What is Elsevier's policy on using patient photographs? +
Can I obtain permission from a Reproduction Rights Organization (RRO)? +
Is Elsevier an STM signatory publisher? +
Do I need to request permission to re-use work from another STM publisher? +
Do I need to request permission to text mine Elsevier content? +
Can I post my article on ResearchGate without violating copyright? +
Can I post on ArXiv? +
Can I include/use my article in my thesis/dissertation? +
Yes. Authors can include their articles in full or in part in a thesis or dissertation for non-commercial purposes

Which uses of a work does Elsevier view as a form of 'prior publication'? +

ABOUT THE AUTHOR

Reginald Atkins began his college education in 1997 at Eckerd College in St. Petersburg, Florida. Reginald played soccer for the Tritons and was awarded a bachelor of arts degree in Psychology in 2001. After deciding to direct his career in a different direction, he returned to school at the University of South Florida where he was awarded a bachelor of science degree in chemical engineering and a bachelor of arts in chemistry in 2011. It was during this time that he performed research in the field of gene delivery, which motivated him to pursue higher education in biomedical engineering. In 2013, he received his masters of science degree in biomedical engineering. This document constitutes the research component required to obtain the doctor of philosophy degree in biomedical engineering.